



Research Report 2010
Volume 22

In this volume...

Report Summaries

On the memory stick...

Complete Reports
CREWES Channel Model Data
Student Theses
Software



UNIVERSITY OF
CALGARY



CREWES Project faculty, staff and students, September 2010

Left to Right:

Back Row: Kris Innanen, Jean Cui, Chris Bird, Larry Lines, Byron Kelly, Brock Hargreaves, Hormoz Izadi, Akshay Gulati, Peng Cheng, Matt McDonald, Michael Lamoureux, Mahdi Almuttaq, Zaiming Jiang, Lily Han, Ritesh Sharma, Kevin Bertram, Rob Ferguson.

Second Row: Xinxiang Li, Andrew Nicol, Steve Kim, Rolf Maier, Peter Gagliardi, Roohollah Askari, Marcus Wilson, Vanja Vracar.

Third Row: Jessie Arthur Heather Lloyd, Mostafa Naghizadeh, Liliana Zuleta, Thais Gurigay, Hassan Khaniani, Todor Todorov, Helen Isaac, Don Lawton, Dali Zhang, Diane Lespinasse.

Fourth Row: Baolin Qiao, Dave Henley, Laura Baird, Faranak Mahmoudian, Gary Margrave (Director), Kevin Hall, Abdallah Al Zahrani, , David Cho, Naser Yousefzadeh, Ben Wards, Melissa Hernández.

Front Row: John Bancroft, Joe Wong, Agnieszka Pawlak, Virginia Vera.

CREWES in 2010

This is proving to be a banner year at CREWES. We have the highest number of students ever in the project and, as of this writing, we are on track to set a project record for the most research reports ever. Of course, quantity does not necessarily imply quality, but I can assure you that our research is truly first class. One thing that inspires such confidence is my interaction with the authors of this tremendous scientific outpouring, by which I understand the intensity of their motivation. Another thing is that we are addressing a very broad spectrum of problems critical to seismic exploration. Our report contains work on acquisition design, low-frequency recording, numerical and physical modelling, wave theory, rock properties, anisotropy and fractures, data processing, imaging, inversion, interpretation, time-lapse seismic, and case studies.

Another event of note is that we are pleased to welcome two new sponsors: Tullow Oil p.l.c. of the United Kingdom, and Geoprosados, SA de CV of Mexico. Tullow is one of the largest independent oil companies in the world and is actively pursuing advanced seismic technology. Geoprosados provides leading-edge solutions to Mexico's major oil and gas E&P companies. We welcome to CREWES our new colleagues from Tullow and Geoprosados!

Beginning in 1995 with a major field effort, CREWES has done a lot of work related to low-frequency recording and inversion. In 1995 we acquired a 2D line at the Blackfoot field that recorded dynamite shots into a variety of standard and low-frequency geophones. Called the Blackfoot broadband experiment, these data are being released this year through the SEG Book Mart. The results from the low-frequency inversions were published in subsequent years. More recently we have compared geophones and MEMS accelerometers to seismometers in the low frequency range. In the coming year, we plan to conduct another low-frequency experiment using modern geophones and accelerometers and more than just dynamite sources. We have not yet chosen a site but would prefer something comparable to Blackfoot: a known field near Calgary with good well control. If you have a possible site or would like to participate in the planning and conduct of the survey, we would like to hear from you.

We thank you all for your support in 2010 and we look forward to another year of vigorous activity in 2011. Please enjoy our meeting and do not hesitate to give us feedback or guidance.

Season's greetings from CREWES to you!

Calgary, Alberta
December, 2010

Gary F. Margrave
Director of CREWES

Table of Contents

| | |
|-----------------------------------|--------------|
| CREWES in 2010 | i |
| Table of Contents | ii |
| 2010 CREWES Sponsors | viii |
| CREWES Personnel | ix |
| Student Theses | xviii |

| | |
|---|----|
| Towards a surface consistent match filter (SCMF) for time-lapse processing Mahdi H. Almutlaq and Gary F. Margrave | 1 |
| Tutorial: AVO inversion Mahdi H. Almutlaq and Gary F. Margrave | 2 |
| Interpretation of 3D multicomponent seismic data for investigating natural fractures in the Horn River Basin, northeast British Columbia Abdallah Al-Zahrani* and Don C. Lawton | 3 |
| Dispersion and the dissipative characteristics of surface waves in the generalized S transform domain Roohollah Askari*, Robert J. Ferguson..... | 4 |
| A MATLAB version of Equivalent Offset Migration (EOM) John C. Bancroft* | 5 |
| Investigating reflections from smooth transition boundaries John C. Bancroft | 6 |
| Microseismic sensitivity for four receivers on a square grid John C. Bancroft | 7 |
| Recovery of low frequency data from 10 Hz geophones Malcolm B. Bertram* and Gary F. Margrave..... | 8 |
| Seismic acquisition projects 2010 Malcolm B. Bertram, Kevin L. Bertram, Kevin W. Hall, Eric V. Gallant | 9 |
| Amplitude calibration of a fast S-transform algorithm Chris Bird, Mostafa Naghizadeh, Kristopher Innanen..... | 10 |
| Determination of anelastic reflectivity: how to extract seismic AVF information Chris Bird*, Kristopher Innanen, Larry Lines, Mostafa Naghizadeh..... | 11 |
| Color correction for Gabor deconvolution: a test with 2D synthetic data and field data Peng Cheng*, Gary F. Margrave and David C. Henley | 12 |
| Estimation of elastic stiffness parameters in weakly anisotropic rotated HTI media David Cho and Gary F. Margrave | 13 |

* Presenter

| | |
|---|----|
| Histograms of the Kirchhoff migration operator | |
| James Close and John C. Bancroft | 14 |
| A comparison of exact, approximate and linearized ray tracing methods in transversely isotropic media | |
| P.F. Daley, E.S. Krebs and L.R. Lines* | 15 |
| A comparison of finite difference analogs for hyperbolic equations in inhomogeneous media | |
| P.F. Daley | 16 |
| A linearized group velocity approach for two point qP ray tracing in a layered orthorhombic medium | |
| P.F. Daley | 17 |
| P-S_V wave propagation in a radially symmetric vertically inhomogeneous TI medium: Finite difference hybrid method | |
| P.F. Daley | 18 |
| Quasi-compressional ray propagation in a linearized general anisotropic media | |
| P.F. Daley | 19 |
| Reflection and transmission coefficients in TI media: exact and linearized phase velocities, eikonals and polarization vectors | |
| P.F. Daley, E.S. Krebs and L.R. Lines..... | 20 |
| Shot record depth migration of georadar | |
| Robert J. Ferguson*, Adam Pidlisecky, and Colin Rowell | 21 |
| Borehole geophone repeatability experiment | |
| Peter Gagliardi* and Don C. Lawton..... | 22 |
| Converted wave processing in the EOM domain | |
| Thais A. Guirigay and John C. Bancroft..... | 23 |
| A simple algorithm for the restoration of clipped GPR amplitudes | |
| Akshay Gulati and Robert J. Ferguson | 24 |
| Kaiser Bessel gridding kernel for seismic data regularization | |
| Akshay Gulati and Robert J. Ferguson | 25 |
| Near-field effects in VSP-based Q-estimation for an inhomogeneous model | |
| Arnim B. Haase and Robert R. Stewart | 26 |
| Spectral ratios for the Pembina Cardium formation computed with virtual sources | |
| Arnim B. Haase, Donald C. Lawton and Abdullah Alshuhail..... | 27 |
| Stratigraphic attenuation (Q) effects in heavy oilfield VSP data | |
| Arnim B. Haase and Robert R. Stewart | 28 |
| GPS accuracy part 2: RTK float versus RTK fixed | |
| Kevin W. Hall, Peter Gagliardi and Don C. Lawton..... | 29 |
| Priddis low-frequency seismometer test, part 2 | |
| Kevin W. Hall, Malcolm B. Bertram, Gary F. Margrave, and Dave W. Eaton | 30 |

| | |
|--|----|
| Back-propagation analysis for hypocenter location Lejia Han, John C. Bancroft, and Joe Wong..... | 31 |
| The nearest approach to multiple lines in n-dimensional space Lejia Han and John C. Bancroft..... | 32 |
| Pattern-search inversion for hypocenter location Lejia Han, Joe Wong, and John C. Bancroft..... | 33 |
| Earthtones: nonstationary colour correction in ProMAX David C. Henley, Peng Cheng, and Gary F. Margrave..... | 34 |
| Raypath interferometry for dummies: a processing guide David C. Henley..... | 35 |
| Recent ProMAX module upgrades David C. Henley and Kevin W. Hall..... | 36 |
| Integrated well-log, VSP, and surface seismic analysis of near-surface glacial sediments: Red Lodge, Montana Jingqiu Huang, Robert R. Stewart, Joe Wong, and Carlos Montana..... | 37 |
| A particle/collision model of seismic data Kris Innanen..... | 38 |
| A theoretical note on scattering and diffraction of radar waves from a seismic disturbance propagating in the near-surface Kris Innanen..... | 39 |
| An acoustic description of nonlinearity in seismic exploration Kris Innanen..... | 40 |
| Decomposition of acoustic and elastic RP into contributions from one-parameter reflection coefficients Kris Innanen..... | 41 |
| Determination of time-lapse perturbations directly from differenced seismic reflection data Kris Innanen* and Mostafa Naghizadeh..... | 42 |
| More absorptive AVF inversion - attenuating incidence media and general dispersion laws Kris Innanen..... | 43 |
| Towards an analytic description of anelastic diffraction, reflection, and conversion phenomena Kris Innanen..... | 44 |
| Physical modelling of a 3D marine seismic survey J. Helen Isaac, Joe Wong and Kevin W. Hall..... | 45 |
| Integrated geological and seismic site characterization at Priddis, Alberta J. Helen Isaac and Don. C. Lawton*..... | 46 |

| | |
|--|----|
| Processing of the 2010 field school 3D and 2D seismic data from Priddis, Alberta J. Helen Isaac* and Don C. Lawton | 47 |
| Reverse-time migration imaging with/without multiples Zaiming Jiang*, John C. Bancroft, and Laurence R. Lines | 48 |
| Rigid boundary conditions for staggered-grid modelling Zaiming Jiang, John C. Bancroft, and Laurence R. Lines..... | 49 |
| Comparison of three Kirchhoff integral formulas for true amplitude inversion Hassan Khaniani, Gary F. Margrave and John C. Bancroft..... | 50 |
| Determination of velocity smoothing operator for prestack Kirchhoff depth migration by Common Scatter Point Gathers Hassan Khaniani and John C. Bancroft | 51 |
| Enhancement of velocity field estimation by Common Scatter Point Gathers Hassan Khaniani* and John C. Bancroft..... | 52 |
| Decomposition of surface consistent statics Steve Kim and John C. Bancroft..... | 53 |
| Gabor multipliers for pseudodifferential operators and wavefield propagators Michael P. Lamoureux*, Gary F. Margrave, and Peter C. Gibson | 54 |
| Fluid substitution in coalbeds Diane J. Lespinasse* and Robert J. Ferguson | 55 |
| The robustness of reverse-time migration for imaging noisy sparse foothills data Laurence R. Lines and P.F. Daley | 56 |
| CREWES channel model: description, acquisition, interpretation and data release Heather J.E. Lloyd and Gary F. Margrave | 57 |
| New MATLAB functions for reading, writing and modifying SEG-Y files Heather J.E. Lloyd, Kevin W. Hall and Gary F. Margrave..... | 58 |
| Evaluation of ice-coupled and elevated GPR antenna acquisition on ice Tyler MacFarlane and Robert J. Ferguson | 59 |
| Determining elastic constants of an orthorhombic material by physical seismic modeling Faranak Mahmoudian*, Gary F. Margrave, P. F. Daley, Joe Wong, and Eric Gallant..... | 60 |
| 2D finite-difference modeling in Matlab, version 1 Peter M. Manning..... | 61 |
| Correction filter use in finite-difference elastic modeling Peter M. Manning..... | 62 |
| Full waveform inversion with wave equation migration and well control Gary F. Margrave*, Robert J. Ferguson and Chad M. Hogan | 63 |
| Nodal Galerkin methods for numerical modelling of linear elasticity Matthew A. McDonald*, Michael P. Lamoureux and Gary F. Margrave | 64 |

| | |
|--|----|
| A least-squares shot-profile application of time-lapse inverse scattering theory Mostafa Naghizadeh and Kris Innanen..... | 65 |
| Seismic data interpolation using a fast generalized Fourier transform Mostafa Naghizadeh* and Kris Innanen | 66 |
| Azimuthal anisotropy of Hudson Bay using seismic interferometry Agnieszka Pawlak and David W. Eaton..... | 67 |
| Picking microseismic first arrival times by Kalman filter and wavelet transform Baolin Qiao and John C. Bancroft..... | 68 |
| Characterization of lava tubes using ground penetrating radar at Craters of the Moon National Monument, USA. Colin R. Rowell, Adam Pidlisecky, James D. Irving, and Robert J. Ferguson | 69 |
| Iteratively re-weighted least squares inversion for the estimation of density from well logs: part one A. Nassir Saeed, Laurence R. Lines, and Gary F. Margrave..... | 70 |
| Iteratively re-weighted least squares inversion for the estimation of density from well logs: part two A. Nassir Saeed, Laurence R. Lines, and Gary F. Margrave..... | 71 |
| Mud-rock line estimation via robust locally weighted scattering smoothing method A. Nassir Saeed, Laurence R. Lines, and Gary F. Margrave..... | 72 |
| Time-lapse AVO inversion: model building and AVA analysis A. Nassir Saeed, Laurence R. Lines, and Gary F. Margrave..... | 73 |
| 9C-3D seismic modelling for VTI media R. K. Sharma and R. J. Ferguson..... | 74 |
| Phase-shift modelling for HTI media R. K. Sharma and R. J. Ferguson..... | 75 |
| Reflection and Transmission coefficient for VTI media R. K. Sharma and R. J. Ferguson..... | 76 |
| Seismic interpretation of the Redwater Leduc Reef, Alberta Taher M. Sodagar and Dr. Don C. Lawton | 77 |
| Time-lapse of multi-component seismic modeling of CO₂ fluid replacement in Redwater Leduc Reef, Alberta Taher M. Sodagar* and Don C. Lawton..... | 78 |
| An assessment of natural and man-made vibrations in Lake Kivu, Rwanda Robert R. Stewart | 79 |
| CDP noise attenuation using local linear models Todor I. Todorov and Gary F. Margrave | 80 |
| The seismic quest for estimating heavy oil viscosity Fereidoon Vasheghani and Laurence R. Lines* | 81 |

| | |
|--|----|
| Fluid substitution and seismic modelling in a sandstone aquifer | |
| Virginia C. Vera* and Don C. Lawton..... | 82 |
| Conventional and non-conventional seismic differencing in time-lapse | |
| Vanja Vracar and Dr. Robert J. Ferguson..... | 83 |
| Reverse time migration in anisotropic media | |
| Ben D. Wards*, Richard Bale, Gary F. Margrave and Michael P. | 84 |
| Asymptotic complexity of inverse nonstationary phase shift | |
| Marcus R. Wilson and Robert J. Ferguson..... | 85 |
| Automatic band limited signal reconstruction | |
| Marcus Wilson, Akshay Gulati and Robert J. Ferguson | 86 |
| Implicit and explicit preconditioning for least-squares nonstationary phase shift | |
| Marcus R. Wilson and Robert J. Ferguson..... | 87 |
| Fermat’s principle and ray tracing in anisotropic layered media | |
| Joe Wong..... | 88 |
| Seismic physical modeling measurements on solid surfaces | |
| Joe Wong, Faranak Mahmoudian, Eric Gallant, and Malcolm Bertram | 89 |
| Synthetic microseismic datasets | |
| Joe Wong* and Peter M. Manning..... | 90 |
| Tutorial on the continuous and discrete adjoint state method and basic implementation | |
| Matthew J. Yedlin*, Daryl G. Van Vorst..... | 91 |
| Feasibility of solving least squares Gazdag migration using method of multigrid. | |
| Abdolnaser Yousefzadeh* and John C. Bancroft..... | 92 |
| A multiple model and Padé approximation | |
| Dali Zhang, Michael P. Lamoureux, and Gary F. Margrave..... | 93 |
| AVO processing of walkaway VSP data at the Ross Lake heavy oilfield, Saskatchewan | |
| Zimin Zhang, Robert R. Stewart, and Don C. Lawton..... | 94 |
| Detecting fractures using time-lapse 3C-3D seismic data | |
| Zimin Zhang*, Don C. Lawton and Robert R. Stewart | 95 |
| Estimating seismic attenuation (Qp & Qs) from rock properties | |
| Zimin Zhang, Robert R. Stewart, and Don C. Lawton..... | 96 |
| P-S survey design | |
| Liliana M. Zuleta and Don C. Lawton..... | 97 |

2010 CREWES Sponsors

| | |
|--|--|
| BHP Billiton Petroleum | INOVA Geophysical Equipment Limited |
| BP p.l.c. | Landmark Graphics Corporation |
| CGGVeritas | Marathon Oil Corporation |
| Chevron Corporation | Nexen Inc. |
| ConocoPhillips | Penn West Energy Trust |
| Devon Canada Corporation | Petrobras |
| Encana Corporation | Saudi Aramco |
| Eni S.p.A. | Sensor Geophysical Ltd. |
| Exxon Mobil Corporation | Shell Canada |
| GDF Suez E&P Deutschland GmbH | Statoil ASA |
| Geoprosesados SA de CV | Talisman Energy Inc. |
| Geophysical Exploration & Development Corporation (GEDCO) | Tullow Oil p.l.c. |
| Husky Energy Inc. | WesternGeco |

Natural Sciences and Engineering Research Council of Canada (NSERC)
- Collaborative Research and Development Grant

CREWES Personnel

DIRECTORS

Gary F. Margrave

Professor, Department of Geoscience, University of Calgary

B.Sc. Physics, 1975, University of Utah

M.Sc. Physics, 1977, University of Utah

Ph.D. Geophysics, 1981, University of Alberta

- Work Experience: Chevron Canada Resources, Chevron Geoscience Company

Don C. Lawton

Professor, Department of Geoscience, University of Calgary

B.Sc. (Hons. Class I) Geology, 1973, University of Auckland

Ph.D. Geophysics, 1979, University of Auckland

- Work Experience: New Zealand Steel Mining Ltd., Amoco Minerals (N.Z.) Ltd.

Robert J. Ferguson

Associate Professor, Department of Geoscience, University of Calgary

B.Sc. Geophysics, 1989, University of British Columbia

M.Sc. Geophysics, 1996, University of Calgary

Ph.D. Geophysics, 1999, University of Calgary

- Work Experience: Chevron Research, University of Texas at Austin

Laurence R. Lines

Professor, Department of Geoscience, University of Calgary

B.Sc. Physics, 1971, University of Alberta

M.Sc. Geophysics, 1973, University of Alberta

Ph.D. Geophysics, 1976, University of B.C.

- Work Experience: Amoco Production Research, Tulsa University, Memorial University of Newfoundland

Kristopher A. Innanen

Associate Professor, Department of Geoscience, University of Calgary

B.Sc. Physics and Earth Science, 1996, York University

M.Sc. Physics, 1998, York University

Ph.D. Geophysics, 2003, University of British Columbia

- Work Experience: University of Houston

David W. Eaton

Department Head, Professor, Department of Geoscience, University of Calgary

B.Sc. Geology and Physics, 1984, Queen's University

M.Sc. Geophysics, 1988, University of Calgary

Ph.D. Geophysics, 1993, University of Calgary

- Work Experience: Arco Exploration and Production Research Centre, Geological Survey of Canada, University of Western Ontario

Robert R. Stewart

Cullen Chair in Exploration Geophysics, University of Houston
Adjunct Professor, Department of Geoscience, University of Calgary

B.Sc. Physics and Mathematics, 1978, University of Toronto

Ph.D. Geophysics, 1983, Massachusetts Institute of Technology

- Work Experience: Arco Exploration and Production Research Centre, Chevron Geoscience Company, Veritas Software Ltd., Gennix Technology Corp., University of Calgary

ASSOCIATED FACULTY

John C. Bancroft

Adjunct Professor, Department of Geoscience, University of Calgary

B.Sc. Electrical Engineering, 1970, University of Calgary

M.Sc. Electrical Engineering, 1972, University of Calgary

Ph.D. Electrical Engineering, 1975, Brigham Young University

- Work Experience: Geo-X Systems Ltd., Veritas Software Ltd., Ulterra Geoscience Ltd.

Michael P. Lamoureux

Professor, Department of Mathematics and Statistics, University of Calgary

Adjunct Professor, Department of Geoscience, University of Calgary

B.Sc. Mathematics, 1982, University of Alberta

M.Sc. Mathematics, 1983, Stanford University

Ph.D. Mathematics, 1988, University of California, Berkeley

- Work Experience: Farallon Computing, NSERC Canada

Brian H. Russell

Adjunct Professor, Department of Geoscience, University of Calgary

B.Sc. Physics, 1972, University of Saskatchewan

Honours Certificate in Geophysics, 1975, University of Saskatchewan

M.Sc., Geophysics, 1978, University of Durham

Ph.D., Geophysics, 2004, University of Calgary

- Work Experience: Chevron Geoscience Company, Teknica Resource Development, Veritas Software Ltd., Hampson-Russell Software Ltd.

Matt Yedlin

Associate Professor, Department of Electrical and Computer Engineering, University of British Columbia

B.Sc. Honors Physics, 1971, University of Alberta

M.Sc. Physiology, 1973, University of Toronto

Ph.D. Geophysics, 1978, University of British Columbia

- Work Experience: Conoco

RESEARCH AND ADMINISTRATION STAFF

Laura Baird

BA, History, 1992, University of Calgary

- Work Experience: Tom Baker Cancer Centre, University of Calgary

Kevin L. Bertram

Electronics Technician Certificate, 2005, Southern Alberta Institute of Technology

- Work Experience: Aram Systems Ltd.

Malcolm B. Bertram

B.Sc. Geology, Auckland, New Zealand

- Work Experience: Allied Minerals NL (Western Australia), GSI (Western Australia), Western Geophysics (Western Australia), Auckland University, University of Calgary

Patrick F. Daley

B.Sc. Mathematics, 1974, University of Alberta

M.Sc. Physics 1976, University of Alberta

Ph.D. Geophysics, 1979, University of Alberta

- Work Experience: Independent contractor associated with research centres of major oil companies

Eric V. Gallant

Journeyman Interprovincial Ticket in Electrical Construction, 1976, Cape Breton Institute of Technology

- Work Experience: IBEW, University of Calgary

Arnim B. Haase

Diplom Ingenieur, 1966, Technische Hochschule Ilmenau, East Germany

M.Sc. Electrical Engineering, 1973, University of Calgary

Ph.D. Electrical Engineering, 1976, University of Calgary

- Work Experience: Sefel Geophysical Ltd., Philips New Zealand Ltd., Geo-X Systems Ltd.

Kevin W. Hall

B.Sc. Geophysics, 1992, University of Calgary

M.Sc. Geophysics, 1996, University of Calgary

- Work Experience: Lithoprobe Seismic Processing Facility, University of Calgary

David C. Henley

B.Sc. Physics, 1967, Colorado State University

M.Sc. Physics, 1968, University of Michigan

- Work Experience: Shell Oil Co., Shell Canada Ltd

Helen Isaac

B.Sc. Mathematics, 1973, Imperial College, London

M.Sc. Geophysics, 1974, Imperial College, London

Ph.D. Geophysics, 1996, University of Calgary

- Work Experience: Phillips Petroleum, Hudson's Bay Oil and Gas, Canterra Energy, Husky, Fold-Fault Research Project

Han-xing Lu

B.Sc. (equivalent) Physics, 1967, Fu Dan University, Shanghai, China

M.Sc. Geophysics, 1982, Chinese Academy of Sciences and Institute of Geophysics

- Work Experience: Institute of Geophysics, Beijing, China, Memorial University of Newfoundland

Rolf Maier

B.Sc. Chemical Engineering, 1978, Technikum Winterthur, ZH, Switzerland

M.Sc. Physical Chemistry, 1984, University of Calgary

Ph.D. Physical Chemistry, 1988, University of Calgary

- Work Experience: Lithoprobe Seismic Processing Facility, University of Calgary

Peter M. Manning

B.Sc. Mathematics, 1961, University of British Columbia

Ph.D. Geophysics, 2007, University of Calgary

- Work Experience: Mobil Oil Canada

Mostafa Naghizadeh

B.Sc. Mining Engineering, 2000, University of Shahid Bahonar, Kerman, Iran

M.Sc. Geophysics, 2003, University of Tehran, Tehran, Iran

Ph.D. Geophysics, 2009, University of Alberta

- Work Experience: University of Alberta, CGGVeritas

Joe Wong

B.Sc. Physics/Mathematics, 1971, Queen's University

M.Sc. Applied Geophysics, 1973, University of Toronto

Ph.D. Applied Geophysics, 1979, University of Toronto

- Work Experience: Ontario Ministry of the Environment, University of Toronto, JODEX Applied Geoscience Limited

GRADUATE STUDENTS

Mahdi Almutlaq

B.Sc. Exploration Geophysics, 1998, Boise State University

M.Sc. Geophysics, 2007, King Fahd University of Petroleum and Minerals

- Work Experience: Saudi Aramco, South Rub Al-Khali Co.

Abdullah Al-Shuhail

- B.Sc. (3rd honour) Geophysics, 2001, King Fahd University
M.Sc. Geophysics, 2006, University of Calgary
- Work Experience: Saudi Aramco

Abdallah Al Zaharani

- B.Sc. Geophysics, 2000, King Fahd University of Petroleum and Minerals
- Work Experience: Saudi Aramco

Joaquin Aristimuno

- M.Sc. Geophysics, Universidad Simon Bolivar
- Work Experience: Imperial Oil – Esso

Jessie Arthur

- B.Sc., Geophysics, 2003, University of Alberta
- Work Experience: Hampson-Russell Reservoir Characterization Services

Roohollah Askari

- B.Sc. Applied Physics, 2002, University of Hormozgan
M.Sc. Geophysics, 2005, University of Tehran
- Work Experience: Institute for Advanced Studies in Basic Sciences, Zanjan, Iran

Christopher Bird

- B.Sc. Geophysics, 2007, University of Saskatchewan
- Work Experience: Husky Energy

Peng Cheng

- B.Sc. Applied Geophysics, 2001, Jilin University, China
M.Sc. Electrical Engineering, 2005, Peking University
- Work Experience: VIA Technologies (China) Inc.

David Cho

- B.Sc. Physics, 2007, University of Calgary
B.Sc. Geophysics, 2007, University of Calgary
- Work experience: Schlumberger, Reservoir Seismic Services, Calgary

Jean Cui

- B.Sc. Geophysics, 1998, Petroleum University
M.sc. Geophysics, 2005, China University of Mining & Technology
- Work experience: CGGveritas Canada

Farshid Forouhideh

- B.Eng. Civil Engineering, Azad University, Central Tehran Campus, Iran
B.Sc. Geophysics, University of Western Ontario

Peter Gagliardi

B.Sc. Geophysics, 2010, University of Calgary

- Work Experience: Talisman Energy

Saul Guevara

B.Eng. Civil Engineering, 1984, National University of Colombia

M.Sc. Geophysics, 2001, University of Calgary

- Work Experience: Ecopetrol ICP

Thais Guirigay

B.Sc. Geophysics, 1994, Universidad Simon Bolivar

M.Sc. Geology, 2001, Colorado School of Mines

- Work Experience: National Oil Company (Venezuela), Geotrace (Houston)

Akshay Gulati

B. Eng. Civil Engineering, 2006, Nagpur University

- Work Experience: Indian Institute of Technology in Mubabi

Lejia (Lilly) Han

B.Sc. Applied Geophysics, 1989, Chengdu University of Technology

B.Sc. Computer Science, 2000, McGill University

- Galdos Systems Inc.

Melissa Hernández

B.Sc. Geophysical Engineering, 2006, Simon Bolivar University, Venezuela

Chad Hogan

B.Sc. Physics/Math, 2000, University of Victoria

- Work Experience: CGGVeritas

Hormoz Izadi

B.Sc. Applied Mathematics, 2010, University of Calgary

Zaiming Jiang

B. Eng., Geology, 1992, Northeast Institute of Technology

M. Eng., Communications & Electronics, 1998, Northeastern University

- Work Experience: Neusoft Group Shenyang Business Software Company

Byron Kelly

B.Sc. Geophysics, 2010, Memorial University of Newfoundland

Hassan Khaniani

B.Sc. Petroleum Exploration Engineering, 2003, Petroleum University of Technology

M.Sc. Petroleum Exploration Engineering, 2006, University of Calgary & Petroleum University of Technology

- Work Experience: National Iranian Oil Company, Terras Persia Seismic Company (TPS)

Steve Kim

B.Sc. Geophysics, 2010, University of Calgary

Diane Lespinasse

B.Sc. Geophysical Engineering, Universidad Simon Bolivar, Venezuela

Oliver Lahr

B.Sc. Pure and Applied Mathematics, 1988, University of Calgary

- Work Experience: Hampson-Russell Software Ltd.

Xinxiang Li

B.Sc. Mathematics, 1987, Peking University, China

M.Sc. Applied Mathematics, 1989, Tsinghua University, China

M.Sc. Geophysics, 1999, University of Calgary

- Work Experience: Sensor Geophysical Ltd.

Heather Lloyd

Diploma in Fashion Design and Technology, 2004, Kwantlen Polytechnic University

B.Sc. Geology, 2010, University of Calgary

B.Sc. Geophysics, 2010, University of Calgary

Li Lu

BSc., Geophysics, 1989, Daqing Petroleum University, China

- Work experience: CGGVeritas, Canada

Tyler MacFarlane

B.Sc. Hons. 2010, Geophysics, University of Calgary

- Work experience: Enerplus

Faranak Mahmoudian

B.Sc. Applied Physics, 2000, Khage Nassir Toosi University

M.Sc. Geophysics, 2006, University of Calgary

- Work Experience: Shell Canada

Matt McDonald

B.Sc. Hons. Applied Mathematics, 2010, University of Calgary

- MMC Construction

Carlos Montaña

B.Sc. Mechanical Engineering, 1995, Universidad Industrial de Santander

- Work History: Geophysical Exploration and Development Corporation

E. Andrew Nicol

B.Sc. Hons. Geophysics, 2010, University of Western Ontario

- Work Experience: Sander Geophysics Limited

Lauren Ostridge

B.Sc. Geology and Biology, 2006, Acadia University

Agnieszka Pawlak

B.Sc. Applied Mathematics, 2007, University of Calgary

Baolin Qiao

- B.Sc. Geology and Ore Surveying, 1992, Northeastern University, China
M.Sc., 1999, Geology and Ore Surveying, Northeastern University, China
- Work Experience: China Geological Survey Centre, Shenyang Institute of Aeronautical Engineering

Colin Rowell

- B.Sc. Geophysics, 2011, University of Calgary
- Work experience: PetroCanada

A.-Nassir Saeed

- B.Sc. Geology, 1991, University of Salahaddin
M.Sc. Geophysics, 1998, University of Science Malaysia
- Work Experience: National Building Company (Libya), University of Sciences and National University of Malaysia

Ritesh Kumar Sharma

- B.Sc. 2004, Choudhary Charan Singh University Meerut, India
M.Sc. Applied Geophysics, 2007, Indian Institute of Technology Roorkee, India
- Work Experience: Vedanta Group

Taher Sodagar

- B.Sc. Geophysics, 1994, King AbdulAziz University
M.Sc. Geology (Geophysics), 2002, University of New Orleans
- Work Experience: Saudi Aramco

Todor Todorov

- B.Sc. Exploration Geophysics, 1994, University of Mining and Geology, Bulgaria
M.Sc. Geophysics, 2000, University of Calgary
- Work Experience: Hampson-Russell Software Ltd., Microtech Computer Systems Ltd., Hampson-Russell Software, Petro-Canada Resources

Virginia Vera

- B.Sc. Geophysical Engineering, 2008, Universidad Simon Bolivar

Vanja Vracar

- B.Sc. Applied and Pure Mathematics, 2007, University of Calgary
- Work Experience: Shell Canada Ltd.

Ben Wards

- B.Sc. Hons. Applied and Pure Mathematics, 2003, University of Calgary
M.Sc. Applied and Pure Mathematics, 2005, University of Alberta

Marcus Wilson

- B.Sc. Hons. Pure and Applied Mathematics, 2006, University of Calgary

Abdolnaser Yousefzadeh

- B.Sc. 1997, Shahid Bahonar University
M.Sc. Geophysics, 2001, Institute of Geophysics, University of Tehran
M.Sc. Geophysics, University of Alberta
- Work Experience: National Iranian Oil Company

Zimin Zhang

B.Sc. Geophysics, 1998, Changchun University of Science and Technology, China

M.Sc. Geophysics, 2005, China University of Petroleum

- Work Experience: China National Petroleum Corporation

Liliana Zuleta

B.Sc. in Petroleum Engineering, 1994, Universidad Nacional de Colombia

Specialization in Safety and Environmental (Major in Safety and Environmental concerns in Mining Activities), 2000, Ecole des Mines d'Als

Graduate Diploma in Geophysics, 2008, Curtin University of Technology

- Work Experience: Nexen Inc.

Student Theses

The following theses are included with the CREWES 2010 Research Report:

| | | |
|-------|------------------------|--|
| M.Sc. | Paul Fyfe Anderson | A Comparison of Inversion techniques for Estimating VP/VS from 3C3D Seismic Data |
| M.Sc. | Salman Bubshait | VSP processing for coal reflections |
| M.Sc. | Joanna Kathleen Cooper | Seismic acquisition footprint: modelling and mitigation |
| M.Sc. | Hussain Hammad | Waveform inversion for areas with complex near surface |
| Ph.D. | Zimin Zhang | Assessing attenuation, fractures, and anisotropy using logs, vertical seismic profile, and three-component seismic data: heavy oilfield and potash mining examples |

Towards a surface consistent match filter (SCMF) for time-lapse processing

Mahdi H. Almutlaq and Gary F. Margrave

SUMMARY

This paper presents a new idea for designing a match filter for processing time-lapse seismic data in a surface consistent manner. We extend the surface consistent data model to the case of designing matching filters to equalize two seismic surveys in the least-square sense. The frequency-domain surface-consistent design equations are similar to those for surface consistent deconvolution except that the data term is the spectral ratio of two surveys. To test this concept we have built a time-lapse synthetic dataset (baseline and monitor) whose subsurface (the reservoir) is unchanging but which show surface-consistent variability. Our synthetic dataset models acquisition over a simple stratigraphic reservoir in both summer and winter. Initial results are encouraging but suggest that our software is not yet optimal.

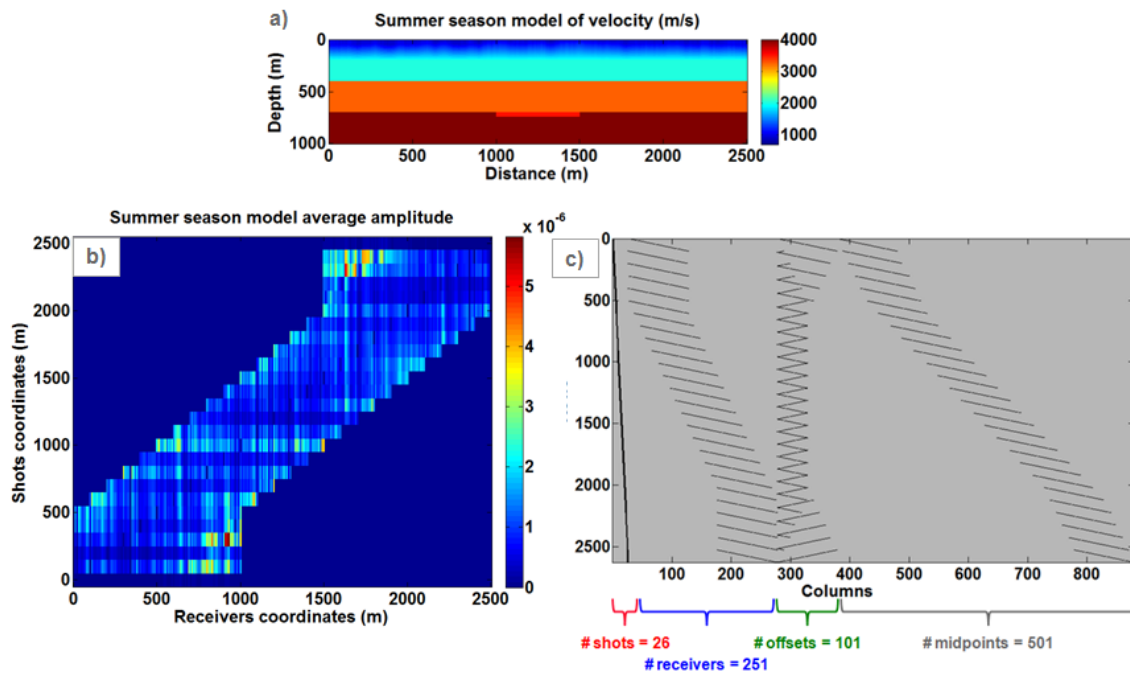


FIG. 1. a) Shows a simple four layer model with a reservoir unit between layers 3 and 4. The near-surface layer is complex with variable velocity in the x-axis. b) Illustrates the source and receiver surface consistent pattern on the extracted average amplitude from a time window around the middle reflector. c) The geometry matrix where the first 26 columns are for the shot positions, then there are 251 columns representing the receiver positions, followed by 101 columns for the offset positions, and finally there are 501 columns for the midpoint positions.

Tutorial: AVO inversion

Mahdi H. Almutlaq and Gary F. Margrave

SUMMARY

This literature review highlights most of the highly referenced work on amplitude variation with offset (AVO) from the past three decades. This review addresses some of the approximations made to the Zoeppritz equations, as well as AVO processing, AVO analysis and inversion. The purpose of this paper is not to provide details of the different AVO methods, but instead to register in chronological order the developments and briefly present the purpose and the outcome of each study. In some instances, we presented a comparison with other methods or listed advantages and disadvantages of one AVO process over the other.

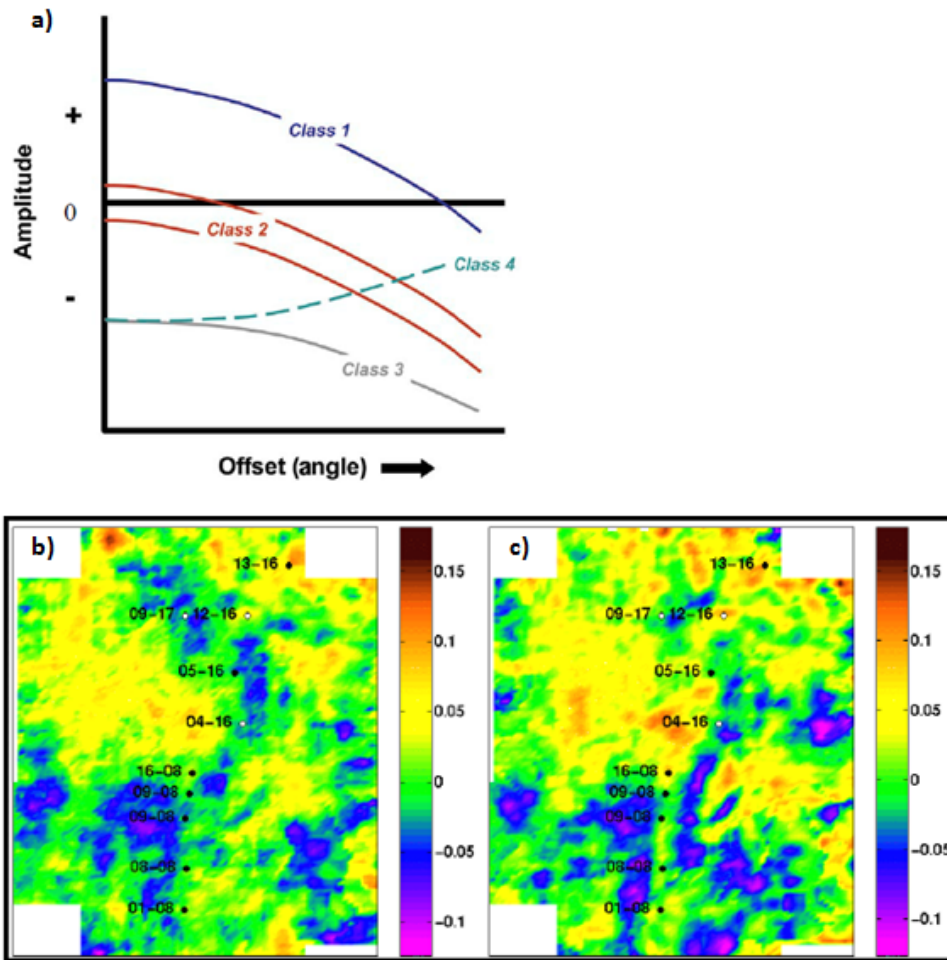


FIG. 1. a) Classification of AVO responses (previously discussed by Rutherford and Williams, 1989) with the addition of Class 4 by Castagna and Swan (1997). b) Weighted impedance reflectivity stacks for the P-P only (left) and simultaneous inversion methods (right) (Larsen, 1999).

Interpretation of 3D multicomponent seismic data for investigating natural fractures in the Horn River Basin, northeast British Columbia

Abdallah Al-Zahrani* and Don C. Lawton

SUMMARY

A 3D multicomponent seismic dataset from the Horn River Basin was assessed for mapping fractures. The data had good fold, offset and azimuth distributions and several approaches were used to interpret the distribution of natural fractures. In addition to amplitude mapping, PP and PS curvature maps enhanced the structural interpretation of the data and enabled the lateral continuity of faults and fractures to be mapped across the area of the seismic survey. Both horizon and volume based most negative curvature were effective in mapping fault and fracture trends within both Exshaw and Muskwa shale gas targets. At the Exshaw level, the curvature shows two main fault trends: northwest-southeast trending normal faults that dip toward the southwest, as well as northeast-southwest strike-slip faults. At the Muskwa level, the curvature image shows different major fault trends, namely north, northeast-south, southwest (normal and reverse faults), and northwest-southeast faults. Fractures interpreted using curvature attributes are close to the major faults and their dominant trends are generally parallel to the major faults in the area. Figure 1 shows a realization of fracture systems in the Muska Formation, based on negative curvature (PP data). Curvature attributes derived from the PS data were found to be contaminated by subtle artifacts from shallow channels in the survey area.

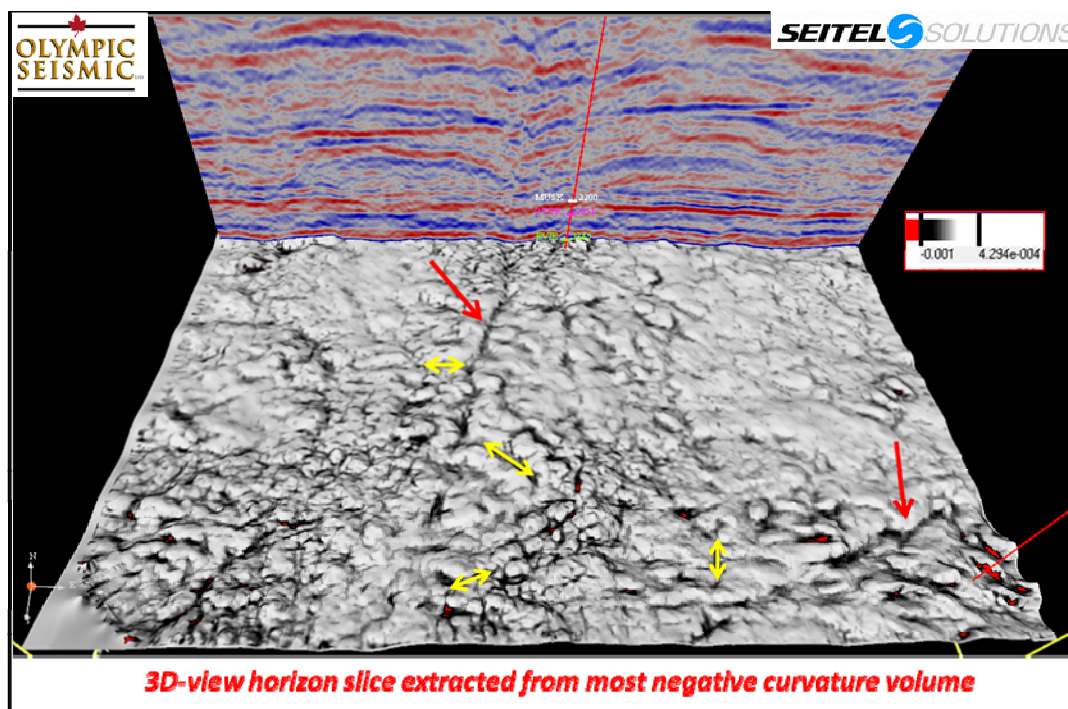


FIG. 1. Horizon-slice through the most negative curvature volume at the base of the Muskwa horizon shows the two major faults indicated by the red arrows and the four fracture trends in the area highlighted by the yellow arrows.

Dispersion and the dissipative characteristics of surface waves in the generalized S transform domain

Roohollah Askari*, Robert J. Ferguson

SUMMARY

Wave number, group velocity, phase velocity and frequency dependent attenuation characterize the propagation of surface waves in dispersive, attenuating media. Here, a mathematical model is developed based on the generalized S transform to simultaneously estimate these characteristic parameters of surface waves from a seismic record. We use a scaling factor in the generalized S transform to enable application of method in highly dispersive medium. We introduce a cost functions in the S domain to estimate an optimum value for the scaling factor. We also use the cost function to generalize the application of the method for noisy data, especially data with a low signal to noise ratio at low frequencies. In that case, experimentally we find that estimated wave number is perturbed. As a remedy, we estimate wave number perturbation by minimizing the cost function using Simulated Annealing. We present synthetic and real data to show the efficiency of the method for the estimation of the propagation parameters of highly dispersive and noisy media. We anticipate that, through inversion of the characteristic parameters of surface waves, near surface shear wave velocity will be obtainable.

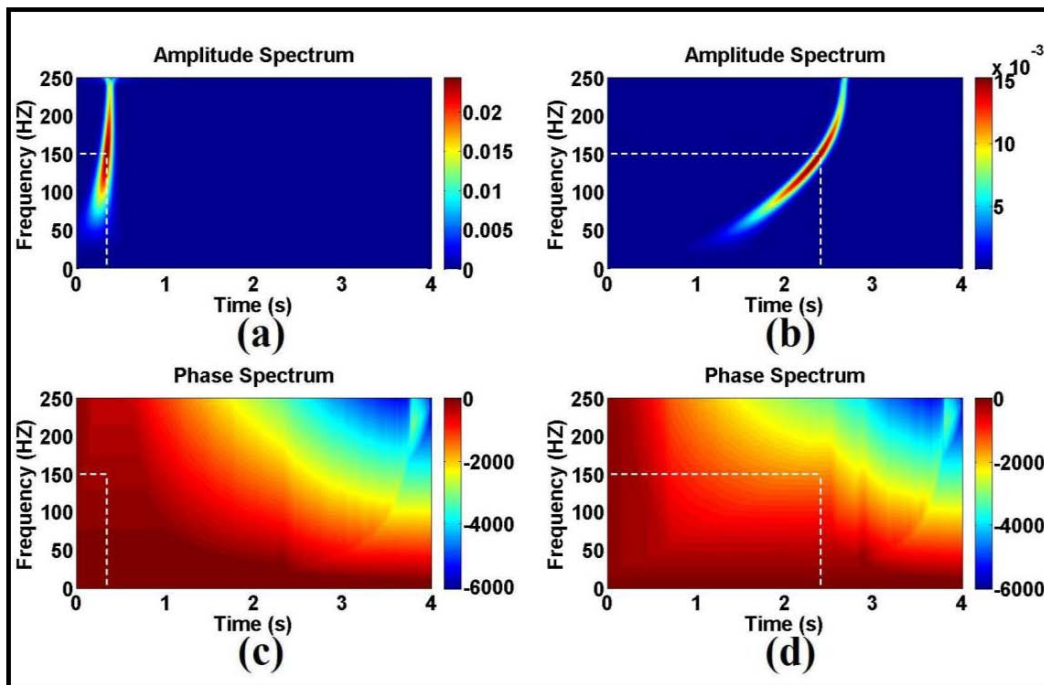


FIG. 1. (a) the amplitude spectra of the first station. (b) the amplitude spectra of the second station. (c) the phase spectra of the first station. And (d) the phase spectra of the second station. The dashed line show how time and phase information of the ridges is estimated.

A MATLAB version of Equivalent Offset Migration (EOM)

John C. Bancroft*

SUMMARY

Equivalent offset migration continues to be a viable method of prestack migration that is used in anisotropic prestack depth migrations, but is more commonly used in prestack time migrations. The continued interest has prompted further developments in a MATLAB computing environment. This version uses a script file (text) to define parameters. The input data are required to be in SEG-Y format that have been corrected to a horizontal datum, all statics applied, but with no moveout correction applied. The output is a SEG-Y file of CSP gathers and a stack based on the given velocities.

The development at this time includes P-wave prestack migration, with converted wave prestack migration to follow shortly.

The following images are from a synthetic numerical data set of an overthrust that has 86 source records, each with 201 traces, and 1251 sample per trace. The velocity model varied from 2815 to 3231 m/s, but only one velocity of 3000 m/s was used to form the CSP gathers. The following migration took approximately 10 minutes on a standard desktop computer.

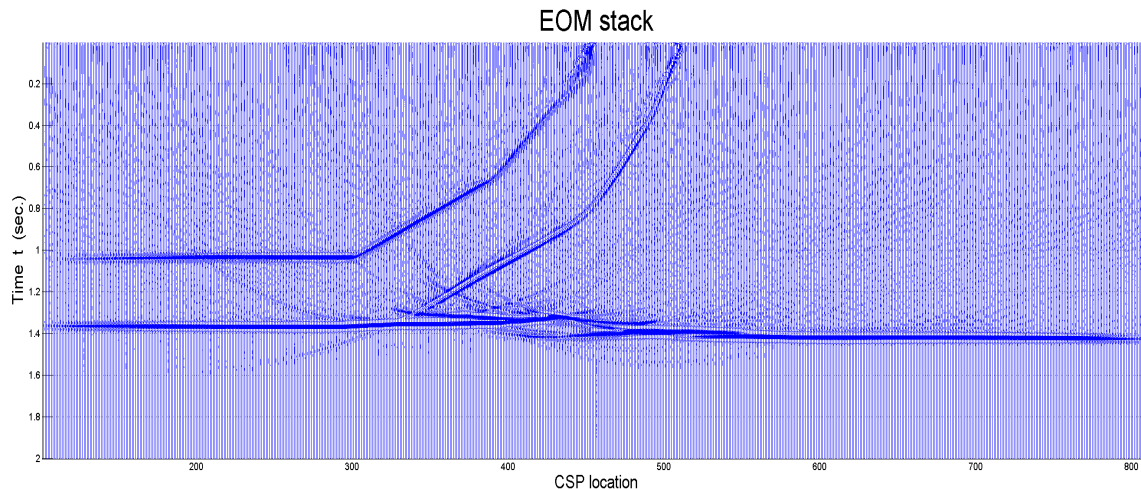


FIG. 1. Prestack time migration of numerically modelled data.

Investigating reflections from smooth transition boundaries

John C. Bancroft

SUMMARY

Reflections from impedance boundaries are well understood in many scientific applications including geophysics. These boundaries are typically assumed to be a step like function that reflects the energy of all frequencies, and are consistent with geological process. Reflections from boundaries with a smooth transition do not reflect all frequencies, and the purpose of this study is to evaluate the reflection energy from various reflector shapes.

The following figures are snapshots from movies of wavelets and chirps that start on the left, propagate to the right, interact with the boundary to produce transmitted and reflected energy. The velocity varies from $V_l = 1000$ m/s on the left to $V_r = 2000$ m/s on the right and the shape of the transition is shown by the red line. The reflection and transmission coefficients are $R = -1/3$, and $T = 2/3$.

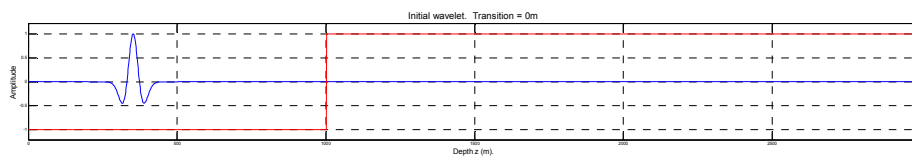


FIG. 1. Starting wavelet that is moving to the left towards the change in velocity.

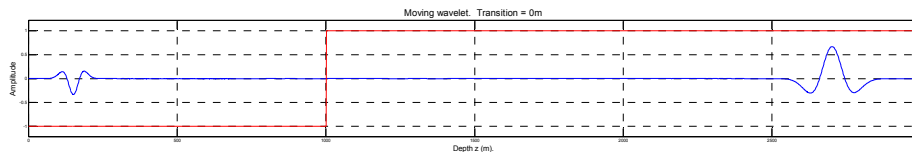


FIG. 2. Wavelets after encountering a step discontinuity. The transmitted wavelet is reaching the right side and the reflected wavelet reaching the left side. The amplitudes and phase are consistent with reflection and transmission coefficients.

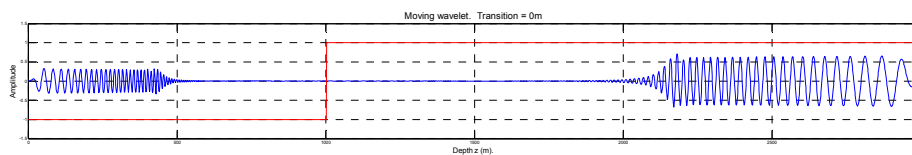


FIG. 3. A chirp after encountering a step discontinuity.

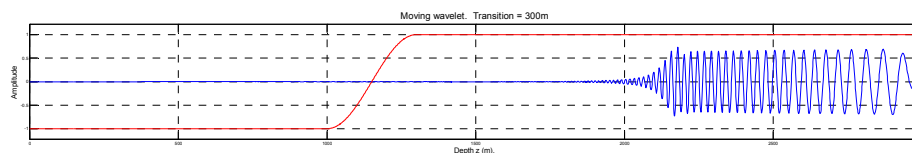


FIG. 4. A chirp after encountering a smooth discontinuity. All energy is transmitted with an amplitude equal to the square-root of the velocity ratio, i.e. $1/\sqrt{2}$.

Microseismic sensitivity for four receivers on a square grid

John C. Bancroft

SUMMARY

There are a number of analytic solutions for estimating the location of a microseismic event using the first arrival clock-times at three or four receivers. This paper evaluates the sensitivity of four receivers on a square grid with respect to jitter on the clock-times, errors in the location of the receivers, and error in the velocity. It is assumed that the four receivers will be part of a larger grid system on the surface.

INTRODUCTION

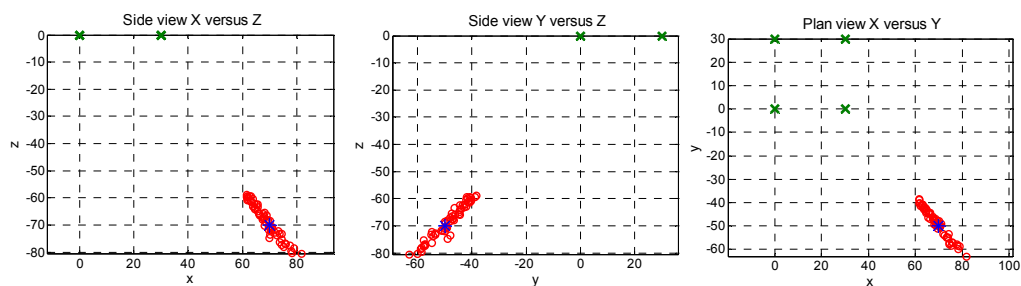


FIG. 1. Estimated locations when a jitter of 0.1 ms added to the clock-times of the receivers.

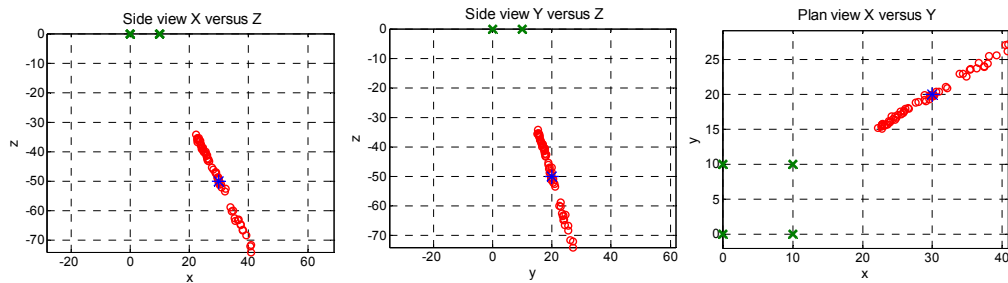


FIG. 2. Estimated locations when a random displacement is added to the location of each receiver. The side of the square is 10 m, and the SD of the displacements are, $\delta x = 0.1$, $\delta y = 0.1$, and $\delta z = 0.01$.

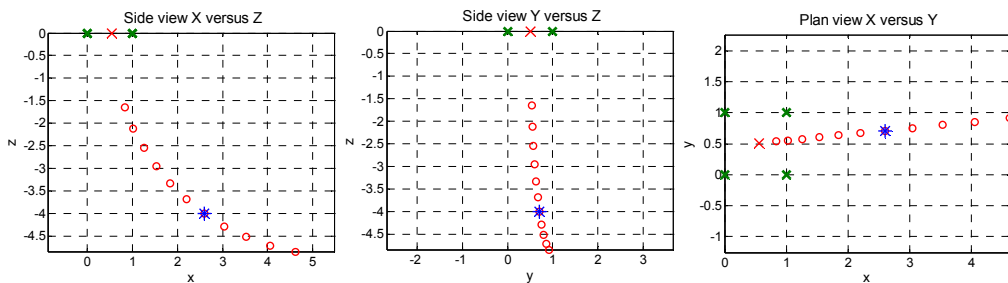


FIG. 3. Estimated locations when the velocity varies from 0.5V to 1.5V.

Recovery of low frequency data from 10 Hz geophones

Malcolm B. Bertram* and Gary F. Margrave

SUMMARY

The use of inverse filtering on the signal from 10Hz geophones to enhance frequencies below resonance is presented, together with a comparison of the enhanced data with that from low frequency receivers co-located with the 10Hz geophones to provide a calibration of the method. Data sets from the 1995 Blackfoot 3C-2D survey, the 2008 Spring Coulee survey, and the 2009 Priddis seismometer tests are used to test the effectiveness of the inverse filter. All three data sets show the method works well down to the frequency at which the noise floor becomes predominant.

A second order minimum phase Butterworth filter is designed in Matlab, a time-domain wavelet is created and inverted, then convolved with the data. By this method, information down to about two octaves below resonance is recovered. The comparison to data from the low frequency sensors shows the correction appears to be returning valid amplitudes.

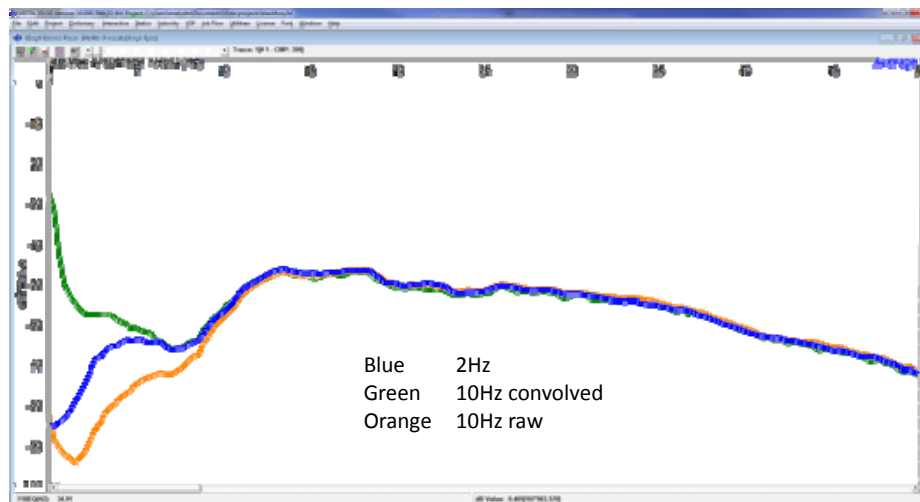


FIG 2. The average amplitude spectra of the Blackfoot data for the 2Hz geophones, the 10Hz geophones and the 10Hz geophones after convolving.

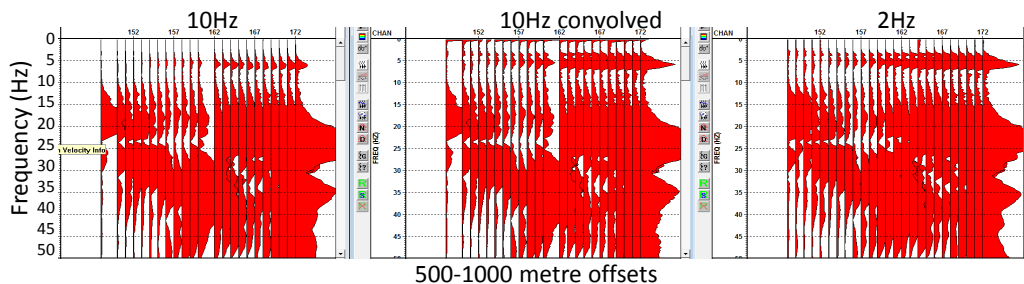


FIG 1. An example of spectra plots of one offset range for the Blackfoot data set showing the effects of the inverse filter. The high noise floor near DC is visible in the 10Hz convolved output, indicating the requirement for a low cut filter following the convolution.

Seismic acquisition projects 2010

Malcolm B. Bertram, Kevin L. Bertram, Kevin W. Hall, Eric V. Gallant

SUMMARY

Acquisition projects since the CREWES meeting in November 2009 include: a) a VSP test of a new downhole tool (developed by High-Definition Seismic Corporation) based on the Vectorseis MEMs sensor at the Priddis test site in the existing 130m deep well; b) a 3C-3D survey over the southern field at Priddis to further investigate locations for the planned injection well site for CO₂ sequestration; c) a test on the University of Calgary campus of the AWD thumper to quantify output versus band tension; d) the 2010 GOPH549 undergraduate Field School project which shot a 3C 2D line along a road allowance on the southern boundary of the Priddis test site, continuing west for a total length of 2.5 Km.

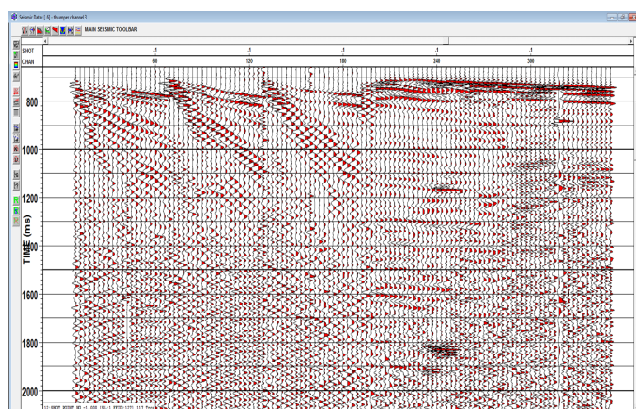


FIG. 1. December 2009 VSP

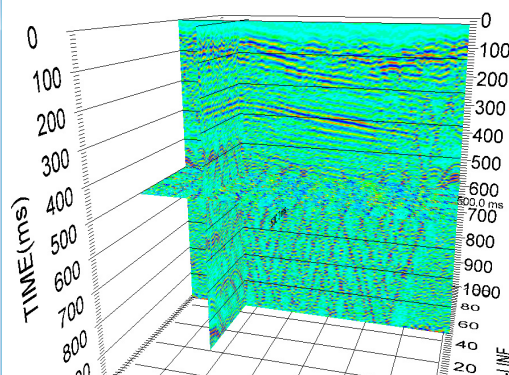


FIG. 2. May 2010 3C 3D survey at Priddis.

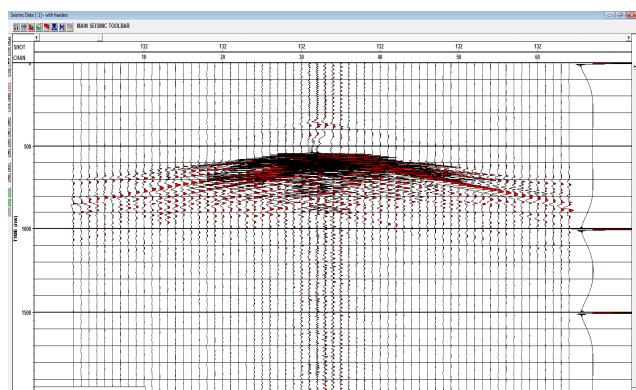


FIG. 3. August 2010 Thumper tests

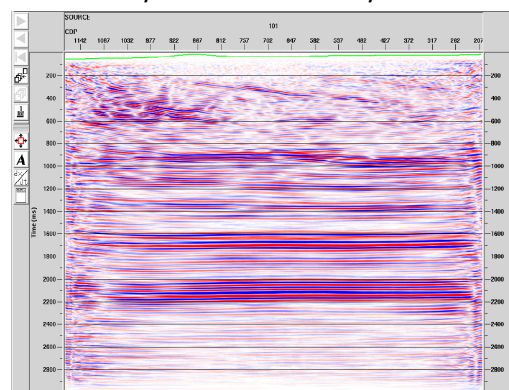


FIG. 4. August 2010 Field School line.

Amplitude calibration of a fast S-transform algorithm

Chris Bird, Mostafa Naghizadeh, Kristopher Innanen

SUMMARY

The S-transform is a time-frequency decomposition technique with a wide range of applications in seismic signal analysis but has been under-used due to the high computational cost needed to employ it. In this paper we present a fast, non-redundant S-transform (FST). The ability of the FST to provide high fidelity estimates of the amplitudes is tested in this paper. Where the FST cannot provide accurate estimates of amplitudes, we calibrate it by normalizing the unit impulse response of the algorithm. Due to the low resolution at low frequency nature of the FST algorithm, the spectra of individual events will interfere with each other at low frequencies and limit the ability of the FST to estimate amplitudes. We discuss the limits of the calibrated S-transform to estimate amplitudes and we propose a set of standards for the fidelity of estimated amplitudes as a function of proximity in time to other events.

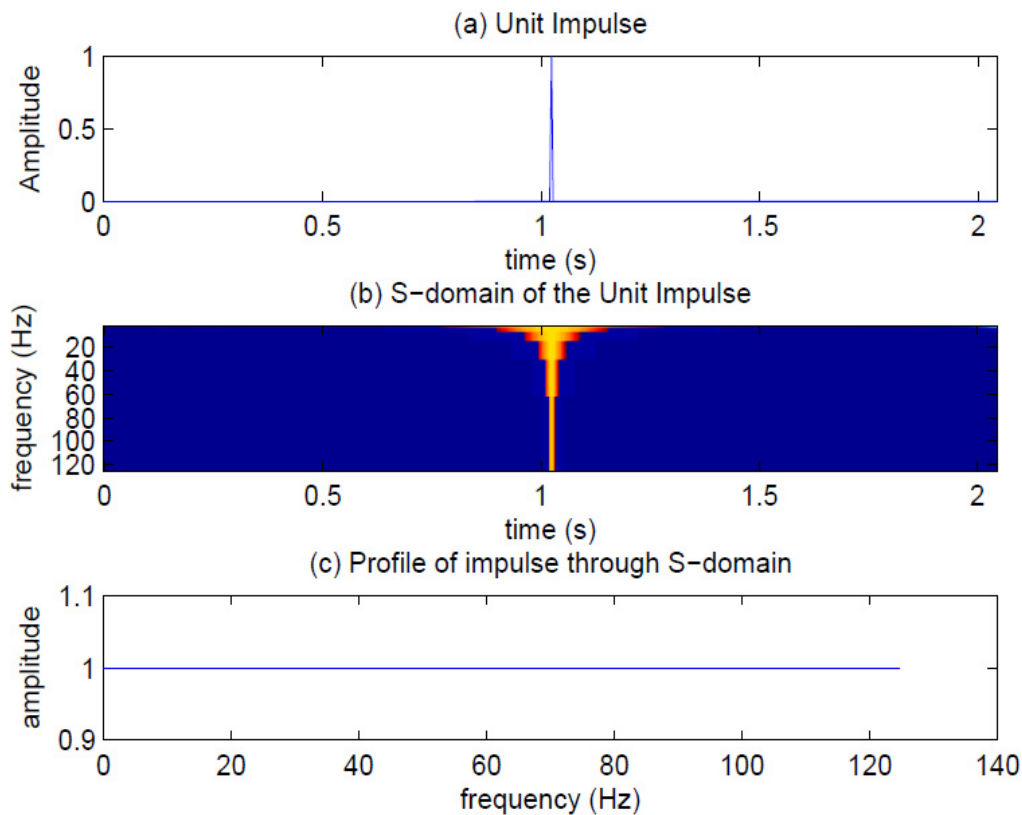


FIG. 1. Unit Impulse Response of the FST after calibration. In (a) we have a unit impulse which is plotted in time. In (b) the calibrated fast S-transform is carried out on the unit impulse identifying the location of the impulse and estimating its spectrum; and in (c) we see the amplitudes picked from the calibrated S-transform and observe the flat spectrum.

Determination of anelastic reflectivity: how to extract seismic AVF information

Chris Bird*, Kristopher Innanen, Larry Lines, Mostafa Naghizadeh

SUMMARY

Strongly dispersive reflection coefficients associated with highly absorptive, hydrocarbon charged targets, have been observed in seismic data. A frequency by frequency method (AVF) for determining Q of a highly absorptive target from measurements of the dispersive reflection coefficient is reviewed in this paper. In order to implement the AVF technique to invert for Q , it is necessary that we have a method of estimating the local spectrum of the reflection coefficient. We develop a method of implementing AVF inversion by using a calibrated, fast, non-redundant S-transform (FST) algorithm to estimate the local spectrum of dispersive reflection coefficients. We test the effectiveness of the FST for estimating the spectrum of reflection coefficients by comparing with the analytic reflection coefficient as calculated by a fast Fourier transform. Using forward modeling to generate synthetic traces for a single absorptive reflection coefficient we observe accurate results of the AVF inversion, using the FST, for a range of Q values.

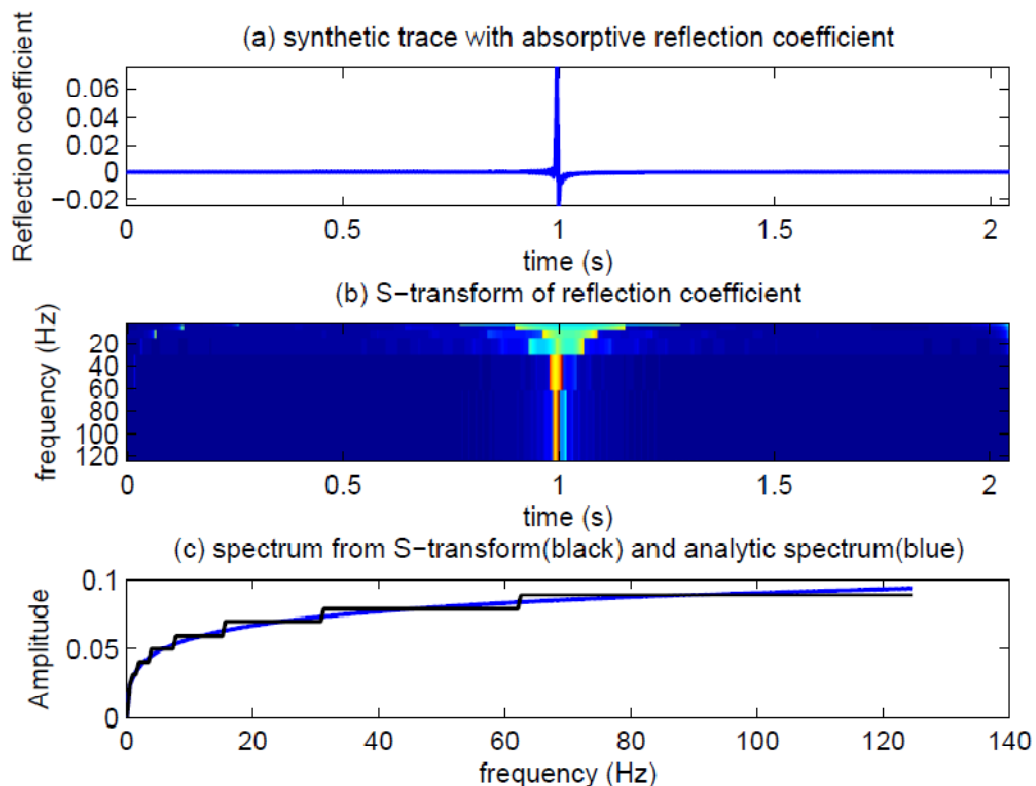


FIG. 1. How to extract a frequency-dependent reflection coefficient from a seismic trace. In (a) the single primary reflection generated by a contrast from acoustic to highly attenuative media is plotted in the time domain; in (b) the calibrated fast S-transform is carried out on the trace in (a), identifying the location of the event and estimating its spectrum; in (c) the amplitudes picked from the S-transform (in black) is compared with the analytic reflection coefficient (in blue).

Color correction for Gabor deconvolution: a test with 2D synthetic data and field data

Peng Cheng*, Gary F. Margrave and David C. Henley

SUMMARY

Conventional deconvolution algorithms usually assume that the spectrum of reflectivity is white. However, the amplitude spectrum of reflectivity calculated from a well log usually demonstrates obvious dependence on frequency, which is referred to as the color of the reflectivity. Consequently, the white reflectivity assumption can lead to distortion of the deconvolution result. A practical color correction method for Gabor deconvolution has been proposed and tested on a synthetic 1D seismic trace. This article tests the proposed color correction method using a synthetic shot record and real field data. Testing on the synthetic shot record shows that color correction gives a better reflectivity estimation than conventional Gabor deconvolution, and can be successfully applied to shot records. Results of processing field data demonstrate that the seismic data have higher resolution and a better tie to the well log data when color correction is applied.

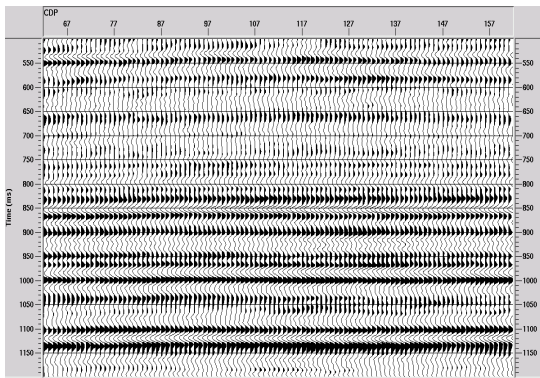


FIG. 1. Migrated seismic data with Gabor. Deconvolution.

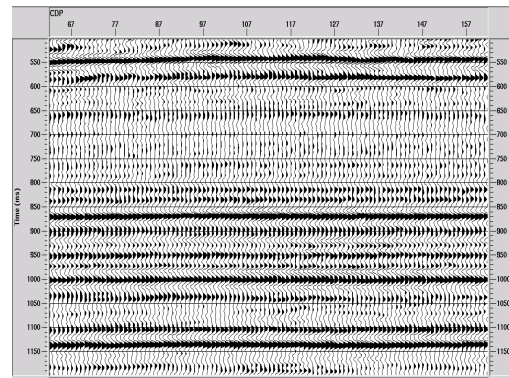


FIG. 2. Migrated seismic data with color correction.

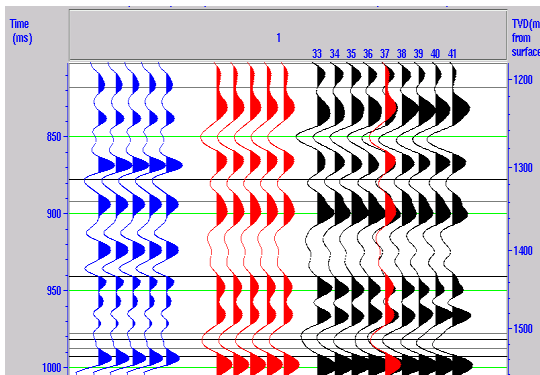


FIG. 3. Correlation of synthetic seismic trace and migrated seismic data with Gabor deconvolution. Blue: synthetic seismic trace; Red: migrated seismic trace with CDP 37, which has the same X coordinate with well location; Black: migrated seismic traces around CDP 37.

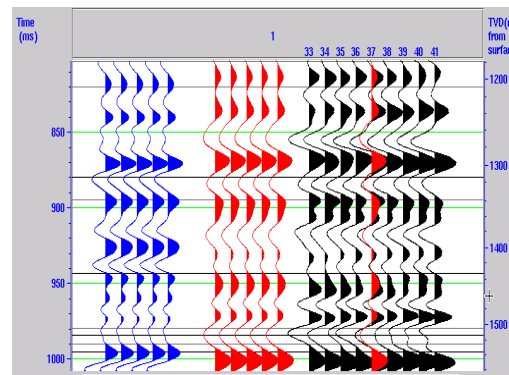


FIG. 4. Correlation of synthetic seismic trace and migrated seismic data with color correction. Blue: synthetic seismic trace; Red: migrated seismic trace with CDP 37 which has the same X coordinate with well location; Black: migrated seismic traces around CDP 37.

Estimation of elastic stiffness parameters in weakly anisotropic rotated HTI media

David Cho and Gary F. Margrave

SUMMARY

The presence of fractures and directional in-situ stress fields in the subsurface has profound implications for numerous geophysical and engineering applications. These phenomenon manifest as azimuthal variations in the seismic response and can be detected in the amplitudes of the scattered wavefield. Therefore, the study of the azimuthal amplitude variation with offset (AVO) can provide information regarding the fracturing or the stress state of the subsurface.

In this study, a transversely isotropic medium with a horizontal axis of symmetry (HTI) was used to model the presence of fractures and directional in-situ stress fields. Previous formulations of the reflections from HTI media invoke conditions that are often unrealistic in the natural world. Therefore, a more generic HTI reflection model was presented. This involves a transformation of the elastic stiffness matrix to represent an unknown symmetry axis azimuth where it is allowed to vary as a function of depth. In addition, we investigate the effect of dipping fracture sets and when the vertical stress is not equal to one of the principle stresses. It is shown that the corresponding reflection coefficients for a transformed HTI medium is capable of resolving the symmetry axis azimuth but lacks the complete set of parameters required to characterize the dipping fractures or when the vertical stress is not equal to one of the principle stresses. However, a different parameterization of the model space in the parameter estimation problem can provide an inference as to the presence of dipping fractures or a non-vertical principle stress component. These concepts are illustrated through a numerical example.

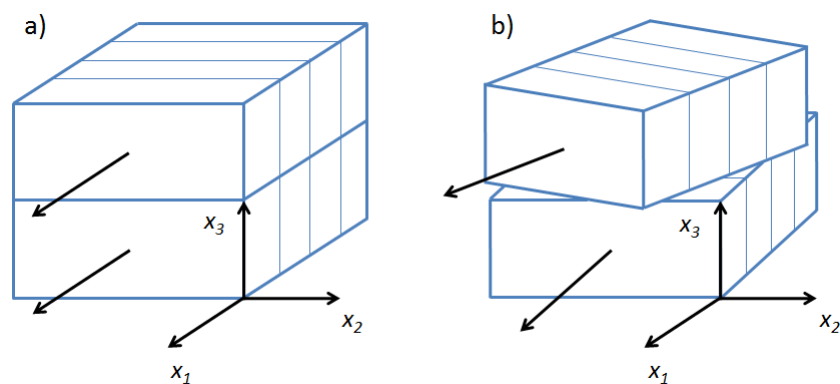


FIG. 4. HTI/HTI interface with a) similar symmetry axis orientations and b) arbitrary symmetry axis orientations.

Histograms of the Kirchhoff migration operator

James Close and John C. Bancroft

SUMMARY

Kirchhoff migration defines a diffraction shape at a scatterpoint location, then sums the recorded energy, identified by that shape, back to the scatterpoint. The process is repeated for all possible scatterpoints in the migration window. Energy that is tangential to the diffraction shape will constructively sum to produce a point of energy on a reflector. The diffraction will also cross events that are not tangential and this energy should sum to zero. However, if the crossed data is aliased relative to the dip of the diffraction, then this energy will not sum to zero but will create aliased energy on the migrated section, which will appear as noise.

Energy acquired along the diffraction may be displayed in the relative location of the diffraction. An examination of this energy is able to identify areas of extended tangential energy, and short porting of energy that are due to crossing non-tangential events. Identifying and using only tangential energy produces a section that can eliminate the aliased noise. Histograms of the diffraction energy aid in identifying the desired reflection energy.

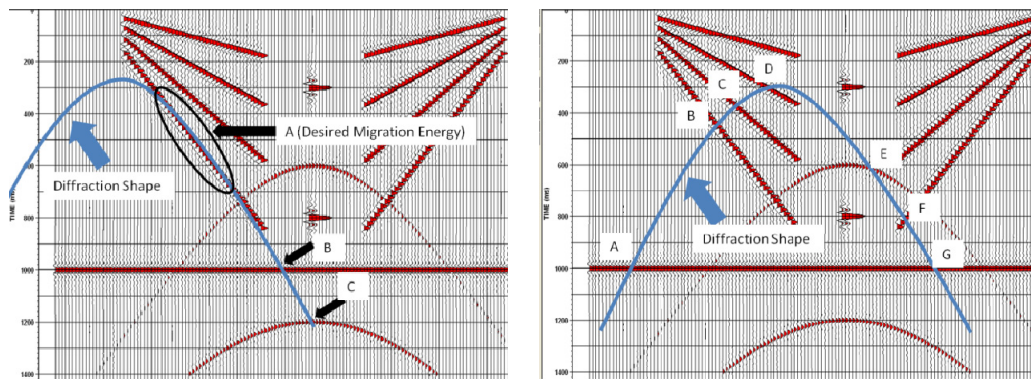


FIG. 1. Two diffractions in blue crossing tangential and non-tangential energy.

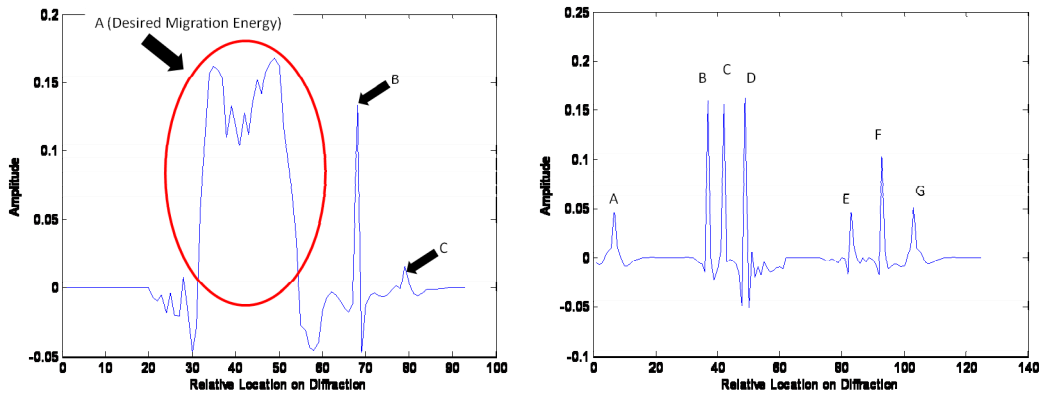


FIG. 2. Energy along the diffractions above, identifying the desired energy to be migrated along with aliased energy.

A comparison of exact, approximate and linearized ray tracing methods in transversely isotropic media

P.F. Daley, E.S. Krebs and L.R. Lines*

SUMMARY

The exact eikonals for the quasi-compressional (qP) and quasi-shear (qS_V) modes of seismic wave propagation in a transversely isotropic (TI) medium are considered. These are compared in a travel time sense with *weak* anisotropic and *linearized* approximations. The comparisons involve ray propagation in a 2D plane layered structure where the axis of anisotropy need not necessarily be aligned with the local coordinate system. The motivation for this is to determine the accuracy of the approximate and linearized eikonals when compared to the exact eikonal for the computation of ray paths in a media displaying weak anisotropy. This exercise is an initial step in addressing an analogous more complex problem, specifically, ray tracing in orthorhombic media. This 3D symmetry is becoming more fundamental in seismic data processing and modeling as 3D seismic acquisition methods become the norm rather than the exception. As a consequence the development of relevant software for processing and modeling of the more complex media types should be available in a variety of forms.

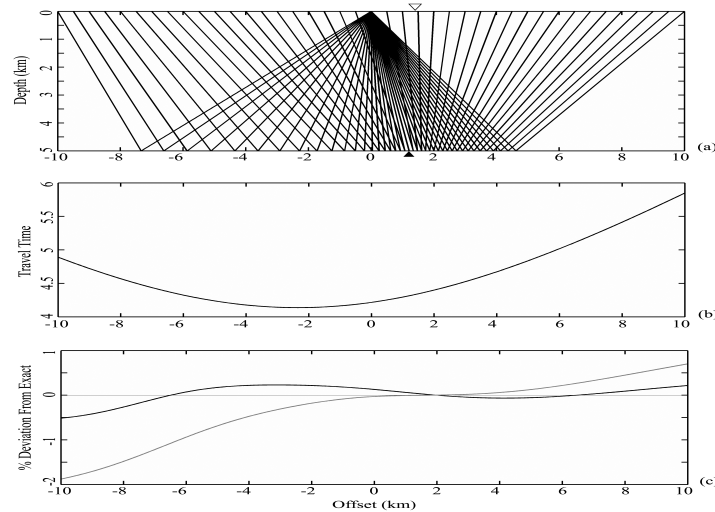


FIG. 1. Two point ray tracing with a qP ray incident and qS_V ray reflected from the plane interface at a depth of 5 km . The ray paths drawn at 0.5 km intervals for surface receivers located at offsets of -10 km to 10 km are shown in panel (a). The exact method discussed in the text was used for this with the anisotropic axis rotated 15° with respect to model coordinates. The solid triangle in (a) indicates the point where the reflected ray returns to the source and the open triangle, the ray which is at normal incidence at the surface. The exact travel time for this reflected $qP - qS_V$ ray is shown in panel (b), while the differences in travel times in percent of the approximate method (gray) and linearized method (black) when compared to the exact are plotted in panel (c).

A comparison of finite difference analogs for hyperbolic equations in inhomogeneous media

P.F. Daley

SUMMARY

In an infinite halfspace with constant media scalar wave equations may be written including one for acoustic wave propagation (pressure wave propagation in fluids) and another for S_H – wave potential propagation. Both of these scalar wave equations will be considered here in a radially symmetric medium with the possibility that parameters related to both problems may vary with depth. This is done such that the different effects of discontinuities with depth of the media parameters may be investigated in the context of the boundary conditions required to be introduced. Once these have been determined, finite difference analogues for the two cases are constructed. The simplest of these cases is to consider incidence at the halfspace boundary with the upper halfspace assumed to be a vacuum as was considered by Aki and Richards and solutions presented in the form of Sommerfeld integrals. For the problem types being investigated here, stress continuity conditions for a horizontal boundary within the two media types will be addressed.

What has often been noticed in the literature is that a scalar wave equation associated with elastodynamic wave propagation in an isotropic homogeneous has its medium parameters modified, without any mathematical justification, to be spatially variable and the resulting equation employed to model elastodynamic (compressional) P –wave propagation using methods such as finite difference modeling. Liberties appear to be taken regarding continuity conditions at discontinuities of media parameters (interfaces). This is not to say that reasonable looking numerical results cannot be obtained but the nature of these equations is questioned.

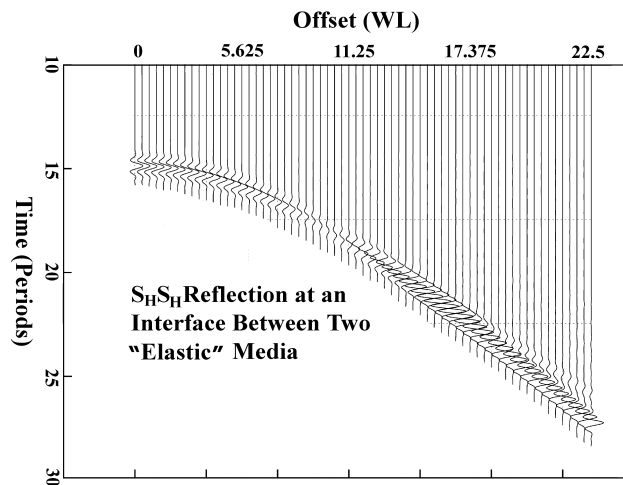


FIG. 1. The reflected $S_H S_H$ (potential) arrival from an interface between two elastic media. The point at which the reflection coefficient passes through zero may be seen, as well as the onset of the critically refracted event at far offset traces.

A linearized group velocity approach for two point qP ray tracing in a layered orthorhombic medium

P.F. Daley

SUMMARY

Using a linearized approximation for the quasi-compressional phase velocity, v_{qP} in an orthorhombic anisotropic medium, which is a subset of the related quasi-compressional (qP) wave propagation in general 21 parameter anisotropic medium, a linearized compressional group velocity may be derived as a function of group angles only. In addition, linearized analytic expressions for the components of the slowness vector in terms of group velocities and angles are also obtained. These expressions are used to define two nonlinear equations which are a generalization of Snell's Law. The solutions of these are used to determine the propagation directions of the reflected and transmitted rays due to an incident ray at an interface between two orthorhombic media. The axes of anisotropy, in both media are, in general, not aligned with the interface separating them. Computer code has been written to consider ray tracing in media defined by a type of large scale $3D$ finite element blocking (blocky structures). However, a plane parallel layered will be used in preliminary investigations. Additionally, in each of these elements (layers) the anisotropic parameters are initially assumed to be constant, although provisions for at least minimal spatial variations of the anisotropic parameters have been considered.

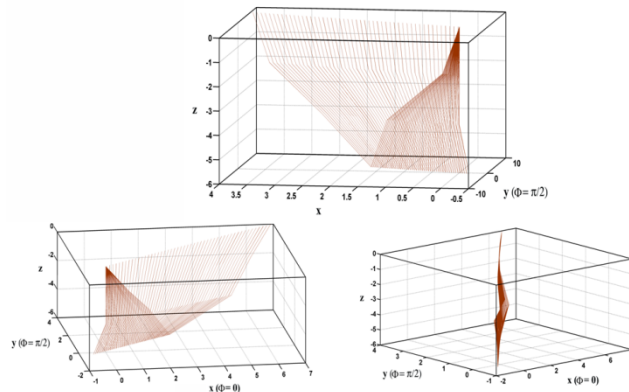


FIG. 1. Three layer model. The first layer is isotropic, the second layer is orthorhombic with a rotation in the $x-y$ plane about the z -axis and the third layer is also orthorhombic with a rotation in the $x-z$ plane. The line shot is very close to two point ray tracing, requiring some minor tweaking. The analogue of Snell's Law at an interface is a system of two coupled nonlinear equation in two unknown angles (sines of the transmitted or reflected angles). The x and y axes in the three panels have different scaling to enhance the effects of the rotations of the orthorhombic ray surfaces. The line is shot at an angle of 70 degrees with respect to the x -axis. The modified two point ray tracing algorithm consists of two coupled nonlinear equations in two unknown angles per layer in which is embedded the other nonlinear equation set for Snell's Law. Different scaling parameters are used on three panels to improve visibility.

P - S_V wave propagation in a radially symmetric vertically inhomogeneous TI medium: Finite difference hybrid method

P.F. Daley

SUMMARY

The hybrid finite difference – finite integral transform method is considered for the coupled $P - S_V$ wave propagation problem in a radially symmetric vertically inhomogeneous (plane layered) transversely isotropic medium. Apart from the development of the equations of motion, a number of numerical considerations are addressed. As in most problems where numerical methods are employed in the solution, there are several areas that are given special attention to indicate how to improve run times and accuracy.

The theory and development of finite difference analogues for coupled $qP - qS_V$ wave propagation in a plane parallel layered transversely isotropic model is presented. The radial coordinate are removed using a finite Hankel transform prior to implementation of finite difference process. What results is a coupled system of finite difference equations in only depth and time. The infinite inverse series summation may be truncated if a band limited source wavelet is used.

The finite difference analogues given are accurate to second order in both time and space (depth). The analogues for a surface point as well as general points within the medium are given. Provisions for either a vertical or explosive point source of $P -$ waves are included in the derivations. A number of points regarding this seismic modeling process, especially where some mathematical rigor is required, are dealt with in a series of Appendices.

This is the second in a sequence of six (currently) related to modeling using hybrid methods in anisotropic medium. At present, a plane layered orthorhombic structure with no anisotropic parameter variations in the two lateral spatial directions, is being tested. Two finite Fourier transforms are employed to remove dependence on the lateral spatial Cartesian coordinates. The theory presently being developed employs these two finite Fourier transforms to reduce the finite difference problem from 3 spatial dimensions and time to one spatial dimension (depth) and time. In the most recent development, the anisotropic parameters are allowed to “slowly” vary with the two lateral coordinates in an orthorhombic medium.

Using the formulae presented here it should be possible write a hybrid finite difference – finite integral transform programs for a transversely isotropic medium for a variety of source – receiver configurations including AVO and VSP.

Quasi-compressional ray propagation in a linearized general anisotropic media

P.F. Daley

SUMMARY

Ray tracing for qP rays in a linearized general (21 parameter) anisotropic medium is investigated. A smoothly varying inhomogeneous medium is initially assumed and the axes of anisotropy within the layers are allowed to be oriented at arbitrary angles with respect to the model coordinates. As in almost all applications of ray tracing the two point problem is the most useful. That is given a source and receiver location within a anisotropic medium, determine the ray path(s) between the two points. This introduces two coupled nonlinear equations which must be solved. Initially, the medium will be chosen to be a smoothly varying inhomogeneous anisotropic medium with no rotations of the axes. These assumptions may appear to be quite restrictive; however, it would seem to be a reasonable foundation upon which to advance to more complicated media types within the context of qP ray propagation in an orthorhombic anisotropic structure. The density normalized anisotropic parameters used to describe an orthorhombic media, which have the dimensions of $(\text{velocity})^2$, will be in Voigt notation, A_{ij} , as this notation is familiar. One of the applications of this ray tracing method is for Born-Kirchoff migration, so that some attention will be afforded that topic.

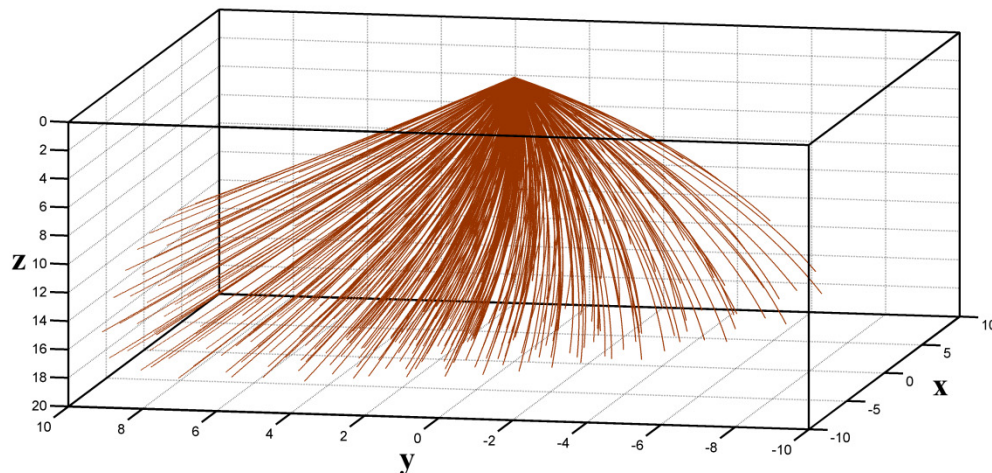


FIG. 1 Rays from a point source locate at the surface at azimuthal phase angles $(0 \leq \phi < 360^\circ)$ at 5° increments. Polar angles $(-80^\circ \leq \theta \leq 80^\circ)$ at 5° increments are used. The rays are forced to lie within the spatial volume $(-10 \leq x \leq 10)$, $(-10 \leq y \leq 10)$, $(0 \leq z \leq 20)$. The dimensions are in km .

Reflection and transmission coefficients in TI media: exact and linearized phase velocities, eikonals and polarization vectors

P.F. Daley, E.S. Krebs and L.R. Lines

SUMMARY

Reflection and transmission coefficients which partition energy due to plane wave incidence at the interface between two transversely isotropic (*TI*) media are considered. The basic forms of these coefficients employed use expressions for certain quantities that may be classified as either exact or linearized. Phase velocities and the related slowness vectors, as well as the polarization vectors for the incident and the four possible reflected or transmitted wave types, are investigated for both levels of accuracy mentioned above. Computed results for these precision types of should be compared graphically for what has been termed weak anisotropy (*WA*). However, liberties will be taken and at least one of the media will be chosen to be strongly anisotropic, to determine the possible limits of the degree of anisotropy which may be considered without a major compromise of results. The results suggest that the degree of anisotropy, for which the linearized quantities are assumed to provide reasonably accurate results, may be larger than that typically associated with “weakly anisotropic” media. A full sensitivity study is not done here as the prime motivation for this work was to develop the linearized formulation of reflection and transmission coefficients, given that the exact solutions are known. This is one of the motivations for undertaking this study, as a linearized reflection and transmission coefficients algorithm for more complex anisotropic media is a future objective.

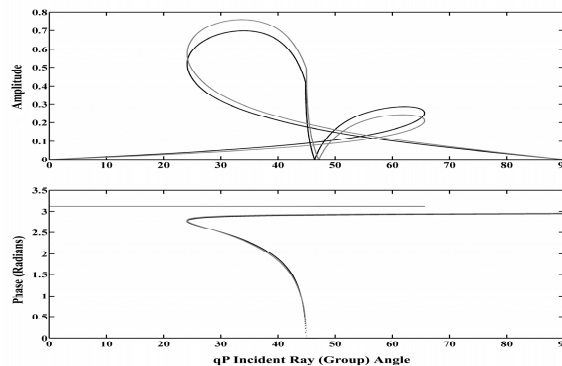


FIG. 1. The reflection coefficient R_{P1S1} due to a qP plane wave incident from the upper medium where the amplitude and phase is plotted versus the incident qP group angle. As is clear from the plotted curves, this was done as another check how well the exact and linearized reflected qS_V amplitudes and phases of the exact and linearized cases matched. The exact curves are black and the linearized curves are grey.

Shot record depth migration of georadar

Robert J. Ferguson*, Adam Pidlisecky, and Colin Rowell

SUMMARY

We modify common shot record migration from seismic imaging into a single trace prestack depth migration (PSDM) specifically for georadar. Implemented using a combination of Linux, Pearl, and Octave programming languages, our georadar PSDM runs in parallel on the CREWES cluster Gilgamesh. This PSDM migrates the radar data from topography, and when compared to conventional migration derived from normal-incidence topography correction followed by zero-offset migration, we find that our PSDM returns significantly improved migrated images. As part of pre-image processing, we find that nonstationary deconvolution implemented in the Gabor domain significantly enhances the sharpness of reflection and diffraction events, and it significantly enhances reflection and diffraction arrivals at later times when compared to conventional spiking deconvolution.

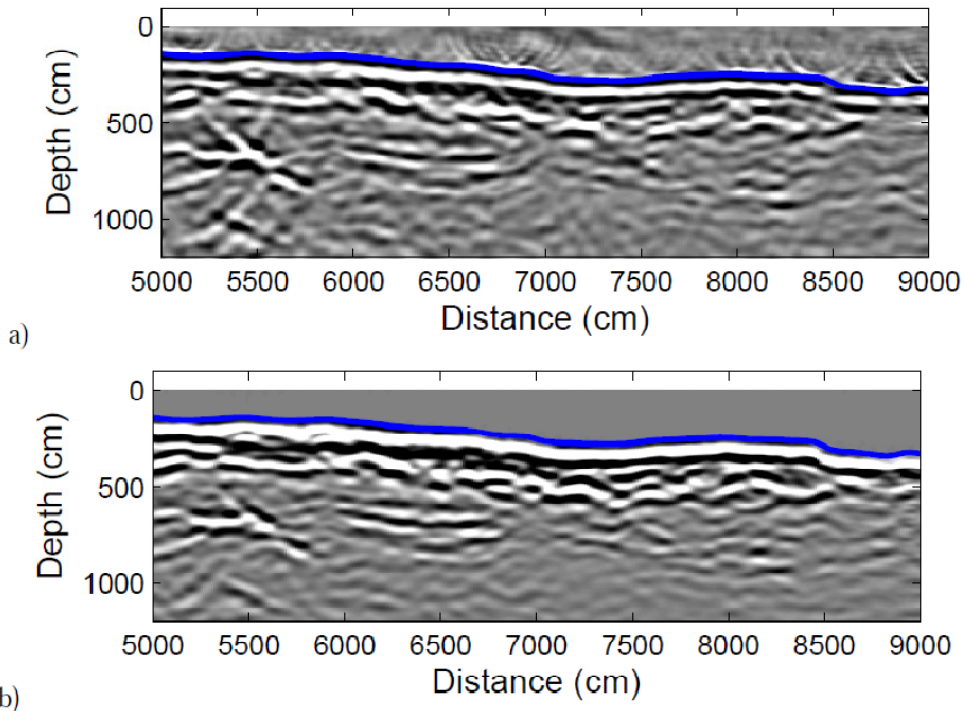


FIG. 1. Migration comparison of 5000-9000 cm. a) Zero offset migration. b) Stacked shot record migration. The shot record migration is less noisy, and energy is more coherent. The elevation profile is overlain as a solid line.

Borehole geophone repeatability experiment

Peter Gagliardi* and Don C. Lawton

SUMMARY

Time-lapse vertical seismic profile data was obtained near Violet Grove, Alberta, using an array of eight 3-component geophones at depths between 1497 m to 1640 m. Baseline data were recorded in 2005 and the monitor recorded in 2007. Analysis of rotation angles was undertaken for both surveys, resulting in differences of less than 2° for 54.2% in Line 2 and 85.9% in Line 3. Rotation angles were found to be more consistent at offsets greater than about 500 m. NRMS analysis gave averages of 61.4% and 45.3% for horizontal components, and 42.8% and 41.4% for the vertical component. Predictability analysis showed averages of 0.72 and 0.83 for horizontal components and 0.83 and 0.86 for the vertical component. In addition, traces were examined visually, and showed good qualitative repeatability. Since the receivers were cemented into place, the greatest effect on the repeatability was judged to be from small differences in the source locations between surveys, and differences in noise.

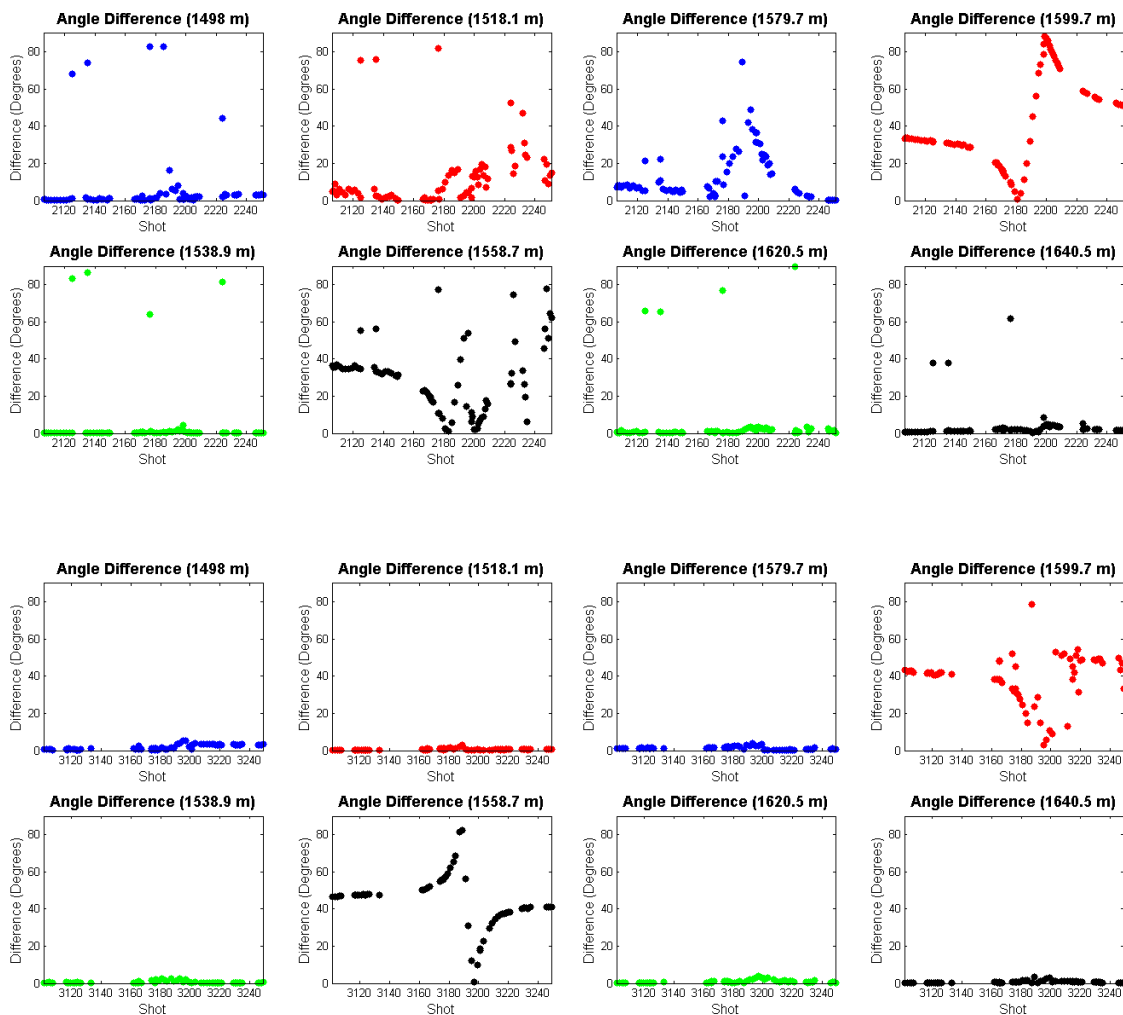


FIG. 1. Time-lapse rotation angle differences for individual geophones (Line 2 top; Line 3 bottom).

Converted wave processing in the EOM domain

Thais A. Guirigay and John C. Bancroft

SUMMARY

Based on the consideration of prestack migration by equivalent offset and common scatter points (CSP), a new approach for converted wave prestack migration and velocity analysis has been developed and works successfully. During the process, a converted wave velocity V_c was estimated from the hyperbolic moveout on a CSP gathers. Moveout (MO) correction and stacking complete the prestack migration. The intent of this paper is to see what additional uses can be made with V_c .

Converted wave CSP are formed by summing all input traces at the equivalent offset migration. V_c can be quickly and accurately estimated using a limited converted wave CSP (LCCSP) gather. This V_c is valid only for zero offset data, however we can extend its application when there is an acceptable small error in the estimated traveltimes.

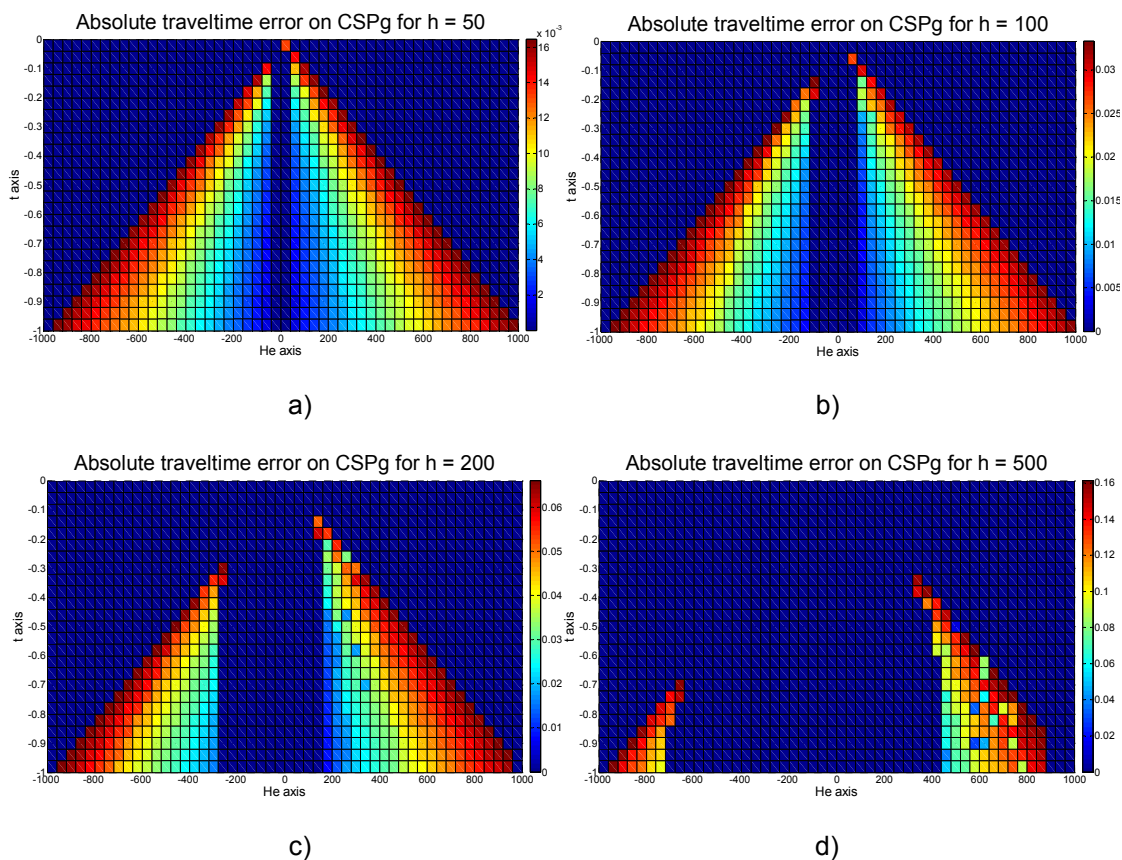


FIG. 1. Traveltimes difference on a CSP gather for various half offsets h equal to: a) 50 m, b) 100 m, c) 2000 m, and d) 500 m. Note that the values on the time scale vary for each figure.

A simple algorithm for the restoration of clipped GPR amplitudes

Akshay Gulati and Robert J. Ferguson

SUMMARY

In this paper, an algorithm for clipped amplitude restoration using hybrid POCS is presented and tested. It is able to completely restore the clipped amplitude of GPR data. Two different methods for estimating the clipping are tested. The first one is the conventional method of spline interpolation, which is widely used in the GPR industry. The second is hybrid POCS, which uses *a priori* information from the signal to recover clipped amplitudes. A comparative study shows that hybrid POCS is better than conventional spline interpolation. Hybrid POCS results in improved lateral continuity of the energy across the horizons in reconstructed data.

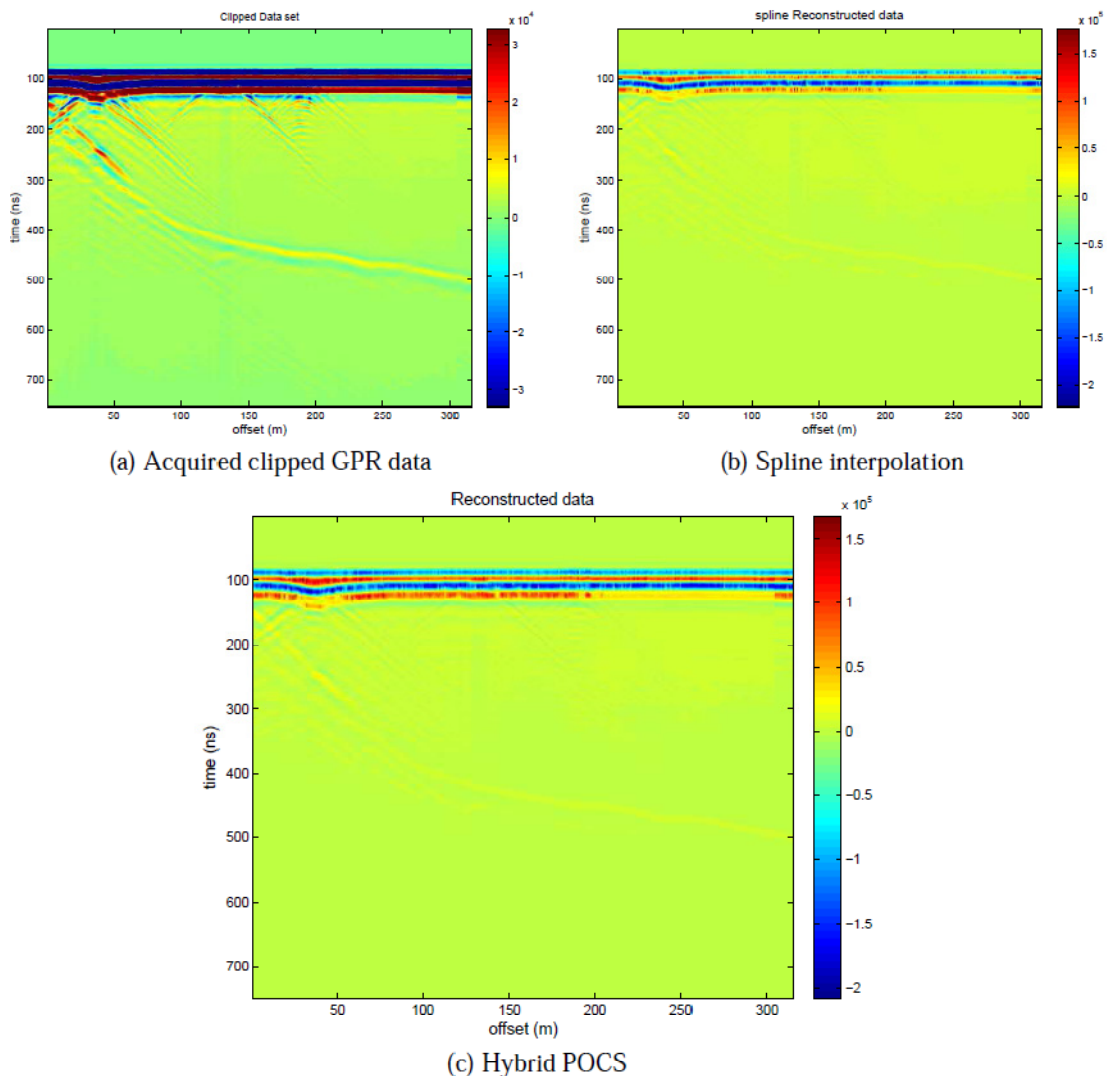


FIG. 1. Reconstruction of clipped Ground Penetrating Radar data.

Kaiser Bessel gridding kernel for seismic data regularization

Akshay Gulati and Robert J. Ferguson

SUMMARY

A new seismic regularization method is presented that is based on gridding using Non uniform Fast Fourier transform Kaiser Bessel kernel. In one dimension, computational complexity of Kaiser Bessel NFFT is $O(N \log N)$ which is a dramatic improvement from the $O(N^2)$ complexity of the Discrete Fourier transform (DFT) and comparable to FFT. Finally, Least squares is used to approximate spectra and this is followed by simple Fast Fourier transform (FFT). The low computational cost of Least square Kaiser Bessel Non uniform fast Fourier transform make it a robust and practical algorithm. This algorithm is effective both in case of random sampled data as well as uniform sampling. NFFT and Adjoint NFFT can be use as an effective tool in other seismic processing steps. The applicability of the proposed method is examined using synthetic examples.

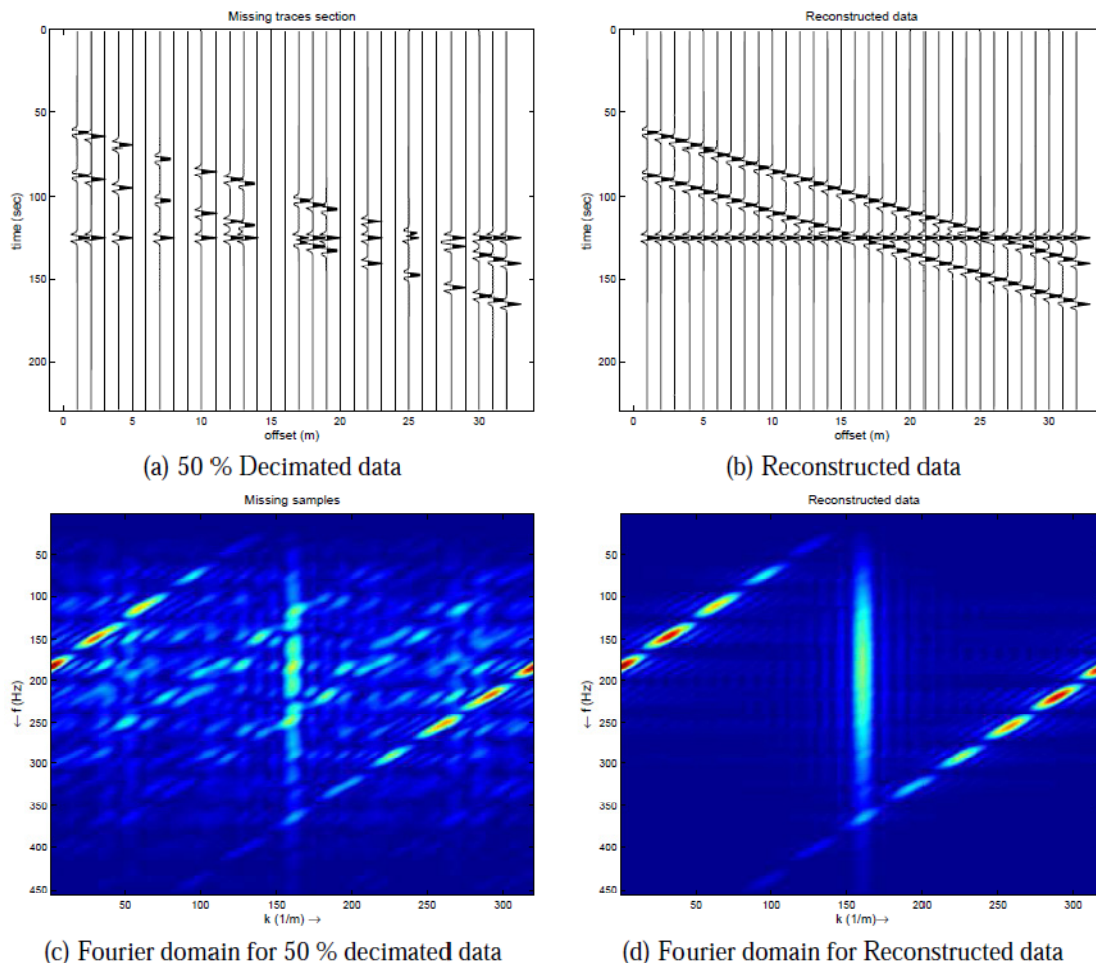


FIG. 1. Reconstruction of random sampled Seismic data.

Near-field effects in VSP-based Q-estimation for an inhomogeneous model

Arnim B. Haase and Robert R. Stewart

SUMMARY

As a continuation of earlier near-field investigations into homogeneous situations we expand our analysis to an inhomogeneous example. We show that depth locations of so-called *wrap-around* points where spectral ratio method Q-estimates change from large negative values to large positive values are controlled by P-wave velocities and intrinsic Q-factors. A velocity-step model and Q-factors derived from these velocities by empirical equation are used to demonstrate near-field Q-factor recovery by inversion. Because VSP model data and forward models are computed with the same multi-interface Sommerfeld integral it is found that, in this noise-free situation where velocities and densities are assumed to be known exactly for the forward modelling step, Q-factors can be recovered exactly also. Even though this VSP model approach is a simplification in many respects it does include near-fields, far-fields and geometrical spreading in the analysis.

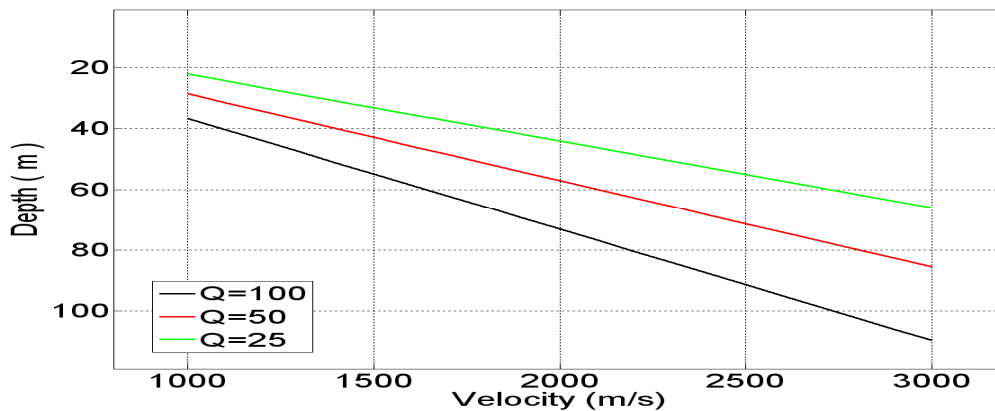


FIG. 7. Wrap-around depth as function of velocity and Q-factor.

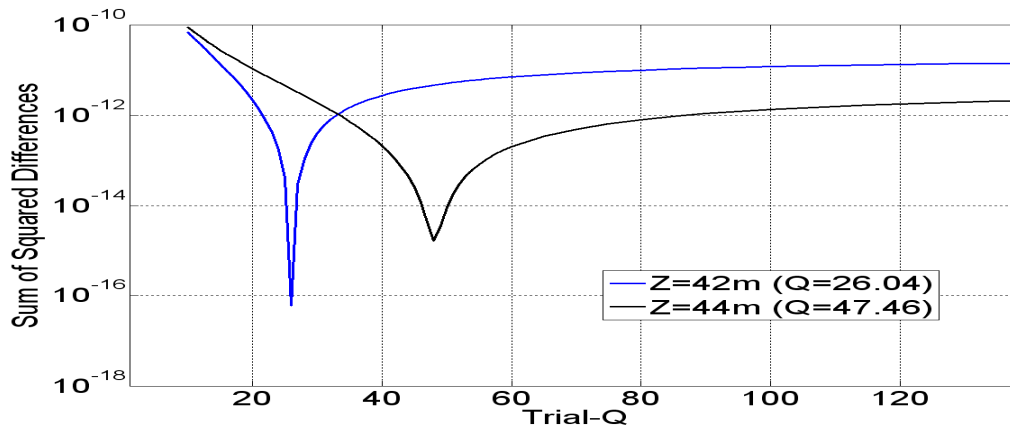


FIG. 11b. Sum of squared differences between data and forward model (log scale).

Spectral ratios for the Pembina Cardium formation computed with virtual sources

Arnim B. Haase, Donald C. Lawton and Abdullah Alshuhail

SUMMARY

Spectral ratios across the Pembina-Cardium formation are computed from surface source lines and down-hole receiver gathers by applying virtual source principles. It is found necessary to apply first-arrival wave package windowing to reduce ringing of these spectral ratios. There is an increase of attenuation across the reservoir layer for all three source line experiments following CO₂ injection. This attenuation increase is confirmed by spherical wave modelling employing a multi-interface Sommerfeld integral algorithm and using monitor well-logs as well as fluid substitution derived perturbations of reservoir parameters. Spherical wave modelling also shows far-offset tuning across the reservoir when offsets are retained rather than applying virtual source methods. Alternate measures of CO₂ injection effects are demonstrated by displaying time domain maximum amplitude differences as function of offset as well as plotting frequency domain magnitude spectral differences as function of frequency and offset.

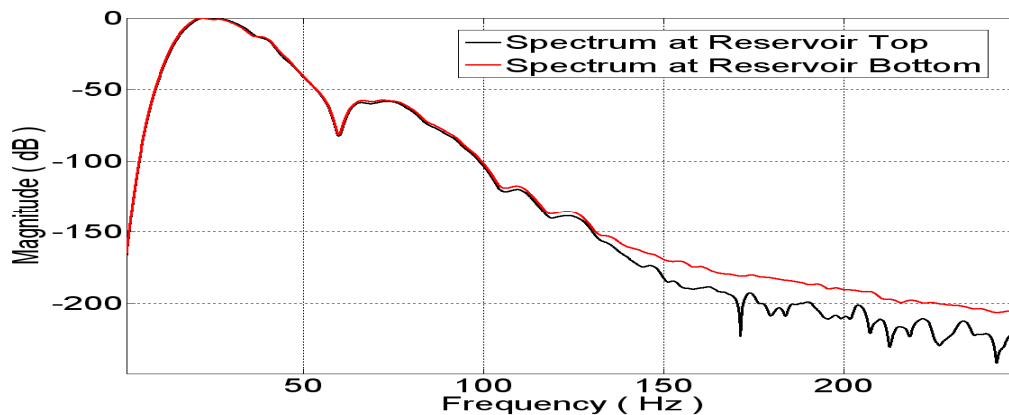


FIG. 8. Base line VSP-trace interferometry spectrum (Gaussian window applied).

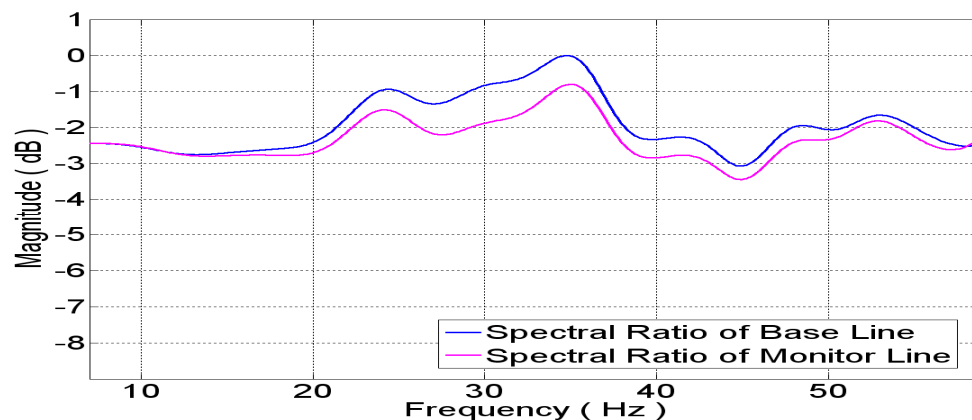


FIG. 10. VSP-trace interferometry spectral ratios of line 3 (Gaussian window applied).

Stratigraphic attenuation (Q) effects in heavy oilfield VSP data

Arnim B. Haase and Robert R. Stewart

SUMMARY

As an extension of work on near-field Q-factor recovery we apply Q(z)-inversion by forward modeling to VSP model data generated from Ross Lake well-logs applying a multi-interface Sommerfeld integral algorithm. An intrinsic Q(z) model is derived from Ross Lake P-wave velocities by applying an empirical equation. When computing swept-Q forward models with the same Sommerfeld algorithm as is used for generating the VSP model data the sum of squared differences show minima at the correct intrinsic Q-values; velocities and densities are assumed to be known in these forward model computations. Applying a Golden-Section-Search algorithm for computational efficiency leads to a local-minimum problem at some depths which is solved by adding a local-minimum search extension. For this ideal noise free model situation intrinsic Q-factor recovery is very successful.

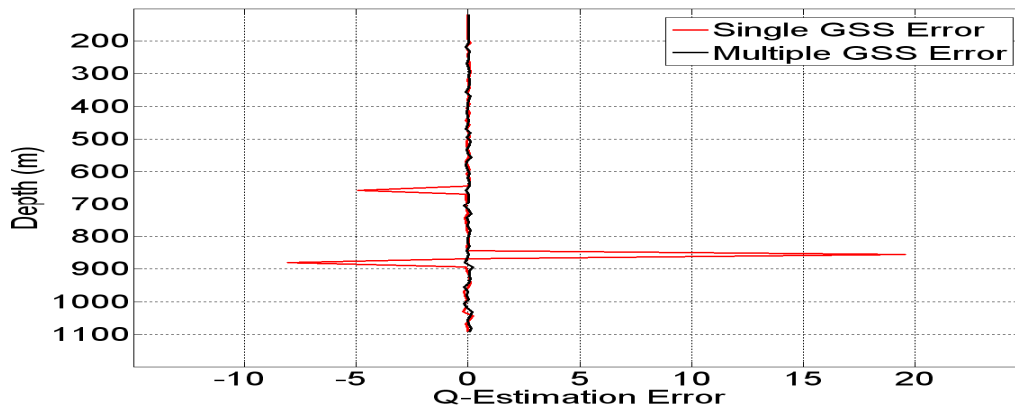


FIG. 7. Ross Lake Q-estimation error following Golden Section Search.

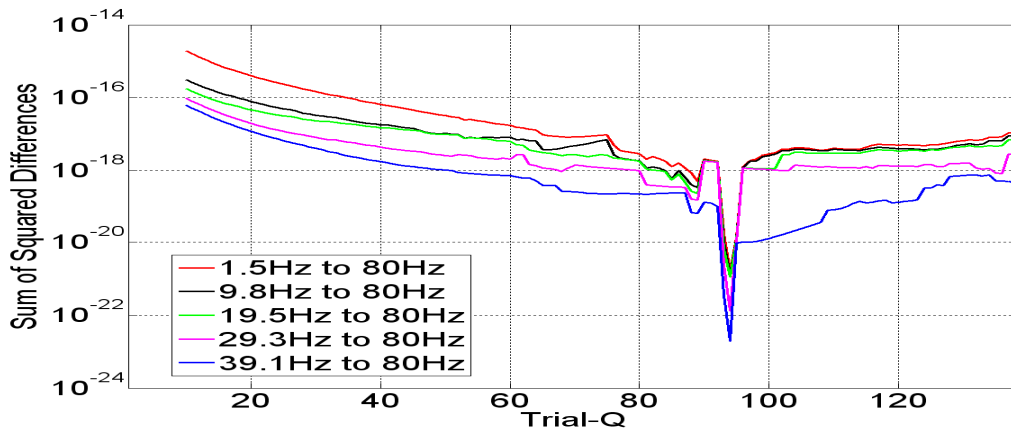


FIG. 8. Bandwidth dependence of *sums-of-squared-differences* at Z=656m (Q=94.3).

GPS accuracy part 2: RTK float versus RTK fixed

Kevin W. Hall, Peter Gagliardi and Don C. Lawton

SUMMARY

During the University of Calgary's 2010 geophysics field school, geophone and source point locations for a 3C-2D seismic line were GPS surveyed by student crews over a period of many days. In the course of the RTK GPS (real time kinematic global positioning system) survey, some geophones were surveyed up to three times, particularly in problem areas on the line. In this case, the problem areas had thick bushes and trees, such that the GPS rover was not able to achieve a good GPS solution due to signal attenuation by the vegetation. Comparisons of the repeated data points show that RTK fixed solutions have the best repeatability (accuracy better than one decimeter). RTK float solutions can be as repeatable as fixed solutions, but can also be out by up to five meters, with no way to tell unless surveying a known point. The authors recommend RTK fixed solutions for small station/receiver spacings.



FIG. 1. Typical daily GPS base station setup, looking roughly southwest. The part of the seismic line that is visible in this picture is high-lighted with a red line.

Priddis low-frequency seismometer test, part 2

Kevin W. Hall, Malcolm B. Bertram, Gary F. Margrave, and Dave W. Eaton

ABSTRACT

CREWES acquired a low-frequency sensor comparison test dataset in 2009. The dataset was acquired using a weight drop trailer and an IVI Minivibe (2-10 Hz and 2-100 Hz linear sweeps with different sweep lengths and peak force levels) at two source points, offset by 50 meters from the ends of the north-south receiver lines. Sensors on the ground included accelerometers (DSU3 and VectorSeis), geophones (SM-24) and broadband seismometers (Trillium 240). Near-offset (50 m) traces for a single 2-100 Hz linear sweep are visually compared as 1) uncorrected, uncorrelated data, 2) converted to common units and corrected for geophone and seismometer instrument response in the velocity and acceleration domains. Least-squares-subtraction-scalar results are also presented. System electrical noise appears to dominate signal below about 7 Hz for all systems, likely due to the long taper used for the low frequencies (< 10 Hz) and the low power used for the sweep in order to not damage the Minivibe. We appear to have a close match (other than a multiplicative term) down to at least 5 Hz for all recording systems and sensors.

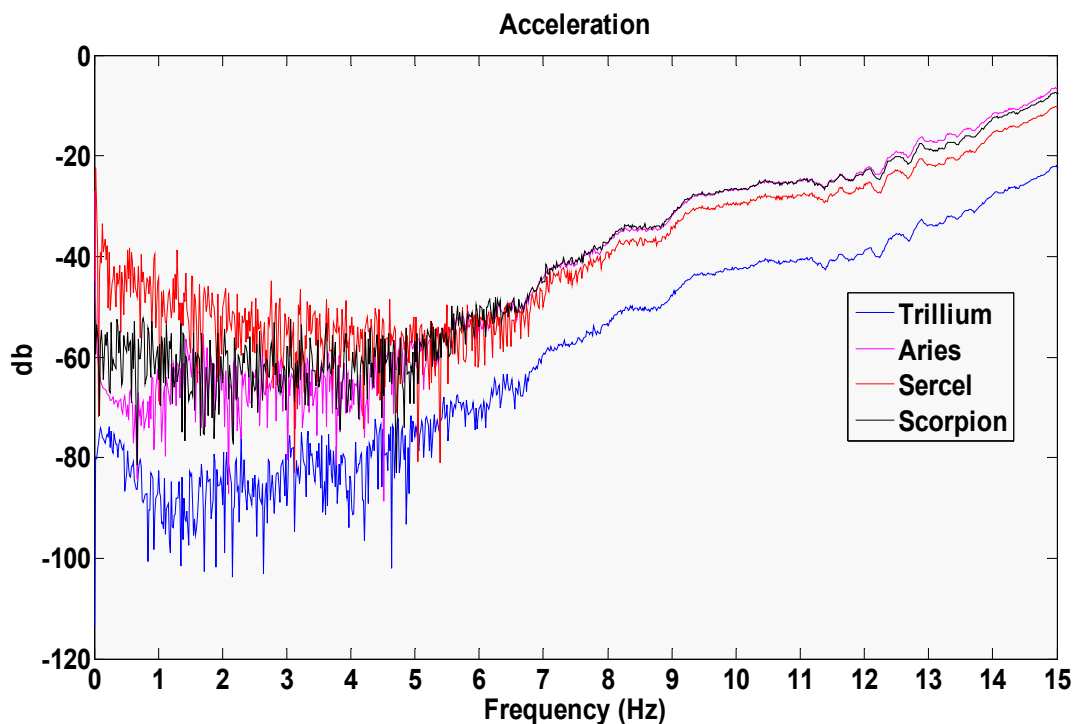


FIG. 6b. Visual comparison after converting raw data to acceleration: data have been corrected for geophone and seismometer instrument response.

Back-propagation analysis for hypocenter location

Lejia Han, John C. Bancroft, and Joe Wong

SUMMARY

Back propagation analysis has been based on the incident propagation directions derived by hodogram analysis with weighted least squares, the nearest points of mutual raypaths, and the statistical clustering optimization with Student's t distribution. The hodogram of each trace is based on MER picking of 1st-arrival time on noise attenuated data as shown in Figure 1.

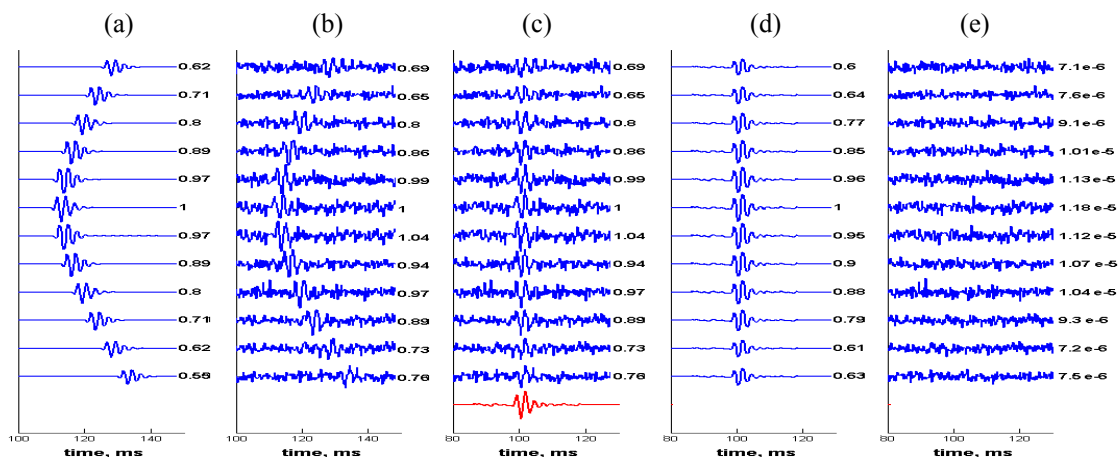


FIG. 1. Noise attenuation on synthetic data. (a) true arrivals, (b) noisy traces (SNR=3), (c) trace stacking after bandpass filtering, matched filtering, (d) signal components after noise-signal separation (NSS), and (e) noise components after NSS.

This method exhibits low location uncertainties in both 2D and 3D approaches under sufficient experimental testing (totally with 600 and 180 cases respectively for 2D and 3D) as shown in the two (left and right) tables below.

Table 1. Statics from approaches of 2D (left) with 100 cases and 3D (right) with 30 cases for each (row) set of parameters (SNR and dR).

| Statistics of the Location Uncertainty by the 2D Approach of Back-propagation Analysis | | | | | Statistics of the Location Uncertainty by the 3D Approach of Back-propagation Analysis | | | | |
|---|---------|-----------|------------|-----------|---|---------|-----------|------------|------------|
| Noise | Spacing | Estimated | Hypocenter | Locations | Noise | Spacing | Estimated | Hypocenter | Locations |
| | dR (m) | Xs (m) | Ys (m) | Zs (m) | | dR (m) | Xs (m) | Ys (m) | Zs (m) |
| 10 | 10 | 390 ± 28 | 292 ± 22 | 2148 ± 7 | 10 | 10 | 400 ± 1.8 | 299 ± 2.2 | 2150 ± 2.1 |
| 10 | 25 | 398 ± 13 | 298 ± 10 | 2151 ± 3 | 10 | 25 | 400 ± 1.9 | 299 ± 1.7 | 2150 ± 1.7 |
| 10 | 50 | 401 ± 8 | 301 ± 7 | 2149 ± 4 | 10 | 50 | 400 ± 2.5 | 300 ± 2.4 | 2150 ± 2.3 |
| 3 | 10 | 264 ± 58 | 195 ± 43 | 2122 ± 14 | 3 | 10 | 405 ± 9.0 | 294 ± 6.4 | 2153 ± 8.2 |
| 3 | 25 | 386 ± 37 | 286 ± 30 | 2151 ± 12 | 3 | 25 | 405 ± 5.0 | 295 ± 6.6 | 2155 ± 5.7 |
| 3 | 50 | 410 ± 27 | 301 ± 23 | 2152 ± 15 | 3 | 50 | 405 ± 7.7 | 299 ± 8.9 | 2158 ± 7.8 |
| The True Location: | | 400m | 300m | 2150m | The True Location: | | 400m | 300m | 2150m |

The nearest approach to multiple lines in n-dimensional space

Lejia Han and John C. Bancroft

SUMMARY

An efficient matrix approach is described to obtain the nearest approach to non-intersecting lines in 3-dimensional or any n-dimensional spaces. By the nearest approach, we mean the nearest point(s) or vector(s) to all lines by matrix inversion. The entire solution set can be provided by the matrix approach simultaneously, ensuring efficiency and accuracy at the same time..

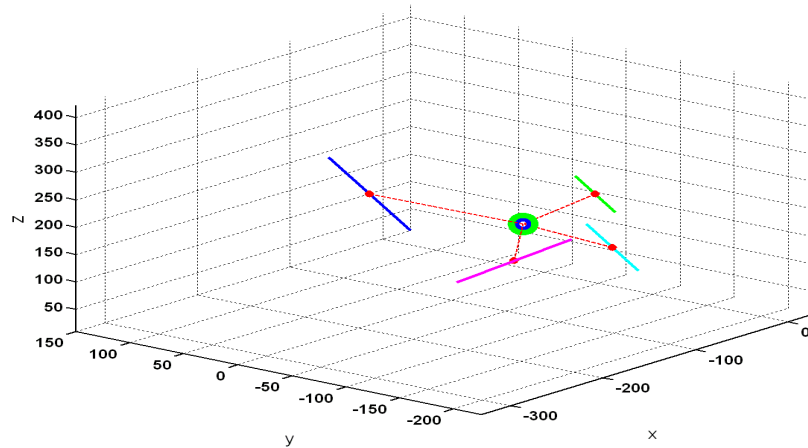


FIG. 1. The nearest points to four non-intersecting but 3 parallel lines (blue, green, and cyan) in 3D space. Results from least squares (green circle) and SVD (blue circle) and respective four on-line nearest points (red dots).

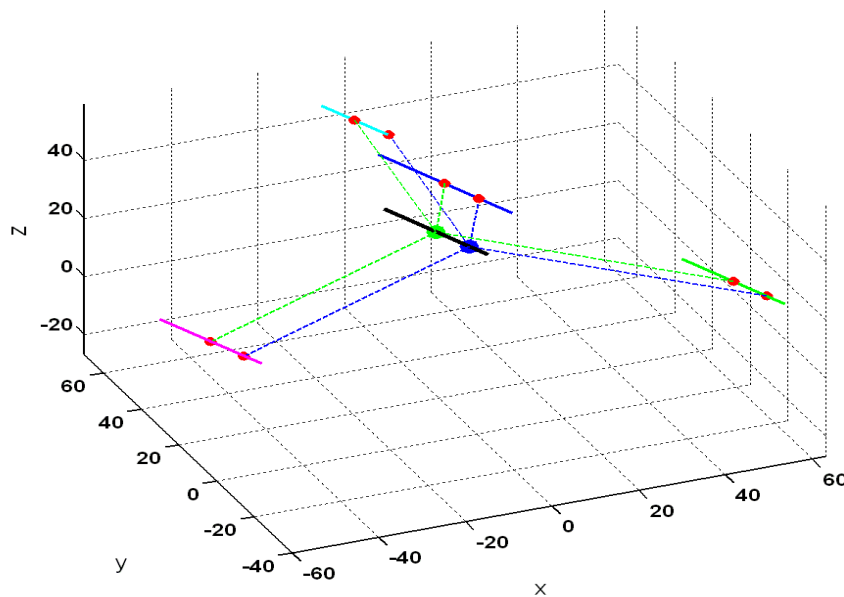


FIG. 2. The nearest points to four non-intersecting but all parallel lines in 3D space lie on the black line. An example solution using least squares is shown at an arbitrary location as the green point. The single SVD solution (blue dot) is closest to the origin of the system.

Pattern-search inversion for hypocenter location

Lejia Han, Joe Wong, and John C. Bancroft

SUMMARY

With one-component recordings, microseismic monitoring and hypocenter location has to employ a conventional imaging method, in contrast to our back-propagation analysis method demanding on three-component recordings. In such situations, we employed the pattern-search inversion algorithm and tested it in three seismic survey geometries with a six horizontal layered velocity model, in wells and on surface. The PS inversion was used to calibrate the velocity model first, and the regressing progress is shown in Table 1. The efficiency of the PS inversion is extensively demonstrated by its regressing efficiency and cost on P-wave observations, where is most favourably in three shallow vertical well with 51 times over in the single vertical well with 155 times, while most expensively on surface with 600 times of searching iterations and function evaluations at the equivalent RMS error of 0.30 milliseconds, as shown in Table 2.

Table 1. PS inversion progress in calibrating the velocity model.

| Iterations (iter) | Evaluations (iter2) | v_1 (m/s) | v_2 (m/s) | v_3 (m/s) | v_4 (m/s) | v_5 (m/s) | v_6 (m/s) | Error (ms) |
|------------------------------|--------------------------------|----------------|----------------|----------------|----------------|----------------|----------------|-----------------------|
| 0 | 0 | 1000 | 2000 | 2000 | 2000 | 2000 | 2000 | 16.5 |
| 10 | 8 | 1012.6 | 4030.9 | 2107.1 | 3040.2 | 4509.3 | 4129.9 | 5.14 |
| 20 | 58 | 1109.8 | 5010.7 | 3059.9 | 4103.2 | 4089.2 | 4035.6 | 1.66 |
| 40 | 229 | 1050.6 | 2510.9 | 4250.3 | 4125.7 | 3509.9 | 4125.1 | 0.45 |
| True | Model: | 1000 | 3000 | 4000 | 4200 | 3500 | 4200 | 0 |

Table 2. PS inversion progress summary for locating a hypocenter in 3 scenarios.

| Observations (1C microseismograms) | RMS error (ms) | Iterations (iter) | Evaluations (iter2) |
|---|---------------------------|------------------------------|----------------------------|
| In a single vertical well | 0.30 | 40 | 115 |
| In three shallow vertical wells | 0.30 | 21 | 30 |
| On surface | 0.30 | 101 | 459 |

Earthtones: nonstationary colour correction in ProMAX

David C. Henley, Peng Cheng, and Gary F. Margrave

SUMMARY

When applying statistical deconvolution techniques to seismic data, it is almost universal to assume that the spectrum of the earth's reflectivity is white over some particular bandwidth. In situations where seismic data are acquired in reasonable proximity to an existing well with one or more reflectivity logs, however, the nonstationary deconvolution of the seismic traces can be improved by replacing the conventional "white" reflectivity spectral assumption with a simple 2D colour function (of frequency and time), whose shape has been derived from spectral analysis of the actual well log. Least-squares fitting of log reflectivity spectra to low-order polynomial curves has been shown to provide a convenient representation of the 'colour' of well log spectra, which may subsequently be used to modify deconvolution operations. This colour-correction scheme has been added to our existing ProMAX Gabor deconvolution and analysis modules. We describe the specifics of those modules, and we demonstrate the updated algorithms on field data.

EXAMPLE

Figure 1 shows a 2D colour correction function obtained from spectral analysis of an actual reflectivity log

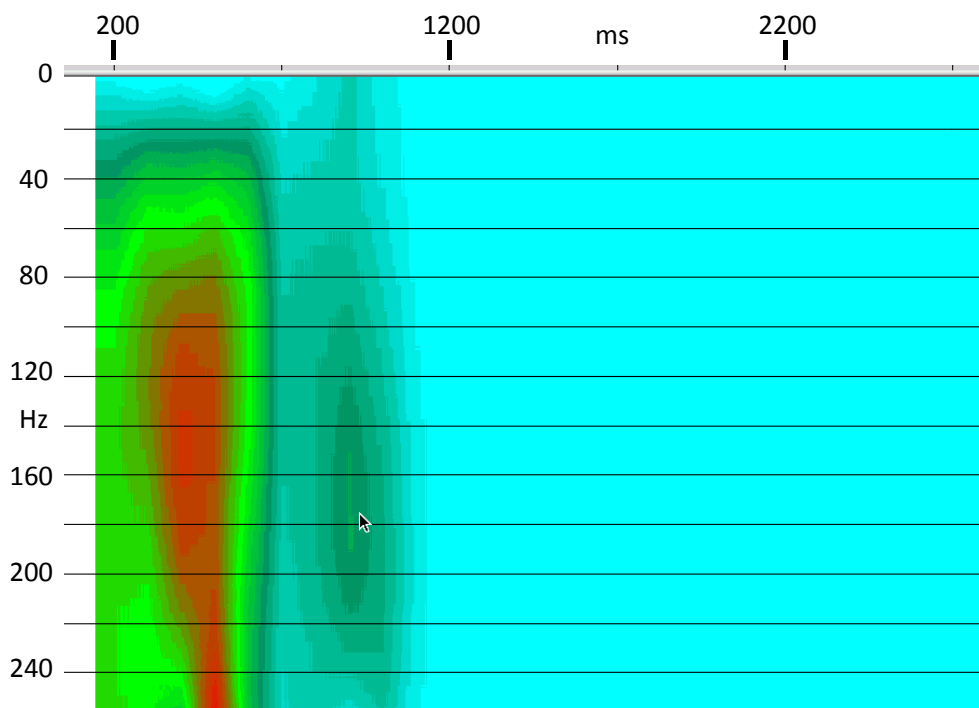


FIG. 1. 2D colour function derived from spectral analysis of a Blackfoot reflectivity log (courtesy of P. Cheng). This plot was made using Gabor_sc in diagnostic mode.

Raypath interferometry for dummies: a processing guide

David C. Henley

SUMMARY

The near-surface layer of the earth often causes serious degradation of seismic reflection images due to the irregularity of its thickness and composition. The effects include loss of signal bandwidth and phase/timing mismatch of specific reflection events between seismic traces recorded at neighbouring shot or receiver surface stations. In earlier work we have introduced interferometric methods to remove these effects, and have shown that what we term the ‘raypath domain’ is an effective one in which to work. We have demonstrated the methods on both synthetic and real data, but have not described the processing details. We present here specific processing flows from the ProMAX processing environment and describe in detail how to apply raypath interferometry to a 2D seismic line. Raypath interferometry actually embodies two distinct and independent concepts, either of which can be utilized on its own: raypath-consistency, and interferometry. The processing flows we have constructed are modular enough that while they are easily combined to apply the complete raypath interferometry method, they may be also be used separately to apply either statics deconvolution or raypath-consistent diagnostics independently.

DIAGNOSTIC DISPLAYS

In the diagnostic displays in Figure 1, we show an example of a set of ‘statics functions’ derived from cross-correlations, which are used to deconvolve a ‘common-angle gather’, the basic processing unit in raypath interferometry. Next, we show a common-angle gather, from an unrelated seismic line, both before and after interferometric correction (deconvolution of the appropriate statics functions).

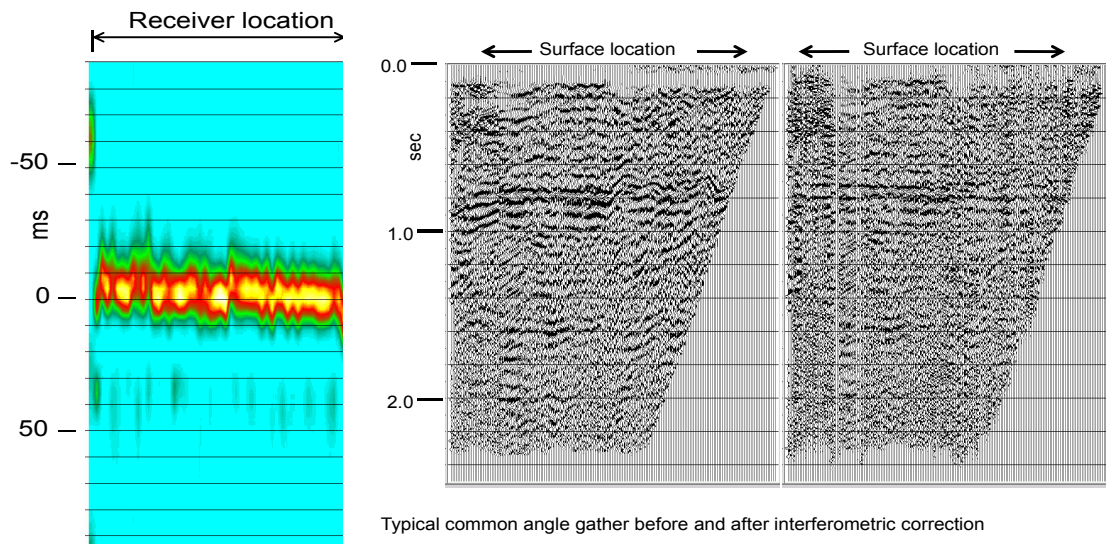


FIG. 1. Example of statics functions (left) used to interferometrically correct (deconvolve) common-angle gathers. Unrelated common-angle gather before (centre) and after (right) interferometric correction (statics deconvolution).

Recent ProMAX module upgrades

David C. Henley and Kevin W. Hall

SUMMARY

We describe here recent modifications and upgrades to several existing ProMAX modules, which are now available to sponsors through our website. Among the more important changes, which were made to all existing modules, were some clean-up of the Fortran code, replacement of obsolete memory allocation subroutines, and re-structuring of the array indexing, to enable the modules to compile and run successfully on 64 bit Linux systems. Specific modules which were given new capabilities are Gabor2 and Gabor_sc (both enabled for colour correction), and Timath (a new function was added to enable computation of Discrete Fourier Transforms).

NEW TIMATH APP: DFT

Figure 1 shows a plot of the very detailed DFT magnitude spectrum obtained using the new DFT function implemented in Timath. The plot shown is only a small portion of the entire spectrum, which extends to 240 Hz. This function is an example of the kind of simple algorithm that can be quickly implemented and tested using Timath

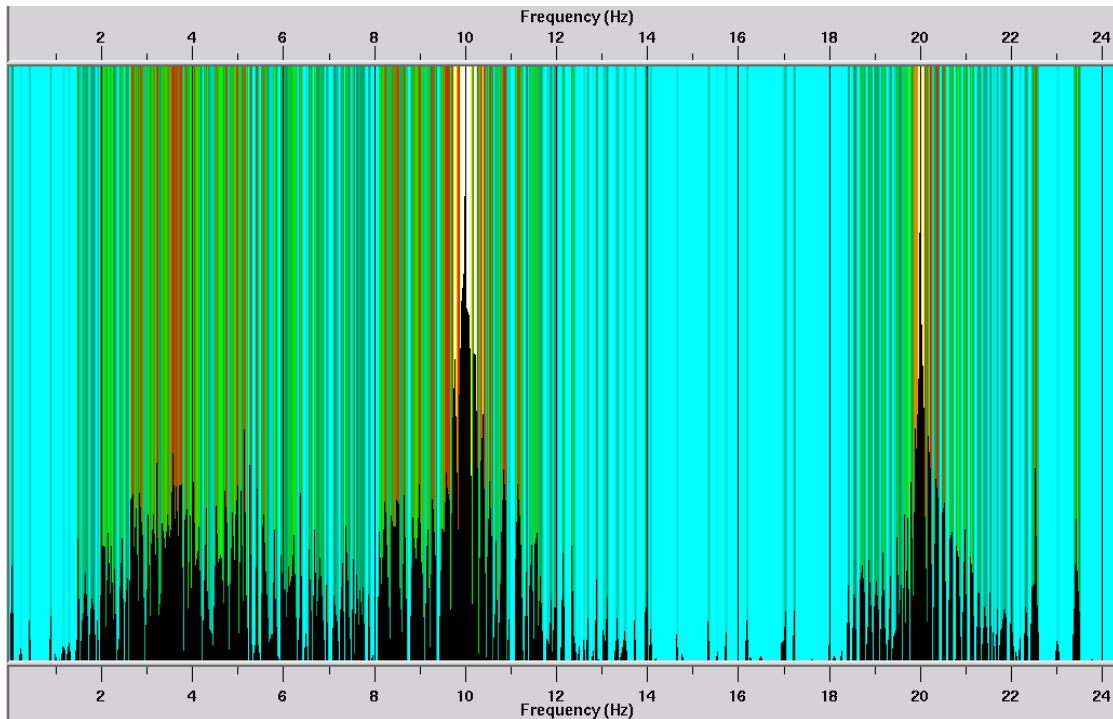


FIG. 1. Example of a DFT magnitude spectrum from a very long monofrequency (10 Hz) vibroseis sweep... which should dispel the notion that there is any such thing as a monofrequency sweep in the real world!

Integrated well-log, VSP, and surface seismic analysis of near-surface glacial sediments: Red Lodge, Montana

Jingqiu Huang¹, Robert R. Stewart¹, Joe Wong², and Carlos Montana³

SUMMARY

We conducted a series of geophysical surveys to characterize a glacial bench deposit and underlying strata near Red Lodge, Montana. Well logs and VSP data were acquired in a PVC-cased, 115m deep borehole. The multi-offset VSP was undertaken using surface sources (an accelerated weight drop and sledge hammer) with a hydrophone string and downhole, wall-clamping, 3-component geophone. The well logs included measurements of conductivity, radioactivity (gamma ray), temperature, and sonic velocity. Sonic and VSP velocities range from 1500m/s in the very near surface to 3000m/s at 85m depth. A distinct black clay (with high conductivity, high gamma ray, and low velocity) is penetrated at 85m. High-resolution 2D and 3D seismic surveys, using a sledge hammer source, show a number of reflectors to about 150ms two-way traveltime. An 80ms seismic reflection correlates to the 85m interface.



FIG. 1. The glacial bench area.



FIG. 2. Seismic and gravity crews at Elk Basin oilfield, Montana.

¹ University of Houston, Department of Earth & Atmospheric Sciences, Houston, TX

² University of Calgary, Department of Geoscience, Calgary, AB

³ Geophysical Exploration and Development Co. (GEDCO), Calgary, AB

A particle/collision model of seismic data

Kris Innanen

SUMMARY

It can occasionally be a valuable exercise to take a familiar phenomenon and observe it from a different point of view. It turns out, for instance, that in the right frame of reference, waves in a VSP experiment seem to act like particles, drifting freely or accelerating in a potential, and thereafter colliding, sticking together, and spontaneously disintegrating. In fact all of the important properties of simple wave phenomena (phase velocities, propagation directions, amplitudes, reflection and transmission coefficients) are correctly captured by speaking of the experiment entirely in terms of a system of colliding particles (with welldefined, though notional, masses, velocities, momenta). In the same framework, a seismic **event**, meaning a coherent arrival of wave energy to which we assign a well-defined history of propagation, reflection, and transmission, can be represented in one of two ways. Either a single particle, whose “world-line” is free to move both forwards and backwards in time, or several particles interacting through a specified set of the aforementioned productions and annihilations.

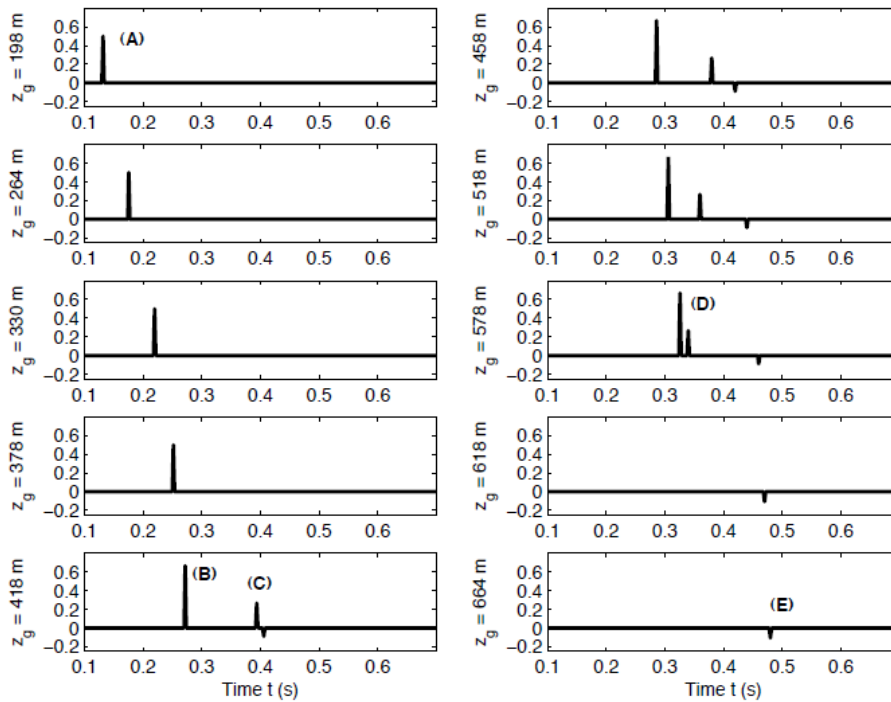


FIG. 1. We may view an event, in, e.g., a zero-offset VSP experiment, in terms of drifting and interacting particles. For instance a first order transmitted multiple appears as three interacting particles. In this Figure we see ten snapshots of the collision model “movie” of the process. At $z_g < z_1$, labelled (A), the multiple consists of a single particle drifting to the right. At $z_g = z_1$ it decelerates (B) and there is a spontaneous production of two more particles (C), one drifting to the right and one to the left. The original, now decelerated particle and the left-going newly created particle approach one another, colliding and annihilating (D) at $z_g = z_2$. The right-going particle drifts on in that direction (E).

A theoretical note on scattering and diffraction of radar waves from a seismic disturbance propagating in the near-surface

Kris Innanen

SUMMARY

A seismic disturbance alters the electrical properties of the Earth. This means, in principle, that within Earth volumes supporting both types of wave propagation, a radar wave field will tend to scatter from a seismic wave field. Given seismic disturbances with lengthscales on the order of that of the radar pulse, such interaction may be detectable as backscattering phenomena. Given seismic disturbances with length-scales much larger than that of the radar pulse, the interaction may be detectable as forward-scattering (e.g., anomalous traveltime) phenomena. Radar data with these characteristics would lend themselves readily to techniques of imaging-inversion, migration, and tomography, and would present the potential for providing “snapshot” images of a seismic wavefield during important stages of its evolution, e.g., as it propagates in poorly characterized and unconsolidated near surface structures. The relative magnitude of these effects are likely very small, and it is not clear whether they could be expected to rise above the noise level in realistic data sets.

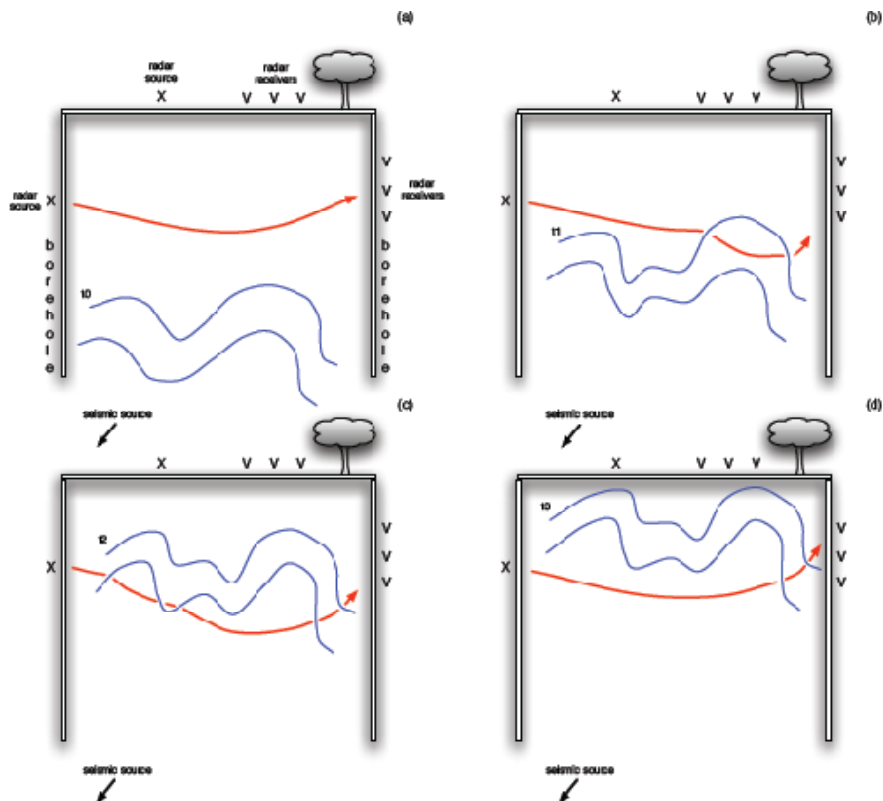


FIG. 1. Schematic diagram of radar transmitting through a seismic wavefield at four times during its propagation. (a)–(d) Times t_0 – t_3 respectively. With a (relatively) slowly varying seismic waveform assumed to induce a perturbation in medium electrical properties, an incident radar field is illustrated undergoing a perturbed, forward scattering process.

An acoustic description of nonlinearity in seismic exploration

Kris Innanen

SUMMARY

In 2008, the Priddis pump-probe experiment, in which the Earth was simultaneously subjected to a vibrating source and a transient source, was carried out by CREWES with the hope of detecting nonlinear behaviour in an exploration seismology setting. In this paper we present a theoretical description of such behaviour, assuming an acoustic medium. Through a simple extension of the order arguments by which the fluid equations are manipulated to form a linear wave equation on the pressure p_1 , we find a nonlinear equation for a corrective term, p_2 , such that in total the field, $p = p_1 + p_2$, is aware of the changes it itself makes in the medium through which it propagates.

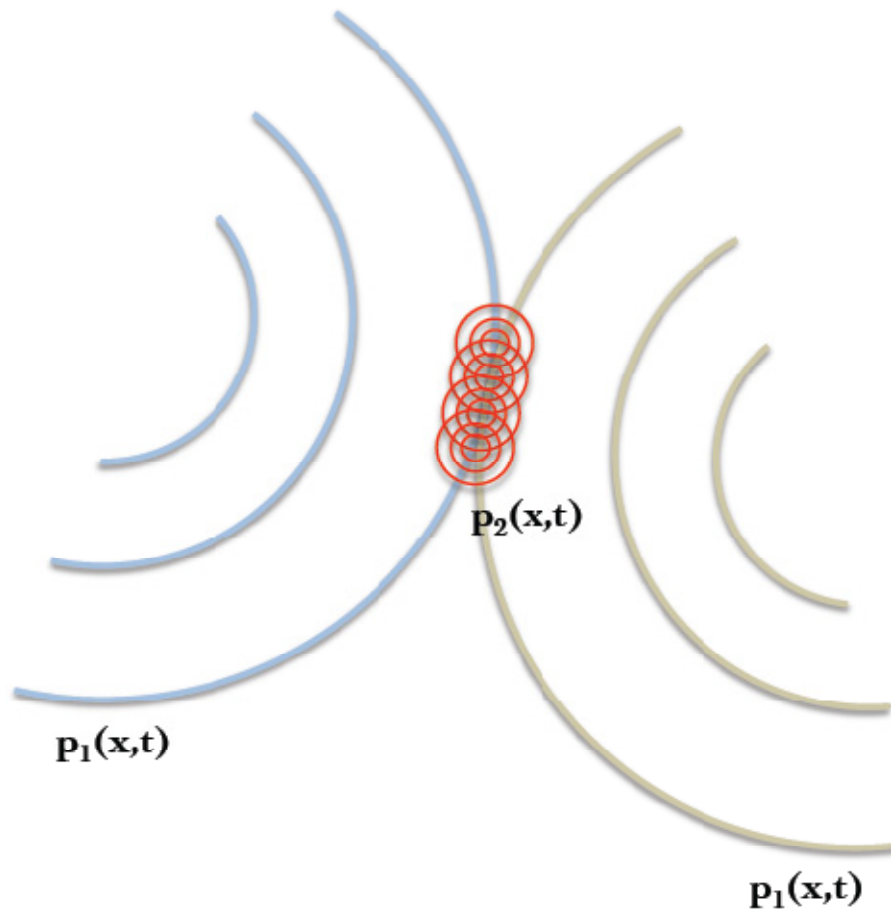


FIG. 1. Seismic waves alter the density and moduli of the Earth as they pass. In principle this means that two incident seismic fields might be seen to scatter from each other. Indeed the amplitude of a local portion of the seismic wave should be expected to influence itself, if its amplitudes are large enough. But if a wave, which depends on the properties of the medium it is in, changes those properties wherever it actually exists, how do you start the problem?

Decomposition of acoustic and elastic R_P into contributions from one-parameter reflection coefficients

Kris Innanen

SUMMARY

In AVO/AVA inversion, a linearized form of the Zoeppritz equations known as the Aki-Richards approximation and variants are used to model R_P . This approximation can be viewed as a linear decomposition of the full reflection coefficient into contributions from the reflectivities of individual medium parameters. A forward/inverse series framework leads to an alternative approach to this type of decomposition. The first order terms in the decomposition are qualitatively similar to the Aki-Richards approximation, with second and third-order terms correcting the approximation at large angle and large contrast. We test the approach both for acoustic and elastic reflection coefficients. In the elastic case, where forward/inverse methods of the kind we use require both the incorporation of R_P and R_S , we proceed in an approximate fashion using R_P only. The elastic nonlinear corrections, in spite of the approximation, provide a significant increase in accuracy over the linear/Aki-Richards approximation in several large contrast/large angle model regimes. Separately determining individual reflectivities could provide useful input to bandlimited impedance inversion algorithms, or the ability to extrapolate data from small to large angle.

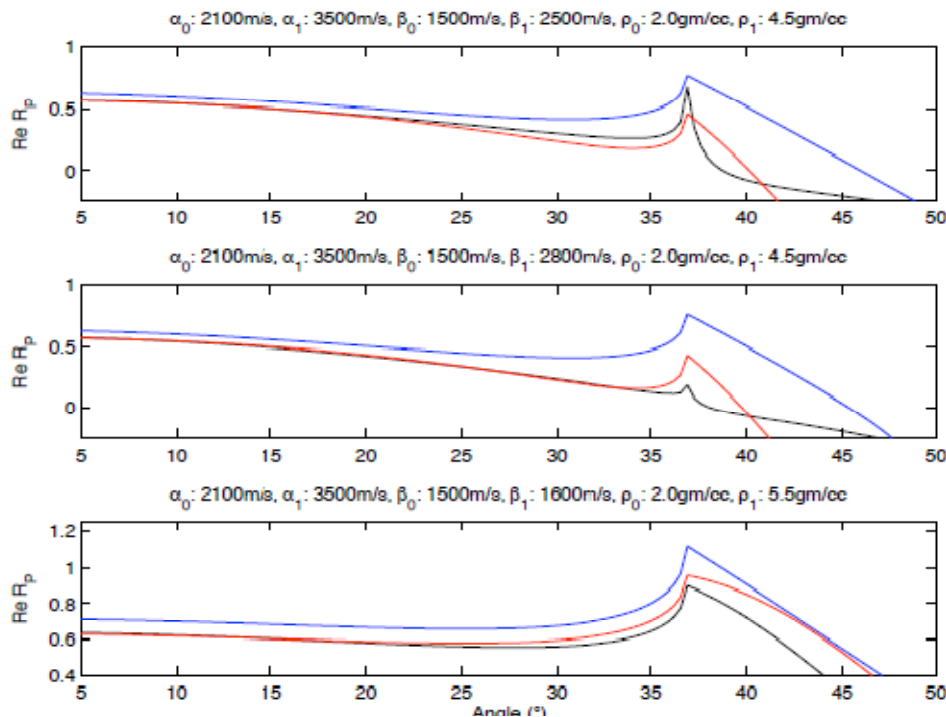


FIG. 1. Reconstitution of elastic R_P in terms one-parameter reflectivities illustrated for three large contrast examples. Black: exact R_P ; blue: linear; red: third order. This approximation seems to perform particularly well in comparison to the AR approximation when either all three parameters undergo large contrasts, or V_P and ρ undergo large contrasts.

Determination of time-lapse perturbations directly from differenced seismic reflection data

Kris Innanen* and Mostafa Naghizadeh

SUMMARY

Scattering theory is a natural framework within which to directly pose the time-lapse seismic inverse problem. Within that theory, if time-lapse difference data are identified with the scattered field, the perturbation becomes a direct measure of the time-lapse acoustic/elastic property and structural changes within the Earth volume of interest. A wave-theoretic relationship of this kind, free of nonphysical artifacts, is not easy to deduce otherwise: think of propagating a 2-way wave through a difference model with a single mobile interface, and the spurious multiples that would be created between the interface and *itself at a later time*. The main complication in the scattering description lies in the heterogeneity of the reference medium, which generates roughly as many reflections as the perturbed medium. Since most existing inverse scattering imaging/inversion methods assume a smooth, non-reflecting reference, the problem would appear to require a complete reformulation. Doing this provides us with both inversion methods of increased accuracy, and an explanation of why inconsistently posed methods do better than one might imagine they should. The complicating influence of the heterogeneous reference medium is suggestive that inversion be considered within certain special cases: multidimensional structural inversion within the linearized regime only, and linear or nonlinear inversion when analyzing a single isolated primary event to determine mechanical property variations within a known, fixed target.

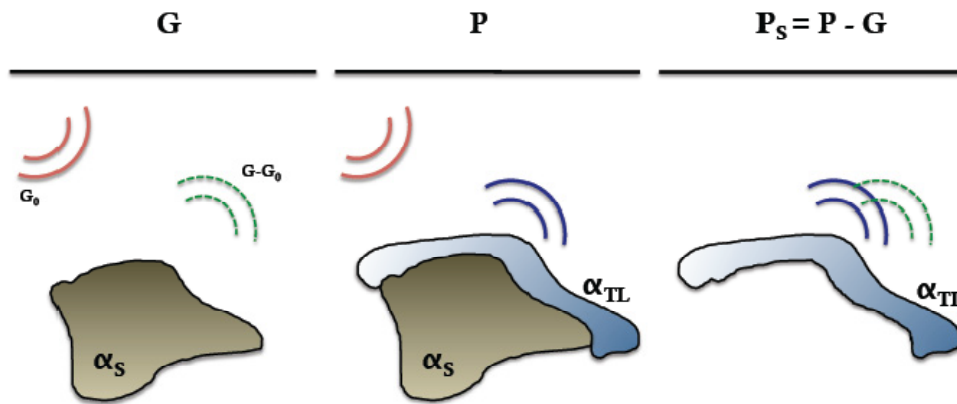


FIG. 1. An illustration of the multidimensional time-lapse scattering problem. To first order, the difference model α_{TL} is related to the difference data P_S as if it were a physical target embedded alone in the background reference medium. To second order and higher, the amplitudes of the scattered field are nonlinearly related to the difference model and the amplitudes in the baseline data amplitudes G . The perturbation framework we are setting out limits the model contrasts within which standard imaging algorithms may be applied to difference data, and provides corrective procedures for determining model parameters that lie outside those limits.

More absorptive AVF inversion - attenuating incidence media and general dispersion laws

Kris Innanen

SUMMARY

In this paper we review our 2009 discussion of direct inversion of absorptive reflectivity, discuss further the requirements for practical implementation, and extend the results to attenuating incidence media and more general attenuation laws. Frequency-dependent seismic field data anomalies, appearing in association with low- Q targets, have, on occasion, been attributed to the presence of a strong absorptive reflection coefficient. This “absorptive reflectivity” represents a potent source of information for determining subsurface rock mechanical properties, and may be of particular relevance to, e.g., reservoir characterization. Series expansions of absorptive reflection coefficients about small parameter contrasts and incidence angles can expose these anomalies to analysis, either frequency-by-frequency (AVF) or angle-by-angle (AVA). Within this framework, for instance, variations in P-wave velocity and Q may be separately estimated through a range of direct formulas, both linear and with nonlinear corrections. Algorithmically, it is a differencing of the reflection coefficient across frequencies that separates Q variations from variations in other parameters. This holds for both two-parameter (P-wave velocity and Q) problems and five-parameter anelastic problems, and would appear to be a general feature of direct absorptive inversion.

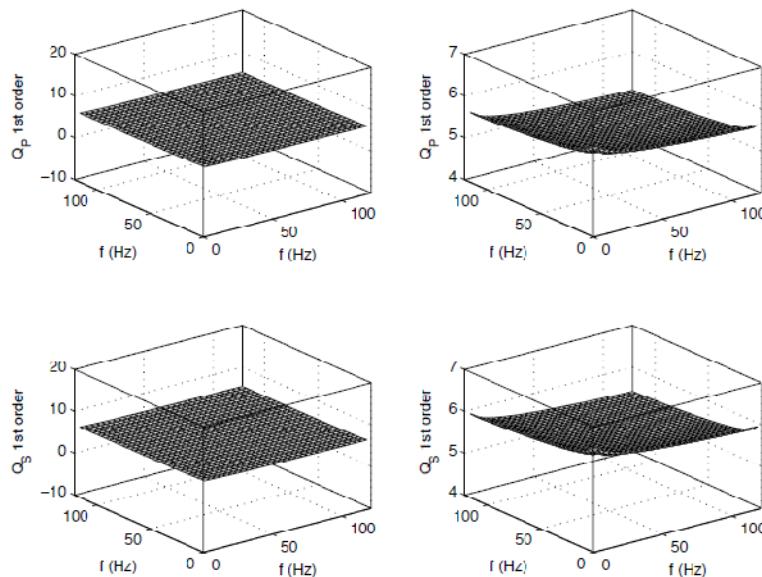


FIG. 1. Recovered Q_P and Q_S values accurate to first order (actual values $Q_P = Q_S = 5$) using exact synthetic R_P , R_S values as input for linear AVF inverse formulas, over a range of frequency pairs and with a fixed angle of incidence. Left column: recovered Q_P , Q_S values; right column: detail of same.

Towards an analytic description of anelastic diffraction, reflection, and conversion phenomena

Kris Innanen

SUMMARY

In this note we lay some of the groundwork for a scattering theoretic description of anelastic wave propagation. The aim is to create a framework for (1) describing the diffraction and conversion of anelastic waves in heterogeneous media, and (2) directly inverting P, S, and converted wave data taken over dissipative media. Here we take the simple but important step of expressing reference and perturbed anelastic wave equations in diagonalized forms, which are then prepared for inclusion in an appropriate Scattering, or Lippmann-Schwinger equation. As a side note we also consider appropriate situations for the use of a popular relationship by which Q_P is used to generate Q_S values.

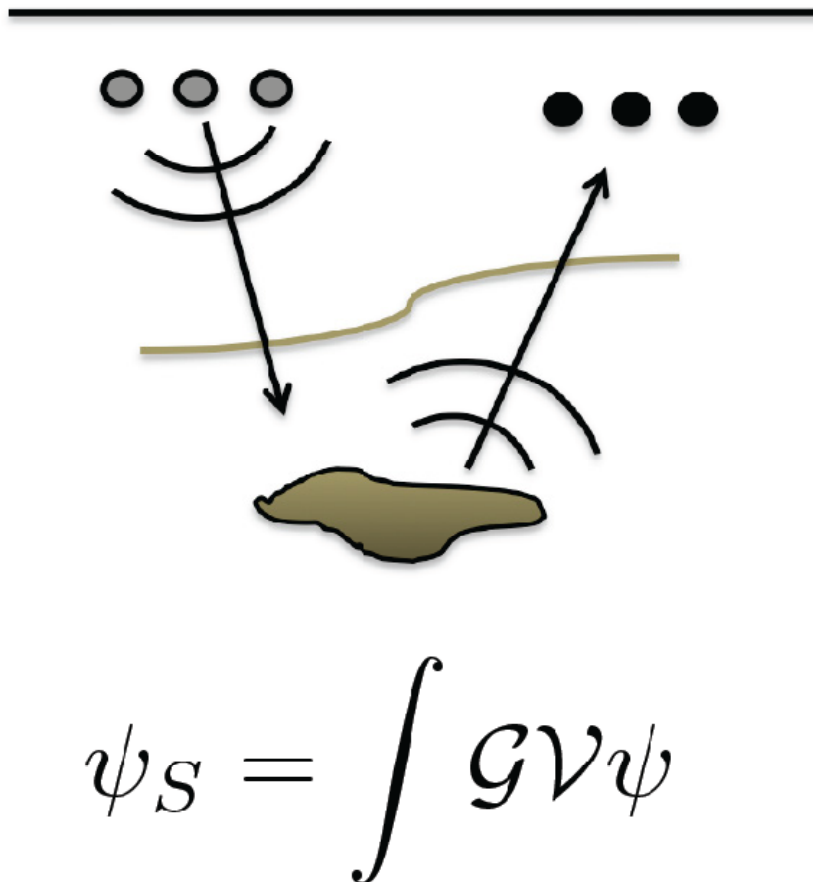


FIG. 1. The aim of anelastic forward/inverse scattering research is to pose in as general as possible a way the relationship between structures with the capability of dissipating seismic wave energy and the attenuated field.

Physical modelling of a 3D marine seismic survey

J. Helen Isaac, Joe Wong and Kevin W. Hall

SUMMARY

A pseudo-marine 3D seismic survey acquired over a physical model was processed and analysed. Although the data contain much noise and the waveform is variable and complex, the target is imaged on offset gathers and limited offset stacks. The target is imaged best on north-south inlines (which are parallel to the transducer array) stacked with limited source-receiver scaled offsets of 300-900 m.

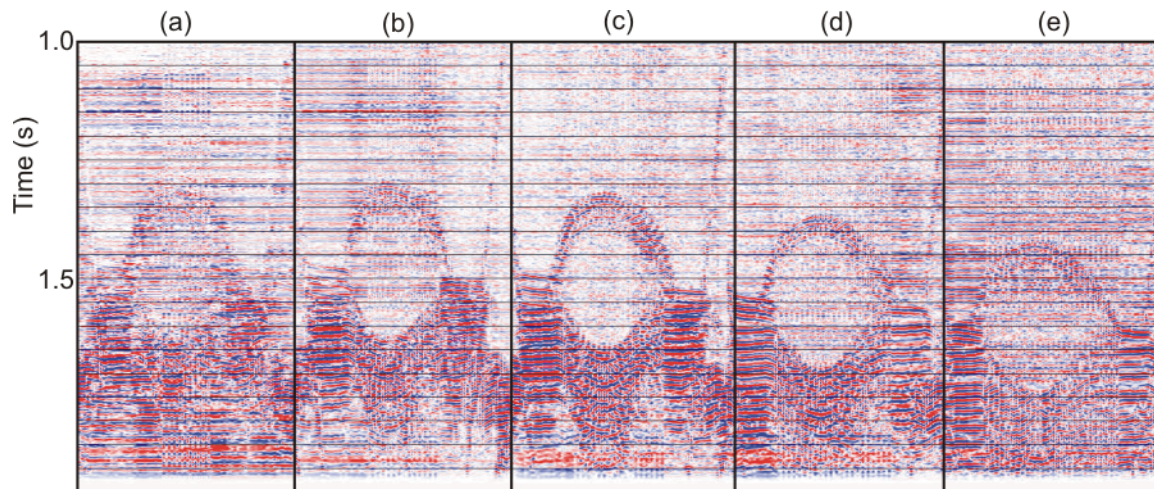


FIG. 1. Source-receiver offset gathers of north-south inline 4 over the limb of an anticline. The offsets are (a) 100 m, (b) 300 m, (c) 500 m, (d) 700 m and (e) 900 m.

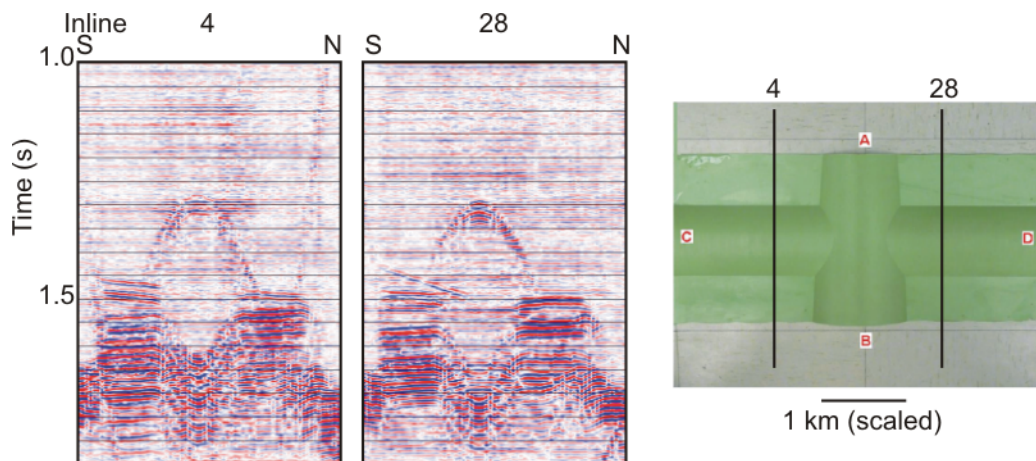


FIG. 2. North-south inlines 4 and 28 which cross the west and east limbs, respectively, of the C-D anticline. Offsets of 300-900 m were included in these stacks.

Integrated geological and seismic site characterization at Priddis, Alberta

J. Helen Isaac and Don. C. Lawton*

SUMMARY

2D and 3D seismic data have been acquired during field school in the last few years on and near university lands at Priddis, Alberta. The data were acquired so that we may characterize the shallowest 800 m for the purpose of future experimental CO₂ injection. Sandstones identified on gamma ray logs are assumed to be correlatable with sandstones observed in outcrop in the west of the study area and to strong reflectors seen on the seismic data. Two sands, termed the Middle Paskapoo A (MPA) and Lower Paskapoo (LP), are interpreted to lie at depths of around 440 and 770 m, respectively, below the surface in the centre of the 2010 Priddis 3D survey. The Lower Paskapoo sand is currently of particular interest as a CO₂ injection target.

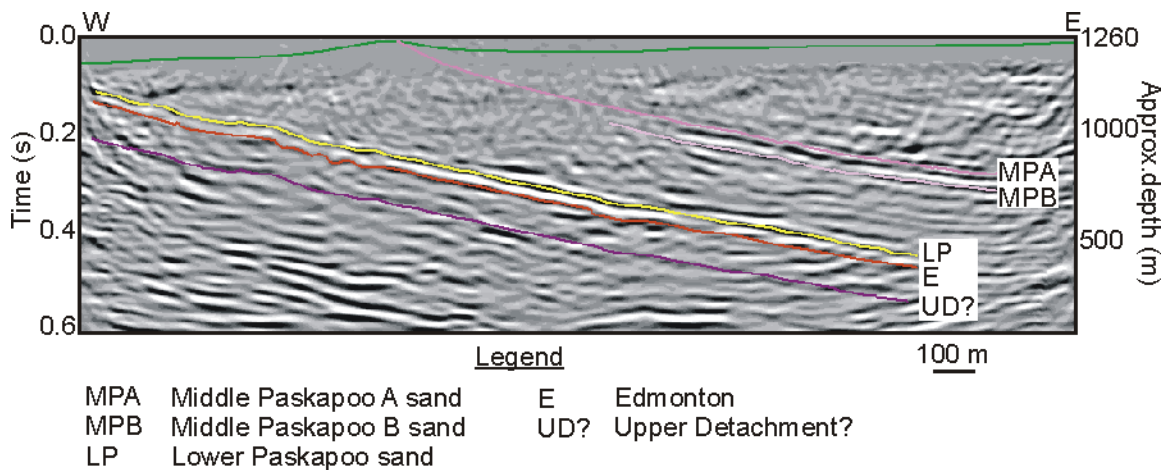


FIG. 1. Vertical component of the 2010 2D3C line.

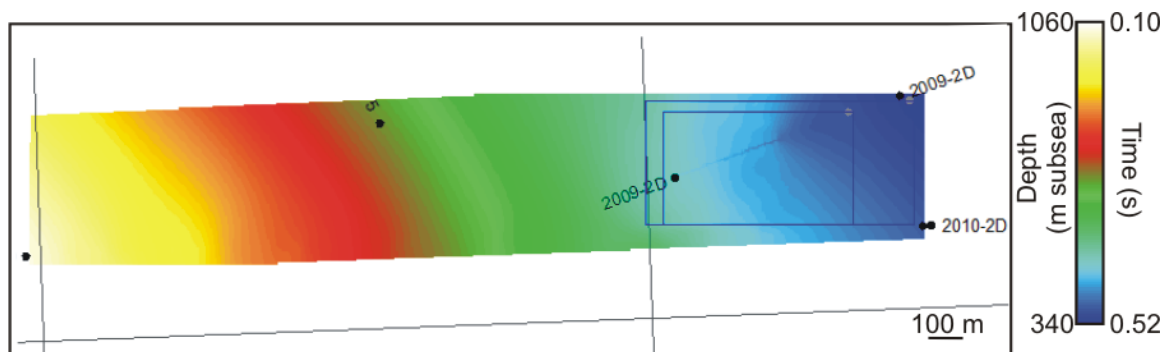


FIG. 2. Map of the Lower Paskapoo sand.

Processing of the 2010 field school 3D and 2D seismic data from Priddis, Alberta

J. Helen Isaac* and Don C. Lawton

SUMMARY

We processed the vertical component of 2D3C and 3D3C seismic data acquired at field schools near Priddis, Alberta, in 2010. The processing was designed to attenuate noise and enhance signal, especially in the section of interest above 0.5s. The quality of the data is good, especially on the prestack time migrated 2D line, where reflections can be seen almost to the surface in the western end of the line. The gentle easterly dip of the Neogene Paskapoo Formation and Early Cretaceous Edmonton Group can be seen above 0.5 s on the processed data. The Paskapoo Formation and Edmonton Group strata dip to the east above the upper detachment while below about 0.9 s the reflections are sub-parallel. The top of the Mississippian carbonate is imaged at 1.7 s.

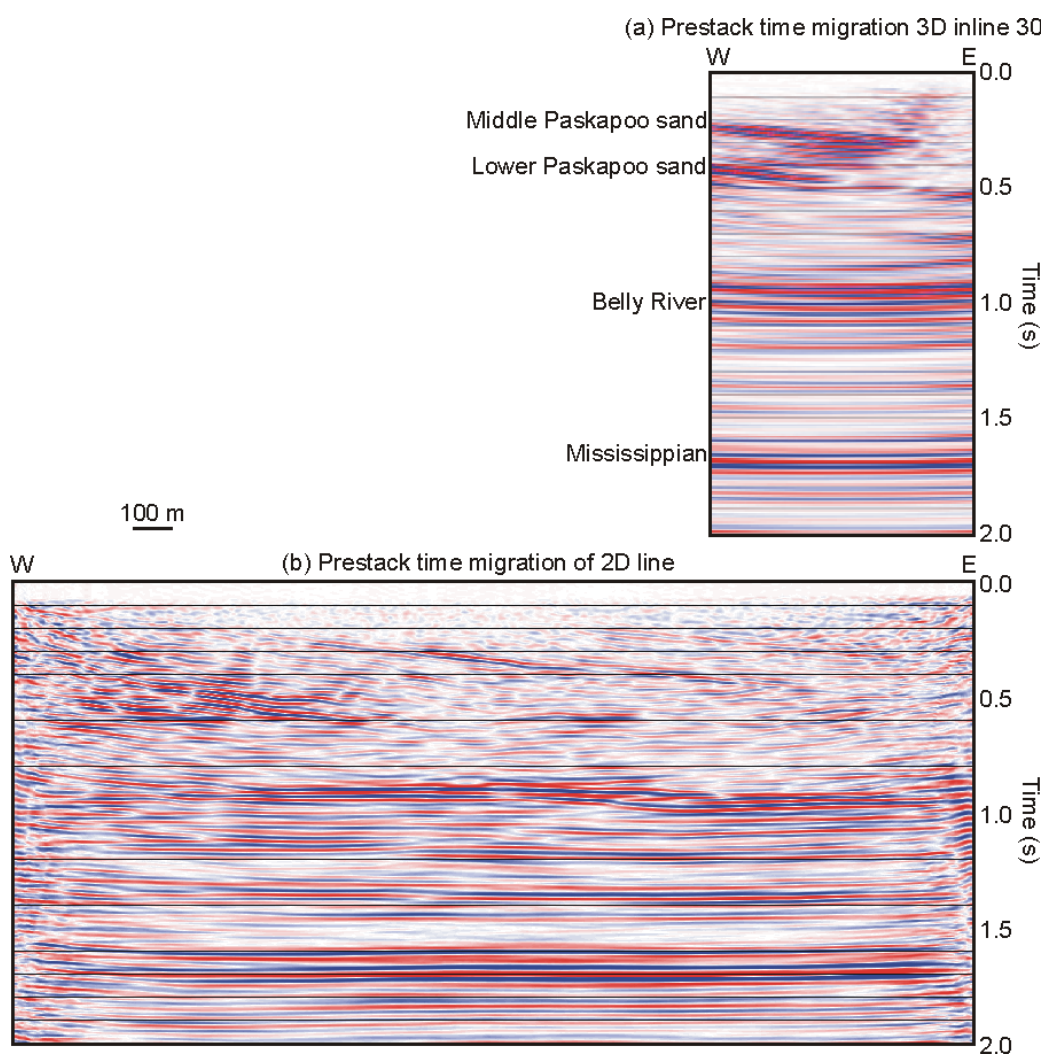


FIG. 1. Prestack time migration of (a) inline 30 from the 3D survey and (b) the vertical component of the 3C2D line. Both lines have had AGC applied.

Reverse-time migration imaging with/without multiples

Zaiming Jiang*, John C. Bancroft, and Laurence R. Lines

SUMMARY

One of the challenges with reverse-time migration based on finite-difference method is the problems of computational costs, in terms of free disk space and/or computational time. This report discusses the principle of a new imaging condition, referred as ‘first arrival imaging condition’, and shows the advantage of less computational costs of this method, compared to the widely used source-normalized crosscorrelation imaging condition for reverse-time migration. Principally, with crosscorrelation imaging conditions, all the multiples inside both forward modelling and reverse-time migration wavefields are involved; on the other hand, with the first arrival imaging condition, the multiples in the wavefields are not included.

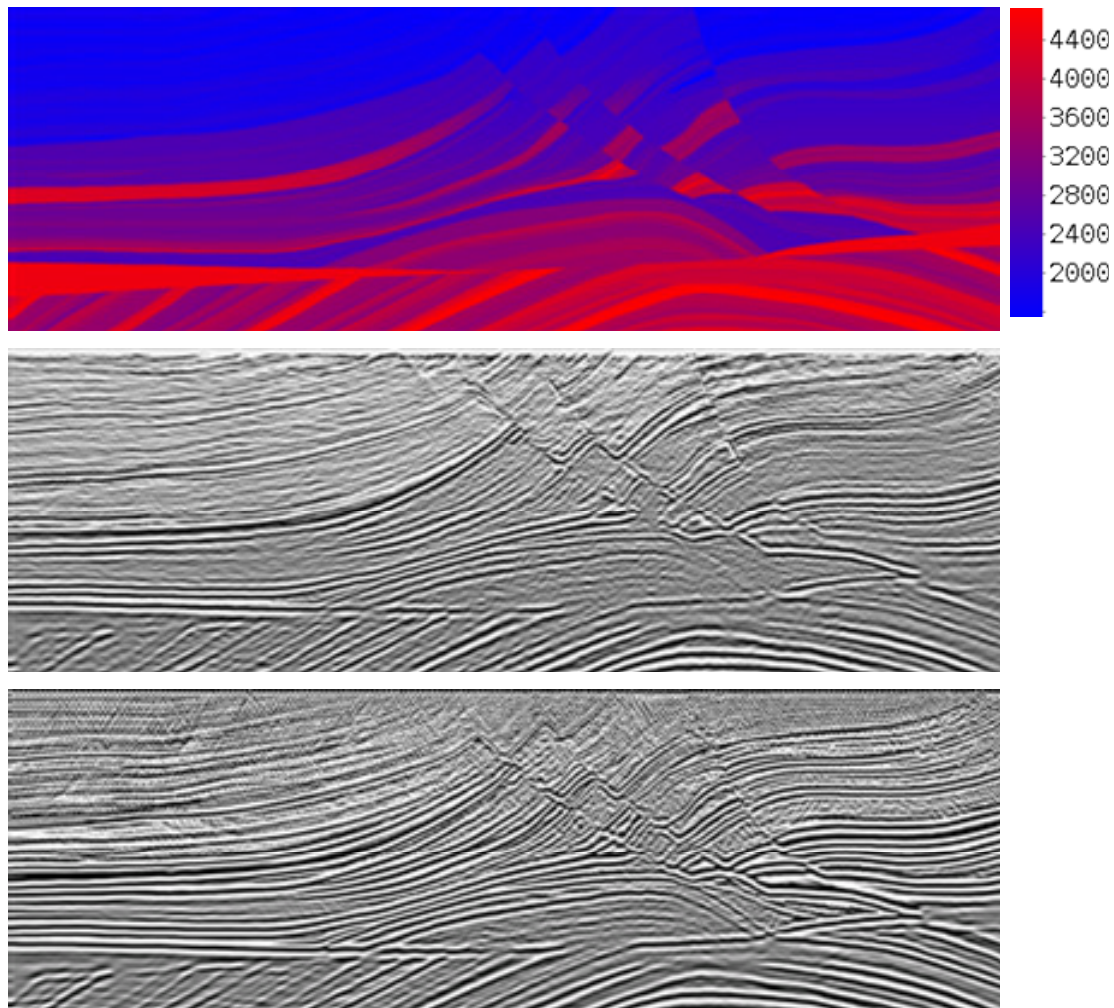


FIG. 1. (Top) A reduced set of Marmousi2, (middle) the result of reverse-time migration by source normalized crosscorrelation imaging condition, and (bottom) the result of reverse-time migration by first arrival imaging condition.

Rigid boundary conditions for staggered-grid modelling

Zaiming Jiang, John C. Bancroft, and Laurence R. Lines

SUMMARY

Staggered-grid modelling methods have been shown previously to be more accurate than non-staggered grid schemes when liquids are involved inside the subsurface models. This report shows that the staggered-grid modelling can also accurately simulate seismic activities when rigid boundaries are involved: the numerical modelling results accurately match the mathematical derivations and qualitative interpretations.

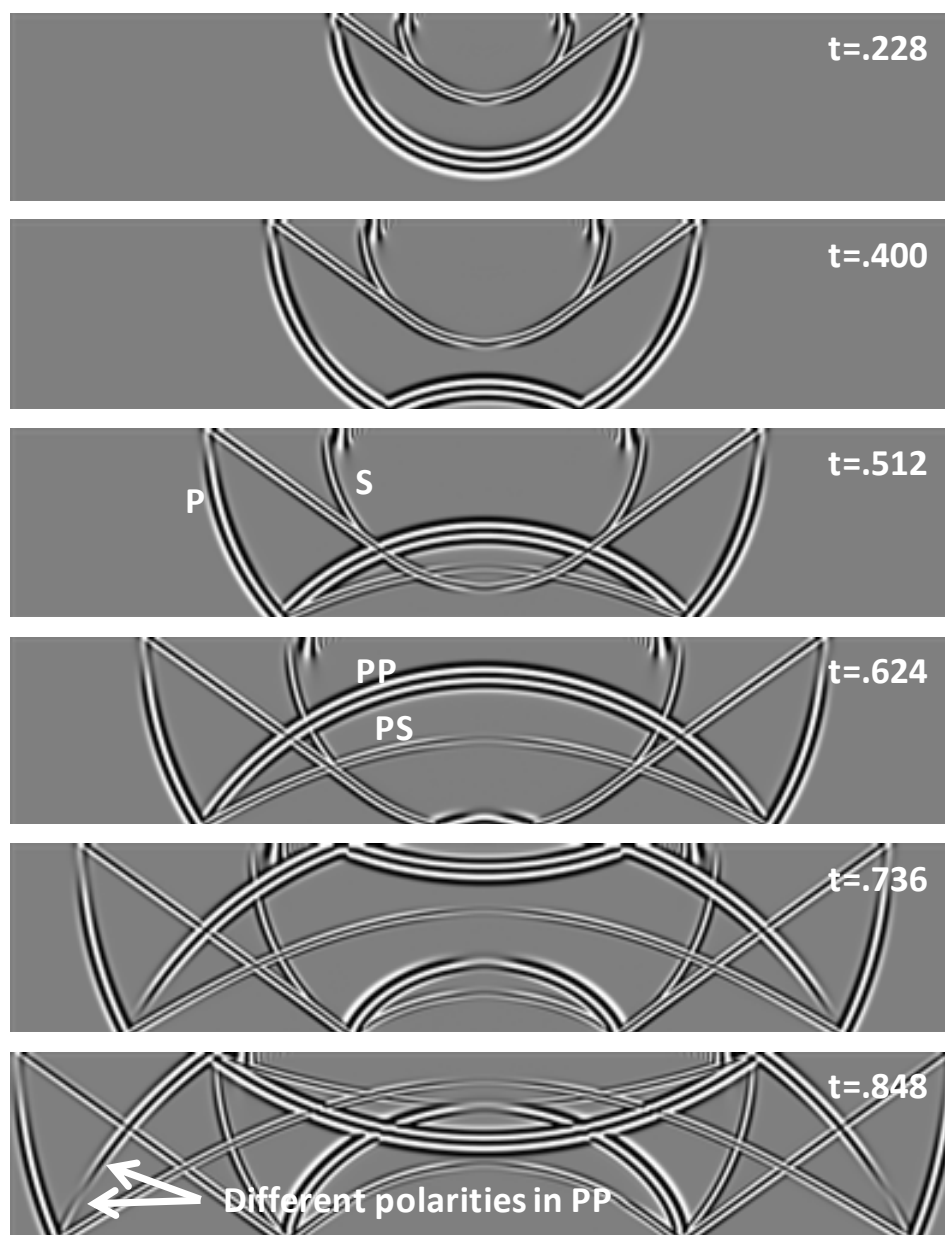


FIG. 1. Vertical component snapshots of numerical modelling in time order.

Comparison of three Kirchhoff integral formulas for true amplitude inversion

Hassan Khaniani, Gary F. Margrave and John C. Bancroft

SUMMARY

Seismic reflection data are the record of a wavefield that originates from a source location, propagates to the reflector, interacts with the reflectivity of the reflector, and returns to the receivers. According to Sun (Sun et al. 1998) the term true-amplitude migration is a new development of Kirchhoff-type migration that uses proper weighting function in the diffraction stack integral to construct the source pulse proportional to reflectivity.

This work summarizes and compares the literatures for three different theoretical approaches for true amplitude Kirchhoff depth migration inversion. These approaches are using paraxial ray theory (Schleicher, 1993), inverse scattering (Bleistein et al., 1987) and applying imaging condition on downward continuation of seismic data (Docherty, 1991).

As a comparison, for a geological model that has a simple and smooth structure, three weight functions are similar, however, as shown in Figure 1, in the complex structures, wavefronts may experience caustics along their path. In this case the formulation of Schleicher (Schleicher, 1993) weight function has advantages compared with the weight functions proposed by Bleistein (Bleistein et al., 1987) and Docherty (Docherty, 1991).

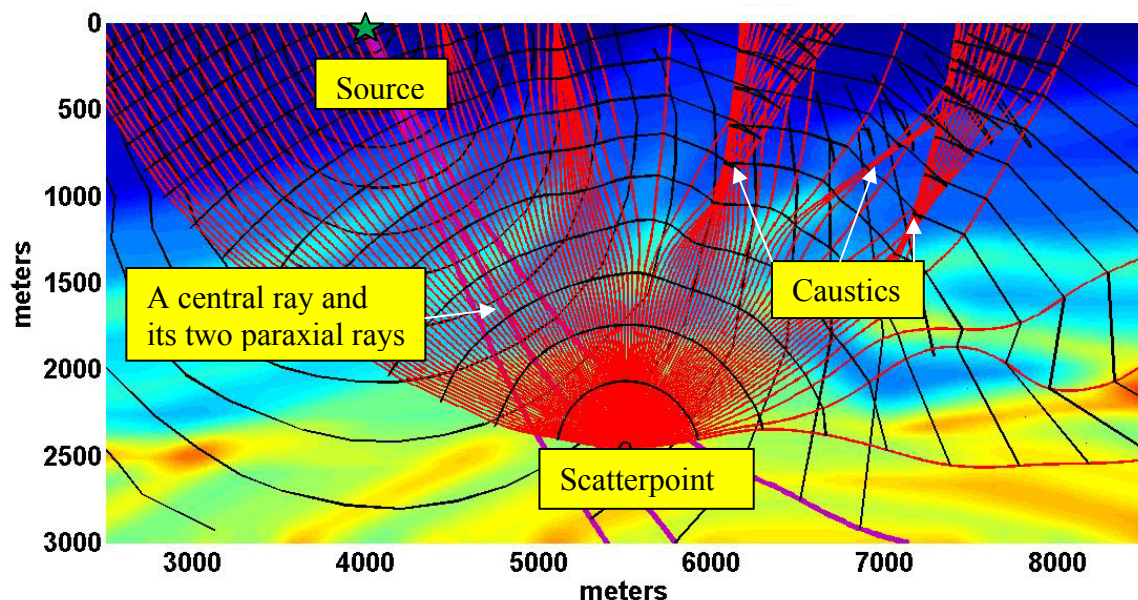


FIG. 1. Simulation for the ray paths and wavefronts of a wave that initiates from a source at (4000, 0) m of the model, then diffracts from (5500, 2500) m to the receivers. The velocity is taken from Marmousi model. Note the behaviour of the wavefronts and the caustics that it experiences.

Determination of velocity smoothing operator for prestack Kirchhoff depth migration by Common Scatter Point Gatherers

Hassan Khaniani and John C. Bancroft

SUMMARY

Optimum smoothing is required in ray based prestack Kirchhoff depth migration to handle complex velocity models. This ensures numerical consistency and validity of modeling of finite difference data using ray tracing methods. Conventional approaches to find an optimum smoothing operator for the velocity field are based on visual inspection of final migrated image which is a time consuming and expensive operation. In this work, to find optimum smoothing, we compared the modeled scatterpoint traveltimes from ray tracing method with corresponding CSP gathers. As an example, a scatterpoint response at coordination of (5500, 2450) m of Marmousi velocity models were selected. This point is located within a highly complex structure. As shown in Figure 1a, first the CSP gather formed from Marmousi synthetic data. Then we modeled the scatterpoint response with smoothing operator lengths of 50 m, 150 m, 250 m and 500 m. Figure 1b shows that the optimum smoothing length is 250 m because the modeled traveltimes has an optimum fit among other smoothing lengths.

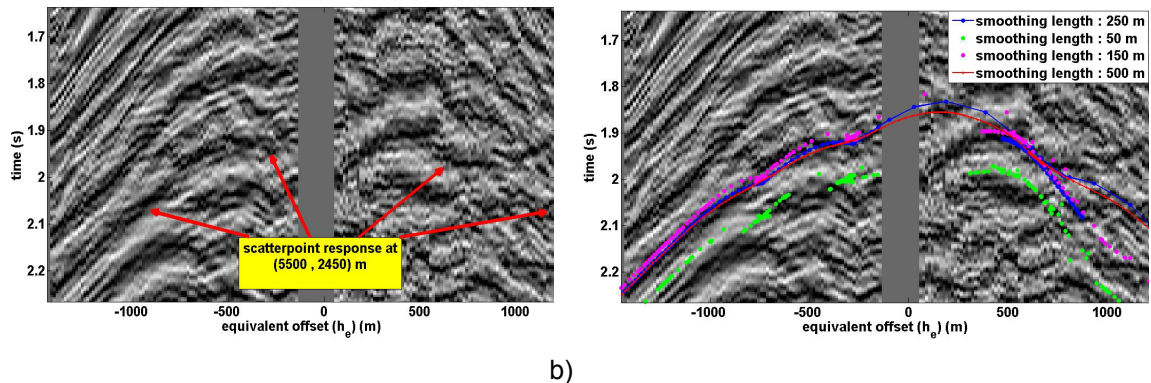


FIG. 1. (a) CSP gather formed at 5500 m from the left edge of the Marmousi model and the (b) modeled traveltimes by four modeled traveltimes curves computed from different smoothed velocities. Here, the blue curve is an optimum fit.

Enhancement of velocity field estimation by Common Scatter Point Gatherers

Hassan Khaniani* and John C. Bancroft

SUMMARY

Equivalent Offset Migration (EOM) maps the energy of DSR equation into an intermediate Common Scatter Point (CSP) gathers. Since the data in the CSP gathers are sorted in hyperbolic paths, it serves as a useful tool for velocity analysis. In this paper, we studied the behaviour of CSP gathers in areas that have strong lateral velocity variation. In this direction, we simulated a CSP gather of a model that has a dipping interface with lateral velocity changes. We observed that the traveltimes response in equivalent offset (h_e) domain is a tilted hyperbola that is not symmetric around vertical axis. The tilted hyperbola is the result of approximately a linear time shifts that depends to the dip angle and the amounts of velocity variation along the dipping interface. This effect reduces the resolution and accuracy of the velocity picking in the semblance plots. We removed the tilt effects by two approaches. First method is estimating the hyperbola parameters using a least squares fitting approach. The second approach is introducing a linear time shifted Radon transform to compute the tilt value in the corresponding semblance cube.

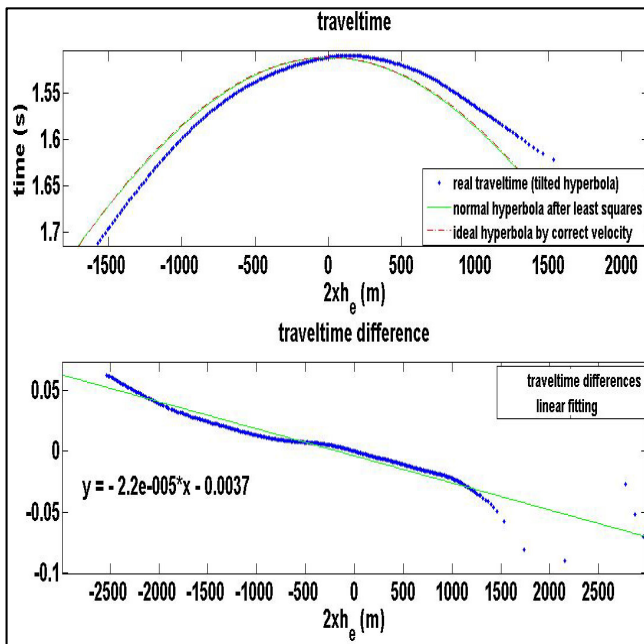


FIG. 1. This figure shows the tilt analysis of a CSP gather formed at 3200 m from left edge of Marmousi model. Comparisons of traveltimes of a CSP event at $t=1.5$ s (the red curve) with its estimated normal hyperbola (green curve) shows the expected tilt coefficient of $\alpha = -2.2 \times 10^{-5}$.

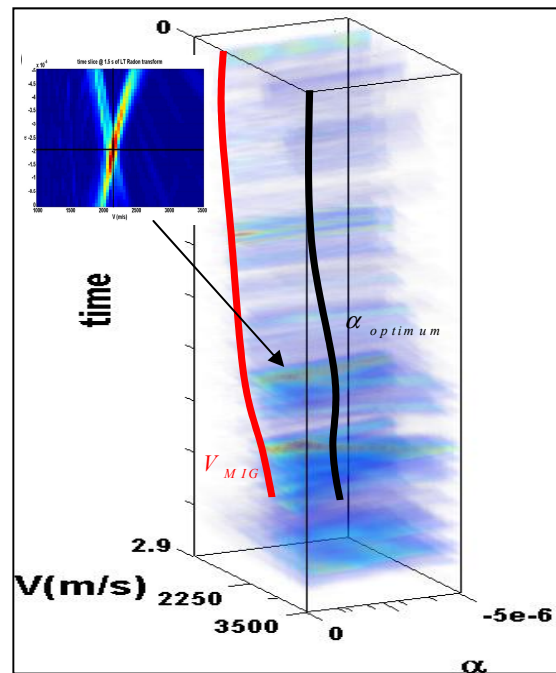


FIG. 2. This figure shows the semblance cube computed based on Linear Time shift hyperbolic Radon transform. The arrow from a semblance slice at time of $t=1.5$ s shows that an optimum focusing energies can be obtained by applying tilt coefficient of $\alpha = -2.1 \times 10^{-5}$.

Decomposition of surface consistent statics

Steve Kim and John C. Bancroft

SUMMARY

Traveltime differences between traces and a model trace may be decomposed into source and receiver statics. The decomposition of these statics is a difficult problem because the inversion process is rank deficient. The rank can be increased by adding a stabilizing equation to make the process invertible. Three stabilizing equations are tested and evaluated to demonstrate their effectiveness in stabilizing the process.

The results of one test is shown below. The figure contains the error plots of the first four trials out of a possible 100 trials, along with the standard deviation of all the trials. The standard deviation of the known statics was 0.010 sec, and the standard deviation of the noise (or jitter) was 0.001, for a signal to noise ratio of 10.

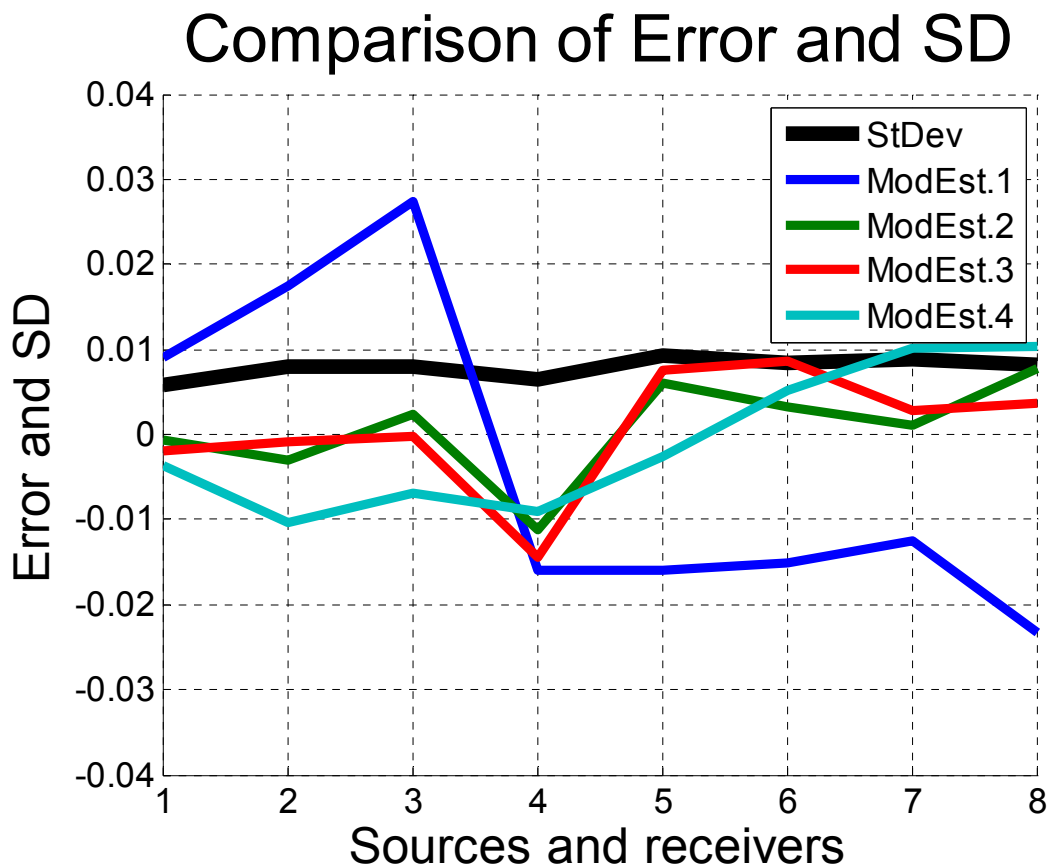


FIG. 1. The errors from four trial solutions are shown and the standard deviation of 100 trials are shown for one stabilizing equation.

Gabor multipliers for pseudodifferential operators and wavefield propagators

Michael P. Lamoureux*, Gary F. Margrave, and Peter C. Gibson

SUMMARY

We summarize some applications of Gabor multipliers as a numerical implementation of certain linear operators that arise in seismic data processing, including differential operators, nonstationary filters, and wavefield propagators. We demonstrate an approximation formula for pseudodifferential operators using Gabor multipliers. We present a demonstration of the almost factorization of Gabor symbols that is used in a fundamental way for nonstationary deconvolution. We give a numerical example of wavefield propagation through the EAGE salt model.

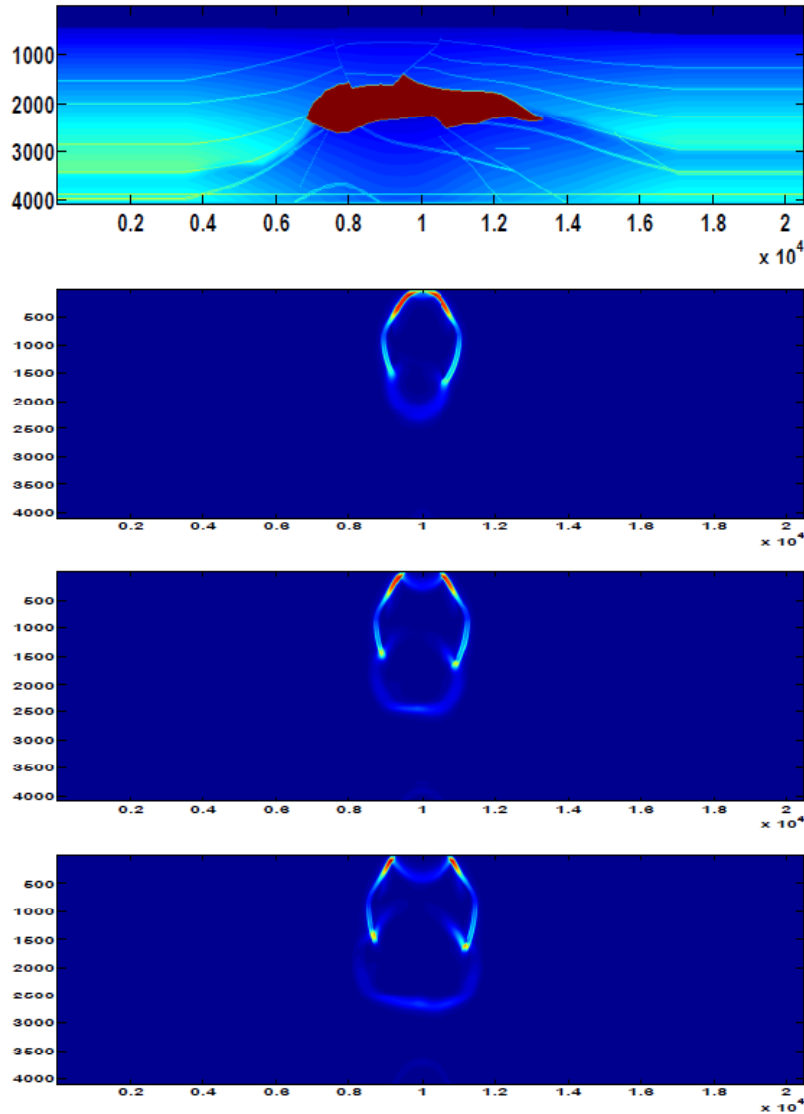


FIG. 1. Numerical simulation of acoustic wave propagation through the EAGE salt model.

Fluid substitution in coalbeds

Diane J. Lespinasse* and Robert J. Ferguson

SUMMARY

We present an evaluation of the seismic response due to fluids in the pore space of coalbeds. The objective of this project is to perform a fluid substitution in coalbeds and generate the associated synthetic seismograms by implementing a work flow previously developed to evaluate seismic as a monitoring tool for CO₂ sequestration in coals.

The Mannville coals are one of the most important coalbed methane resources in the Alberta Province, Western of Canada. In order to study the Mannville Group coals we selected the Corbett Field, located 145Km to the NW of Edmonton, as the area of study. In the Corbett Field the targets are two coal seams of the Mannville Group, the Main Seam with 4m thickness and the Lower Seam, with a thickness of 1.5m.

Using well log data from the well 100-03-22-062-06W500 of the Corbett Field, we perform a fluid simulation to make an assessment of its production forecast in a 10 years period and complete a fluid substitution. We use Gassmann equation to substitute 100% brine (initial state) in the pore space of Main Seam and Lower Seam by a combination of brine and methane.

We also present synthetic seismograms for coalbeds of 10m and 21m thickness in order to establish seismic resolution limits.

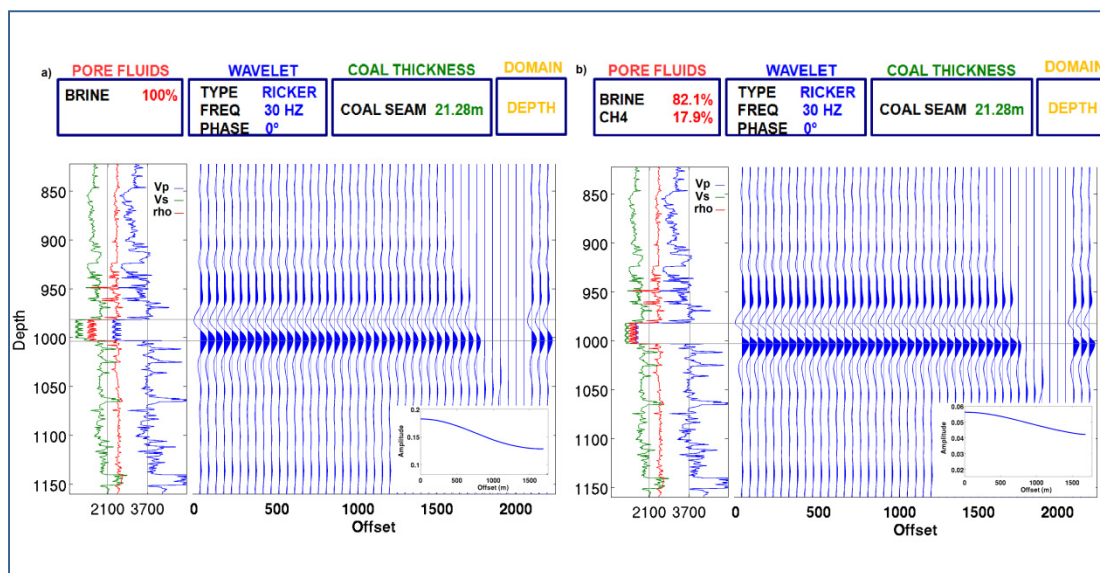


FIG. 1. Depth domain synthetic seismograms for a 21.28m coalbed, generated with a 30Hz zero phase Ricker wavelet. a) Coalbeds are saturated with 100% brine; b) coalbeds are saturated with 82.1% brine and 17.9% methane.

The robustness of reverse-time migration for imaging noisy sparse foothills data

Laurence R. Lines and P.F. Daley

SUMMARY

Seismic data from the Canadian Foothills are often noisy and sparsely sampled with missing traces. We show that reverse-time depth migration (RTM) provides a robust means of imaging sparse noisy data. Traditional RTM computes finite-difference (FD) solutions to the wave equation while back propagating the reflected wavefield to the reflector location at depth. The FD stencil will provide an effective means of interpolating missing traces during the migration process since this implicit interpolation essentially allows the seismic wavefield to heal itself during propagation. The FD operator also provides an effective means of suppressing random noise. Following earlier work by Zhu and Lines (1996), we illustrate the effectiveness of RTM on model data and real data from the Canadian Foothills.

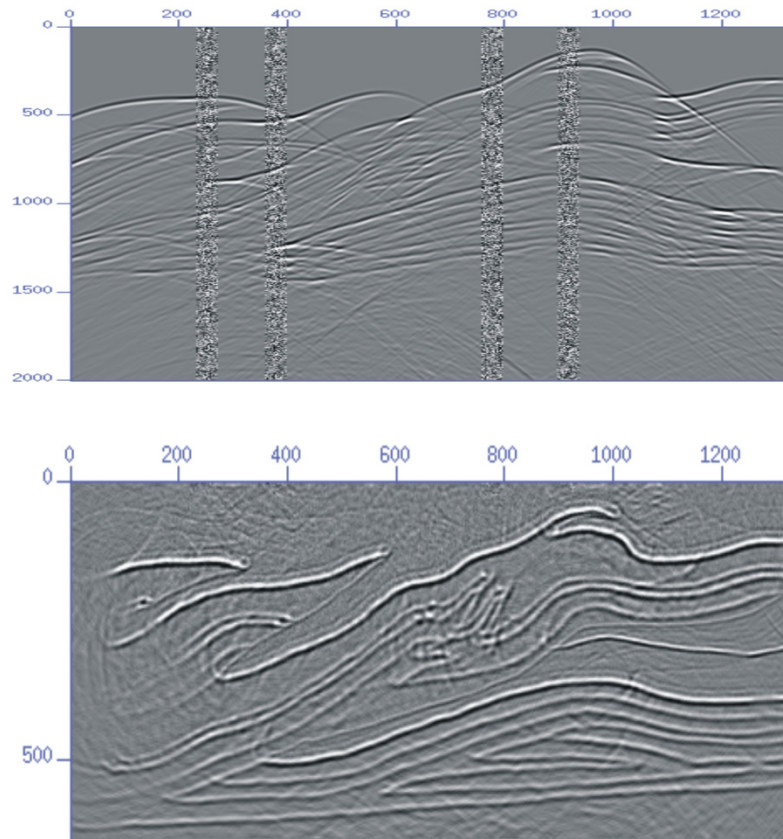


FIG. 1. This figure demonstrates the robustness of reverse-time depth migration by comparing a input time section (top) with noisy traces to the resulting reverse-time depth migration (bottom). The input seismogram has four intervals with noisy traces. The resulting depth migration is very similar to the depth migration of a noiseless seismic section whenever the noisy or missing trace gap is less than the size of a Fresnel zone.

CREWES channel model: description, acquisition, interpretation and data release

Heather J.E. Lloyd and Gary F. Margrave

SUMMARY

The CREWES Channel Model was created in 2008 as a 3D volume of P and S wave velocities plus density. This 3D model represents a 120m channel interval with gradient overburdens derived from the Blackfoot field in Southern Alberta, Canada. The channel was modelled after the present day Bow River and so represents no specific buried channel, but is thought to be typical. Recently this model was used to create a synthetic seismic data using a fully elastic finite difference software package. The data set contains over 1525 shot records with 3C receivers placed on a 10m by 10m grid for each shot. A 2-D line was then selected from the data as an example and to identify its processing flow. This flow includes a bulk time shift of 0.1 seconds, a mute to remove the first breaks, and a F-K filter to remove the ground roll. A pre-stack Kirchhoff migration was then applied to the data creating a section showing undulations in the reflections indicating variations in the channel interval. This data set is very large and is available to sponsors by request.

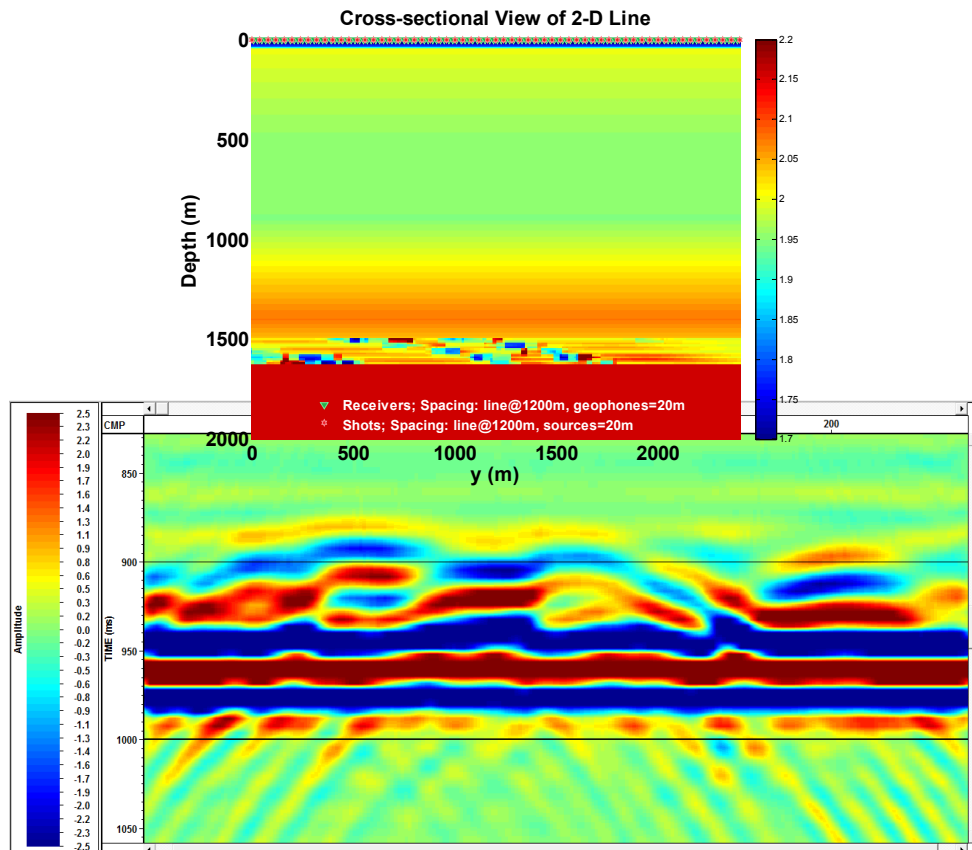


FIG. 1. V_p/V_s ratio and Kirchhoff migrated section of line parallel to channel.

New MATLAB functions for reading, writing and modifying SEG-Y files

Heather J.E. Lloyd, Kevin W. Hall and Gary F. Margrave

SUMMARY

The SEG_Y_Toolbox for MATLAB is a new set of tools that allow SEG_Y files to be read, modified and written. This toolbox adheres to the SEG-Y Revision 1 standards set out in the SEG Y rev 1 Data Exchange format publication. Unlike previous SEG-Y MATLAB tools this toolbox tries to be as flexible as possible when reading SEG-Y files but very stringent when writing SEG-Y files. Currently the following tools are available: `SEG_Y_EditTextHeader`, `SEG_Y_StandardizeHeader`, `SEG_Y_endianSwap`, `SEG_Y_getData`, `SEG_Y_getHeader`, `SEG_Y_getTraces`, `SEG_Y_read`, `SEG_Y_readHeader`, `SEG_Y_readMulti`, `SEG_Y_setHeader`, `SEG_Y_write`, `SEG_Y_writeHeaders`, and `SEG_Y_writeTraces`. Please contact the authors if any further functionality is desired.

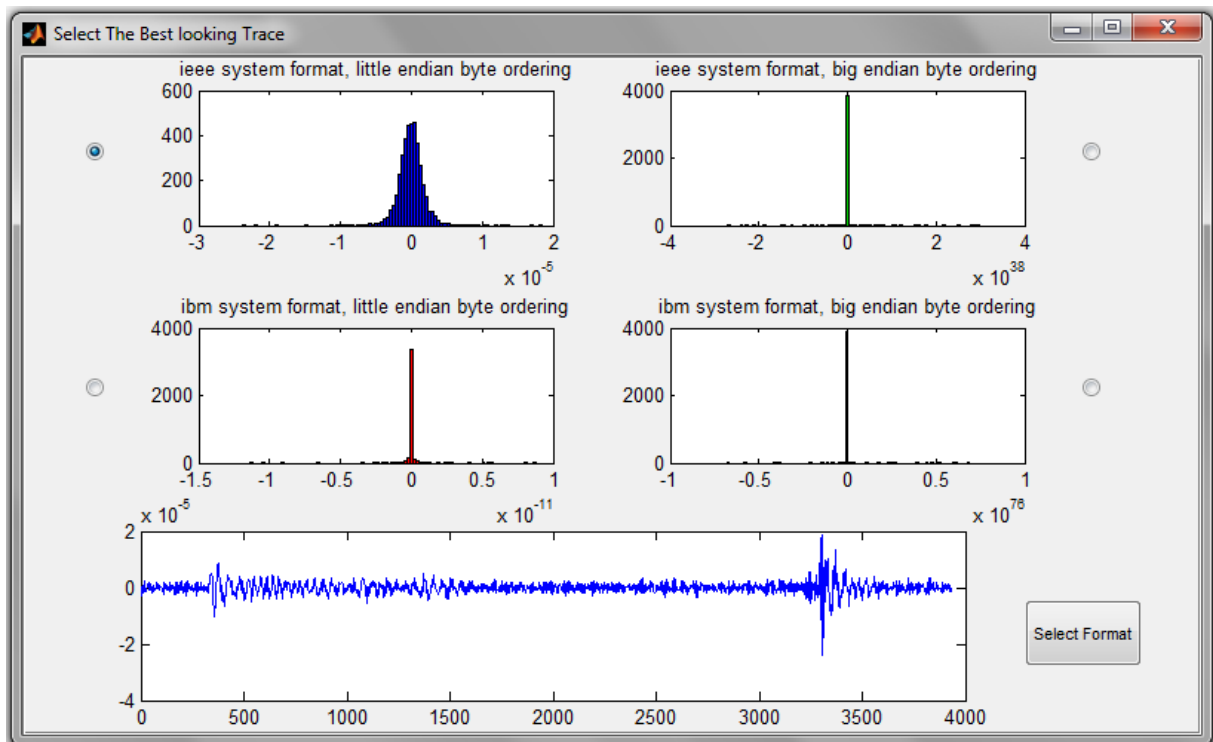


FIG. 1. This figure shows the trace format graphical user interface that helps the user identify the trace format. The four top plots are histograms of the data when decoded using different file formats. The lower window is a plot of the trace using the selected format indicated by the radio button (in this case the upper left option).

Evaluation of ice-coupled and elevated GPR antenna acquisition on ice

Tyler MacFarlane and Robert J. Ferguson

SUMMARY

Two acquisition methods for near surface Ground Penetrating Radar (GPR) are compared for acquisition in ice-over-fresh-water-over-ground environments. In the first method, the antennae are coupled directly to the ice as in conventional acquisition. In the second approach, the antennae are elevated 0.5 m above the ice surface to mimic floatation of the antennae. Numerical comparison of reflectivity suggests that no significant degradation of signal results from elevation of the antennae relative to the ice-coupled. We verify the numerical result with a real-data acquisition at Ghost Lake, Alberta. Data acquired over the same linear traverse are compared, and no significant degradation of the target signal, ice-thickness and the lake bottom, is apparent.

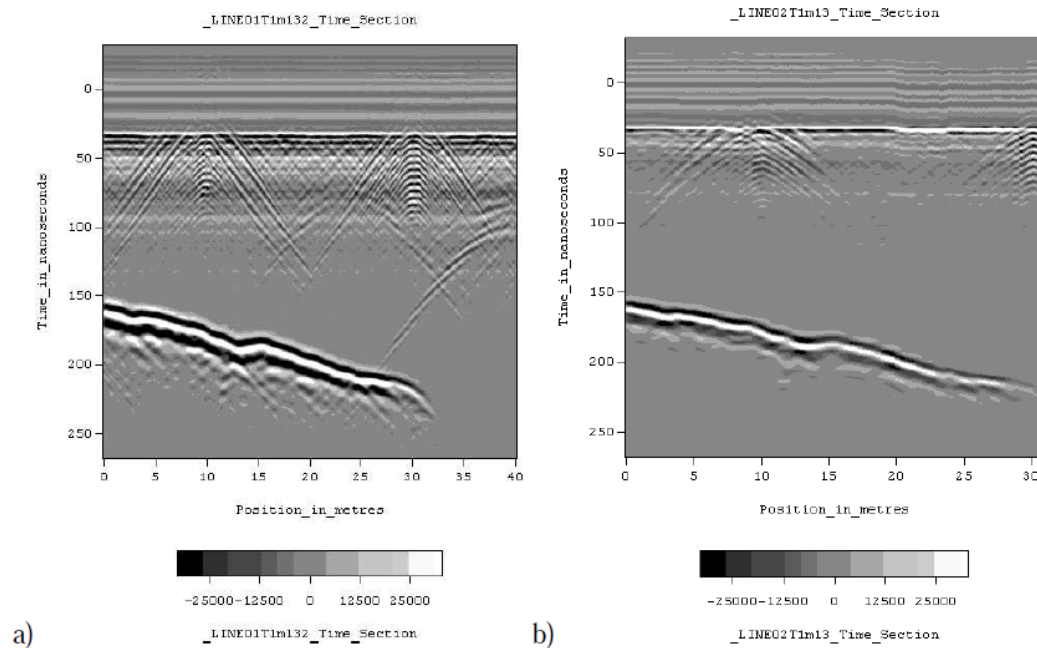


FIG. 1. a) Ice coupled Line 01 migrated. b) Elevated Line 02 migrated. Elevation of the GRP acquisition unit speeds acquisition without a severe amplitude penalty.

Determining elastic constants of an orthorhombic material by physical seismic modeling

Faranak Mahmoudian*, Gary F. Margrave, P. F. Daley, Joe Wong, and Eric Gallant

SUMMARY

Vertically fractured media are commonly described by an HTI (horizontal transverse isotropy) model, which is a degenerate case of the more general orthorhombic symmetry. To study the seismic effects of such a medium, a model from phenolic LE material, which exhibits the orthorhombic symmetry, was constructed. To characterize the anisotropy of the phenolic model the set of nine elastic constants is determined. Elastic constants are most often found from measurements of the phase velocity in a variety of directions, but finding this plane-wave velocity is problematic. Instead of the phase velocity, group velocity, which can be measured easily and more reliably, is used. Scaled physical modeling experiments in the laboratory, in which ultrasonic elastic waves are propagated through the phenolic model, are used to measure the P- and S-wave group velocity in different directions in the principal planes. A linear expression between the P-wave group velocity in an arbitrary direction and elastic constants, has allowed us to estimate all nine elastic constants. Although actually slightly orthorhombic, the phenolic model exhibits approximate HTI symmetry requiring only five elastic constants to characterize the medium.

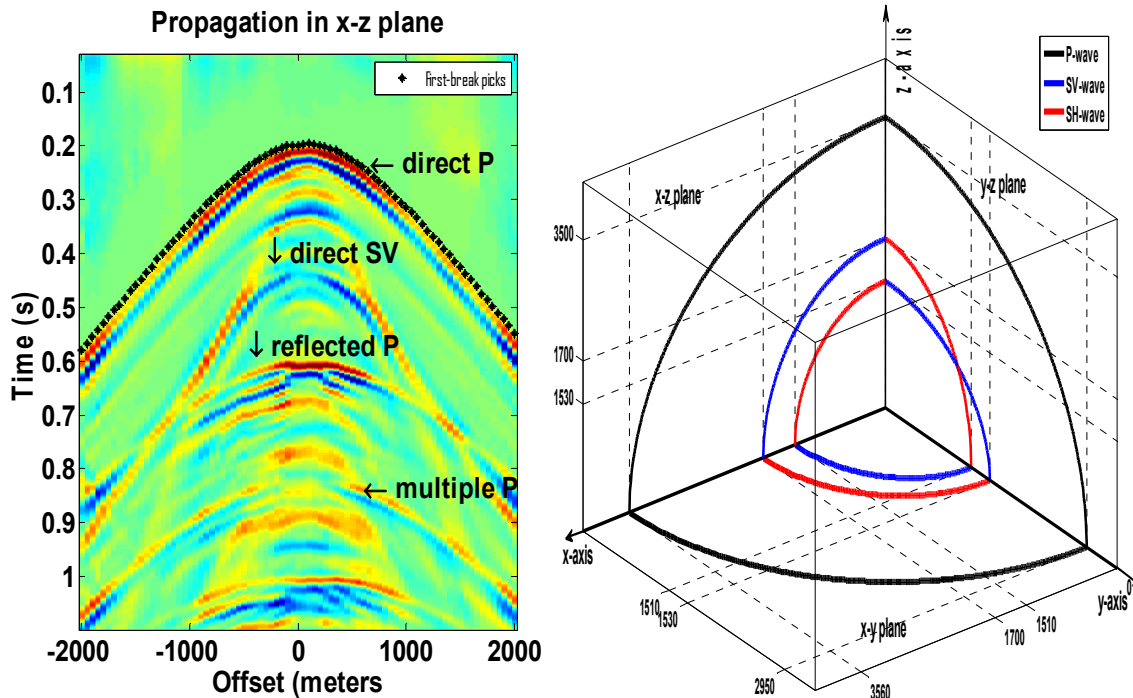


FIG. 1. (left) Vertical component data of a transmission shot gather. (right) The illustration of the P- and S-wave group velocity surfaces of the phenolic model.

2D finite-difference modeling in Matlab, version 1

Peter M. Manning

SUMMARY

An updated CREWES 2D elastic finite-difference modeling program is offered for general use. It has many of the features of the original workbench version, but it may be set up so that very little Matlab coding is required. The program runs from two ascii files which must be named and stored in the working directory. The first file describes the geology, and is easiest to use for layer cake cases. The second file specifies how the finite-difference gridded data is obtained from the geology file, and gives the parameters of the finite-difference operations. The main controls of the program are by menu, and besides the main command to start the computations, there are commands to save or continue computations, and to output in various ways. An essential feature of this version is the capacity to apply a wavenumber correction filter.

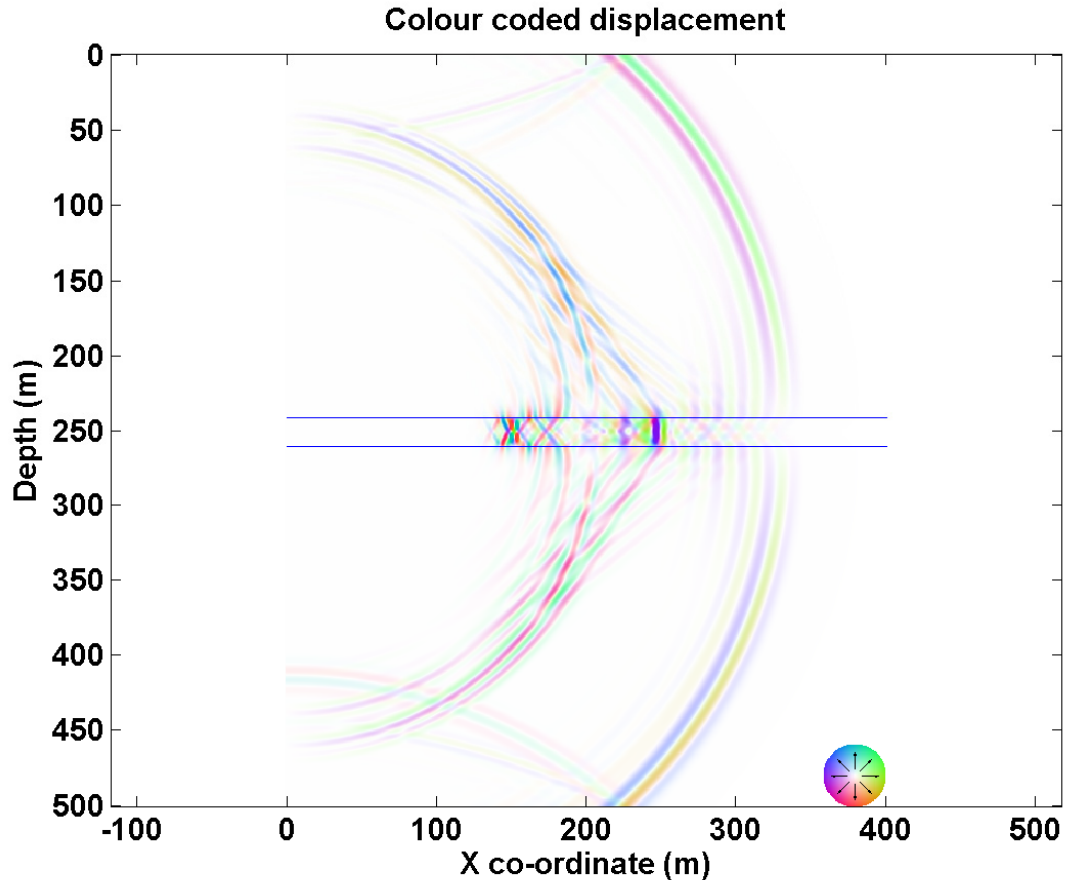


FIG. 1. The program was used to model this seismic response of a 300 Hz source within a 20 m. low velocity zone. The headwaves create complex wavefields from a relatively simple geological model.

Correction filter use in finite-difference elastic modeling

Peter M. Manning

SUMMARY

Correction filtering of the finite-difference elastic wavefield has been found to be a practical and efficient process. In a particular case shown, the cost of the beneficial effects was obtained by using a minimal convolution filter with an overall size of 3 by 3 points, and this resulted in a 80 percent increase in run times. Comparable results obtained by reducing sampling intervals required a one third reduction, which cost a 180 percent increase in run times. Further tests showed that the particular corrections filter set used was still quite effective when used on models with velocities 25% lower than the design velocities.

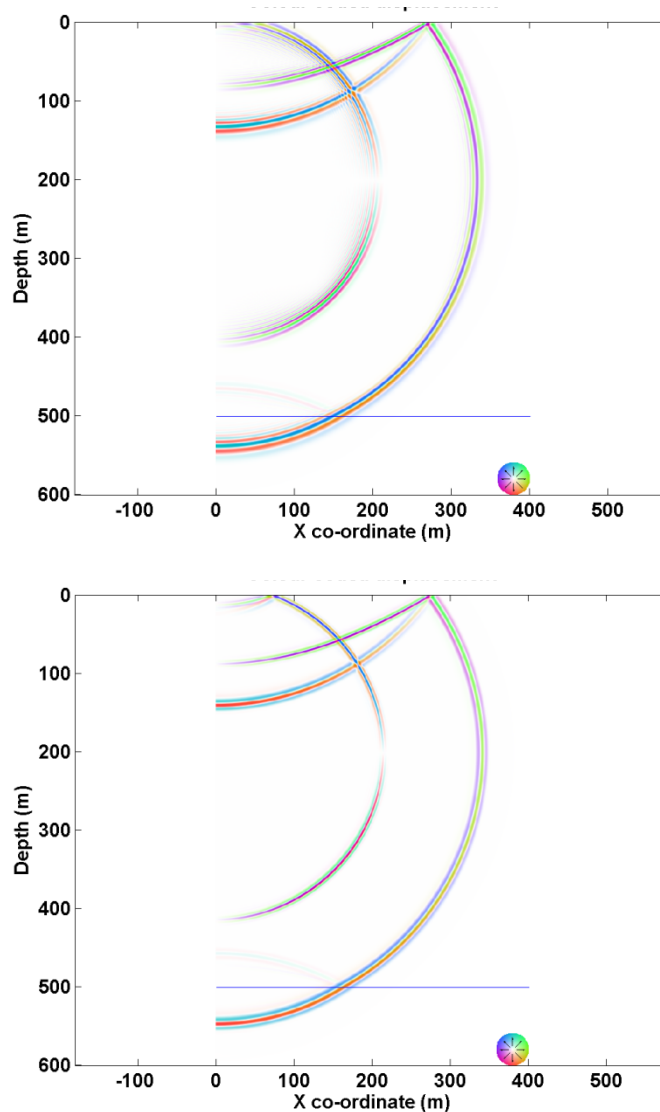


FIG. 1. Uncorrected wavefronts (top); corrected (bottom). Corrections give narrow wavelets and preserve their zero-phase character, shown by the symmetric colour patterns.

Full waveform inversion with wave equation migration and well control

Gary F. Margrave*, Robert J. Ferguson and Chad M. Hogan

SUMMARY

We examine the key concepts in full waveform inversion (FWI) and relate them to processes familiar to the practicing geophysicists. The key theoretical result behind FWI is presented as a mathematical theorem, the Fundamental Theorem of FWI. This theorem says that a linear update to a migration velocity model can be obtained from a reverse-time migration of the data residual, or the difference between the actual data and data predicted by the model. Critically, this migration is only proportional to the required update and the proportionality must be estimated. We argue that in many cases this proportionality factor will be complex-valued and frequency dependent, or in the time domain, a wavelet. The estimation of the velocity update from the migrated section is closely related to the common process of impedance inversion. Then we argue that FWI can be viewed as a cycle of data modelling, migration of the data residual, and calibration of this migration to deduce the velocity update. We present an extended example using the Marmousi model in which we use wave-equation migration of the data residual and we calibrate the migration by matching it to the velocity residual (the difference between actual velocity and migration velocity) at a well. Our example produces an encouragingly detailed inversion but raises many questions.

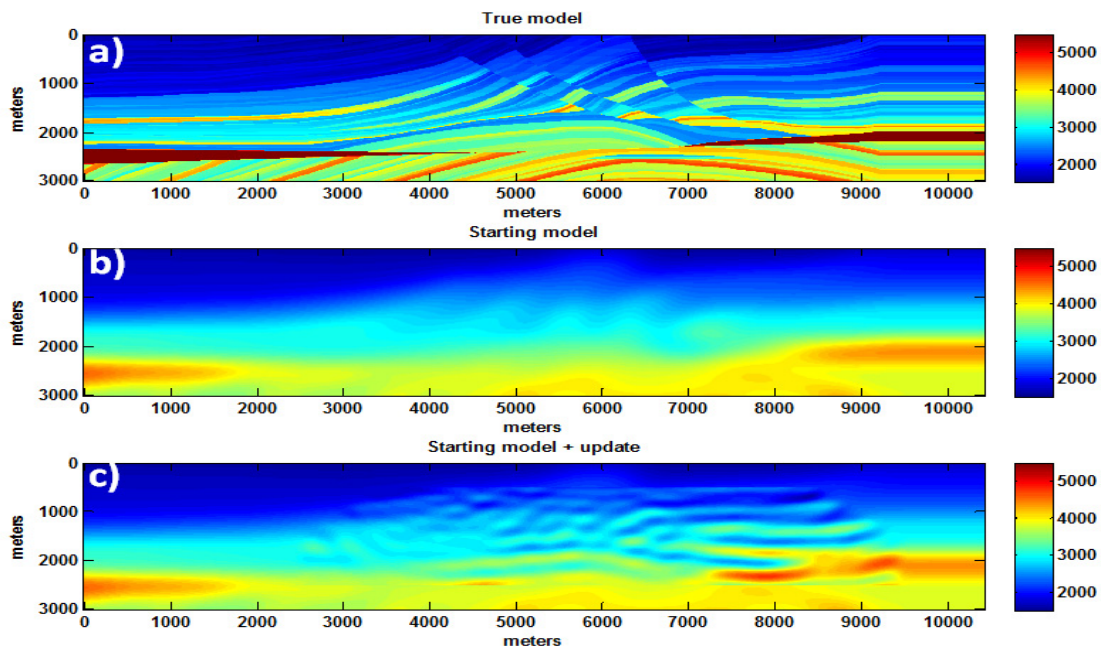


FIG. 1. a) The exact Marmousi velocity model. b) The smoothed starting model used in the migrations of 0-5 Hz data. c) The velocity model after updating with the calibrated migration stack. The update was a scaled and phase rotated version of that stack. The phase rotation and scale factor were estimated at a well at 6000m.

Nodal Galerkin methods for numerical modelling of linear elasticity

Matthew A. McDonald*, Michael P. Lamoureux and Gary F. Margrave

SUMMARY

We consider here a method for numerical propagation of elastic waves in heterogeneous media based on the weak formulation of the elastodynamic equilibrium equations. Find $u \in \mathcal{H}$ such that, for all $t \geq 0$,

$$\langle \rho \ddot{u}, v \rangle_{\Omega} + a(u, v) = \langle f, v \rangle_{\Omega} + \langle T, v \rangle_{\Gamma}, \forall v \in \mathcal{H}. \quad (1)$$

This is converted to a second order system of ordinary differential equations for the nodal values of the displacements in Ω at time $t > 0$,

$$M\ddot{U}(t) + A\dot{U}(t) + KU(t) = F(t),$$

which is evolved in time by the relationship

$$\left[M + \frac{dt}{2}A \right] U(t_{j+1}) + [dt^2K - 2I] U(t_j) + \left[M - \frac{dt}{2}A \right] U(t_{j-1}) = F(t_j).$$

The method provides high accuracy in the spatial domain and converges exponentially. It is appropriate for any formulation of the elastic wave equation in any number of spatial dimensions, but for simplicity is only presented here for isotropic media. Absorbing boundary conditions are incorporated into the method naturally and in the conclusion we compare various implementations of the method to second and fourth order finite differences.

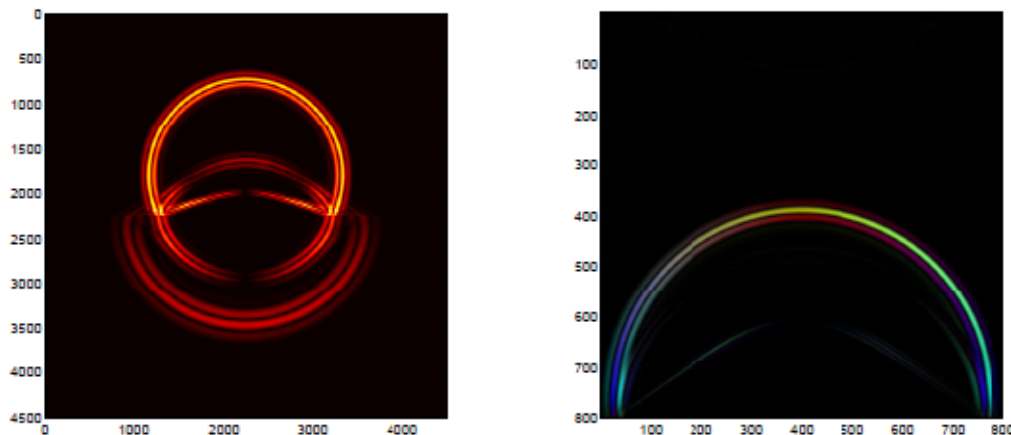


FIG. 1. Numerically propagated P-wave through a jump in the velocity model (left), and at the edge of a model with Stacey P3 absorbing boundary conditions (right). The left figure shows the 2-norm of the displacement and the right figure is colour-coded to direction of displacement (legend in full text).

A least-squares shot-profile application of time-lapse inverse scattering theory

Mostafa Naghizadeh and Kris Innanen

SUMMARY

The time-lapse imaging problem is addressed using least-squares shot-profile migration. The procedure for designing forward (de-migration) and adjoint (migration) operators of shot-profile wave-equation migration algorithm is explained. The least-squares optimization of the problem is achieved using conjugate gradients. Two main approaches for least-squares shot-profile migration of time-lapse data namely, inversion of difference data and joint inversion, are discussed. Some practical considerations for performance of least-squares shot-profile migration are investigated using synthetic data examples. Also, a synthetic data examples is provided for examining the time-lapse shot-profile migration of difference data.

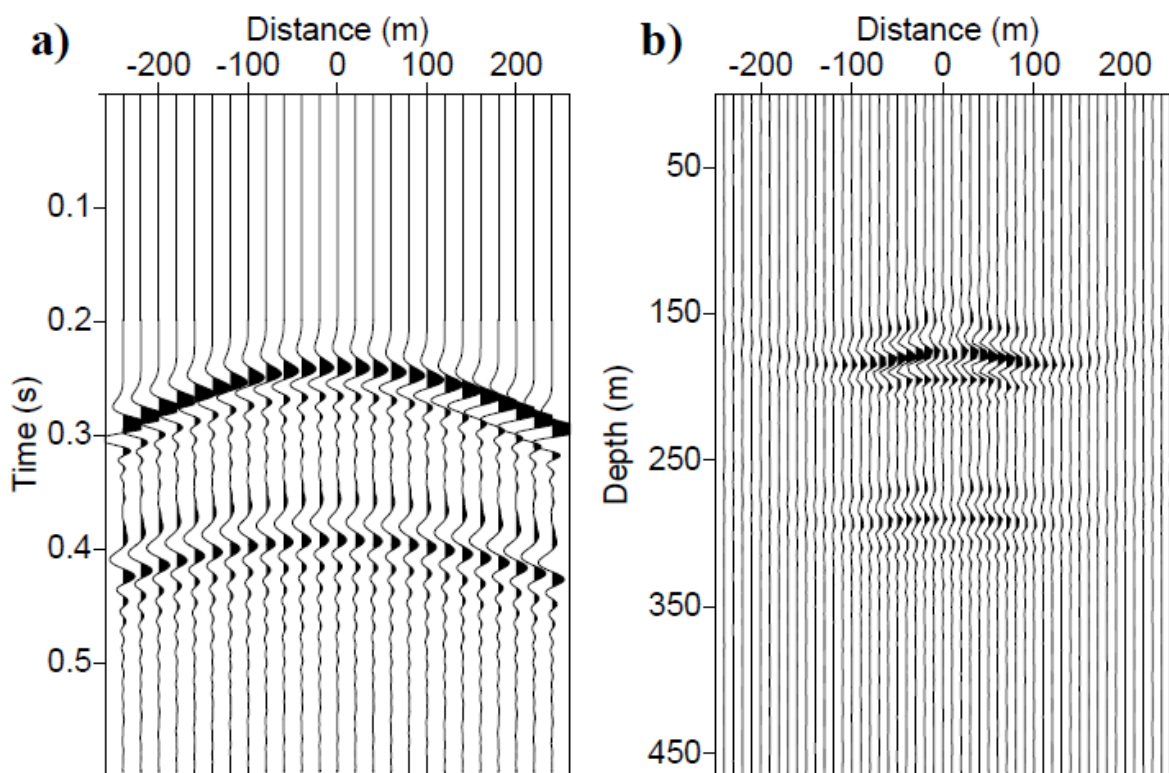


FIG.1. a) The difference section between the base and monitor surveys. b) Migrated data using the least-squares shot-profile migration.

Seismic data interpolation using a fast generalized Fourier transform

Mostafa Naghizadeh* and Kris Innanen

SUMMARY

We propose a fast and efficient method for interpolation of nonstationary seismic data. The proposed method utilizes fast generalized Fourier transform (FGFT) to identify the space-wavenumber evolution of nonstationary spatial signals at each temporal frequency. Next, a least-squares fitting scheme is used to retrieve the optimal FGFT coefficients representative of the ideal interpolated data. For randomly sampled data on a regular grid we seek a sparse representation of FGFT coefficients in order to retrieve the missing samples. Also, to interpolate the regularly sampled seismic data at a given frequency, we use a mask function derived from the FGFT coefficients of the low frequencies. Synthetic and real data examples are provided to examine the performance of the proposed method.

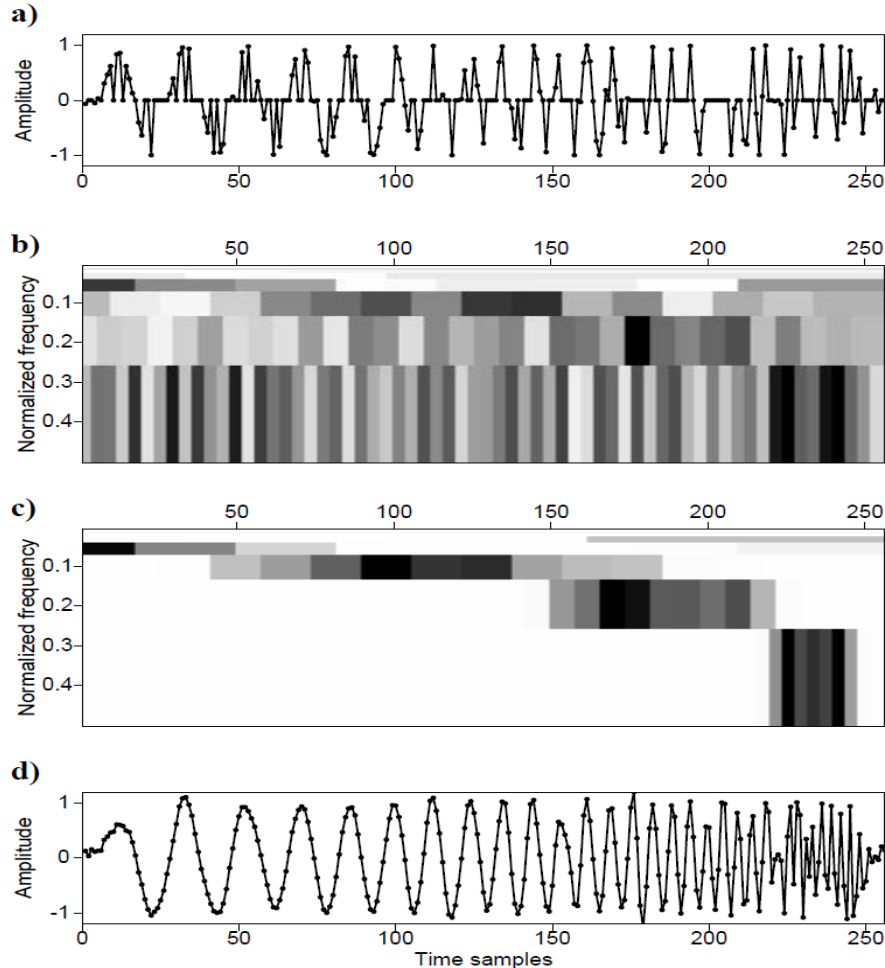


FIG.1. a) Randomly sampled chirp function by randomly replacing 50% of original samples with zeros. b) 2D plot of FGFT coefficients of (a). c) Retrieved FGFT coefficient using algorithm 8. d) The reconstructed chirp signal using the FGFT interpolation.

Azimuthal anisotropy of Hudson Bay using seismic interferometry

Agnieszka Pawlak and David W. Eaton

SUMMARY

The Hudson Bay basin is the least studied of the four major Phanerozoic intracratonic basins in North America, which include the hydrocarbon-rich Williston, Illinois and Michigan basins. Using azimuthal anisotropy results in conjunction with isotropic group velocity maps from previous work, we can further focus our study on determining the formation and regional crustal structure beneath Hudson Bay. Twenty-one months of continuous ambient-noise recordings have been acquired from 37 broadband seismograph stations that encircle Hudson Bay. These stations are part of the Hudson Bay Lithospheric Experiment (HuBLE), an international project that is currently operating more than 40 broadband seismograph stations around the periphery of Hudson Bay. The inter-station group-velocity dispersion curves found from noise-generated seismic-interferometry studies, also known as ambient-noise tomography, are input into a tomographic inversion procedure producing images of crustal azimuthal anisotropy.

This study marks the first where ambient seismic-noise data have been considered in azimuthal anisotropy work. Our resolution testing suggests that the interpretation of the results requires some caution, but good path coverage is available. Preliminary results show a dominant southwest-northeast anisotropic direction, with weak correlation with the tectonic belts (FIG 1). In contrast, previous anisotropic studies have found that crustal anisotropy is strongly correlated with regional geology. Our results suggest that contributions from other forces may be important. Stresses, including large-scale regional stresses from plate motion are considered, but also show little correlation with our data. Local glacial isostatic rebound may be a contributing factor, but further work is required.

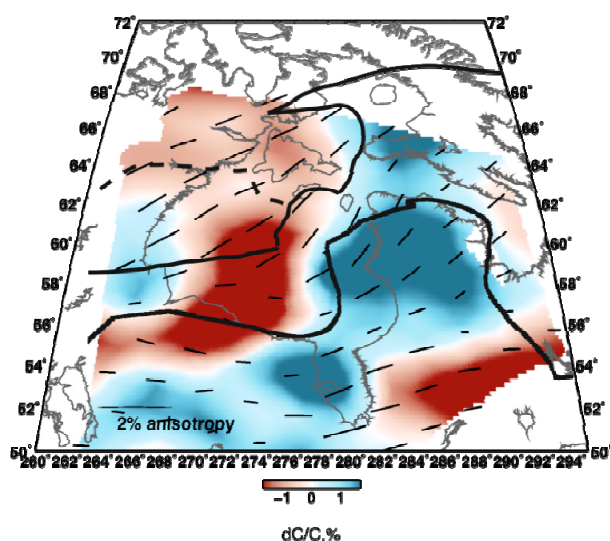


FIG 1. Tomographic reconstruction of Rayleigh-wave group velocity, for periods 20s. Major tectonic boundaries are superimposed. Isotropic velocities are shown in red (lower velocity) and blue (higher velocity). The black bars correspond with anisotropic fast directions.

Picking microseismic first arrival times by Kalman filter and wavelet transform

Baolin Qiao and John C. Bancroft

SUMMARY

To pick up the first arrival times, special techniques must be applied due to the very low signal to noise ratio data. This paper presents three techniques: wavelet transform is applied to de-noising the noisy data; Kalman filter and modified STA/LTA method are implemented to pick up the first arrival times. The results show that the first arrival times are picked up accurately even in very noisy data by incorporating these techniques.

In our test, the real first arrival times are at 150 ms and 400 ms for *p*-wave and *s*-wave respectively. We test our techniques on different levels of noisy data; the results show that the average error is 0.72 ms for *p*-wave and 0.53 ms for *s*-wave.

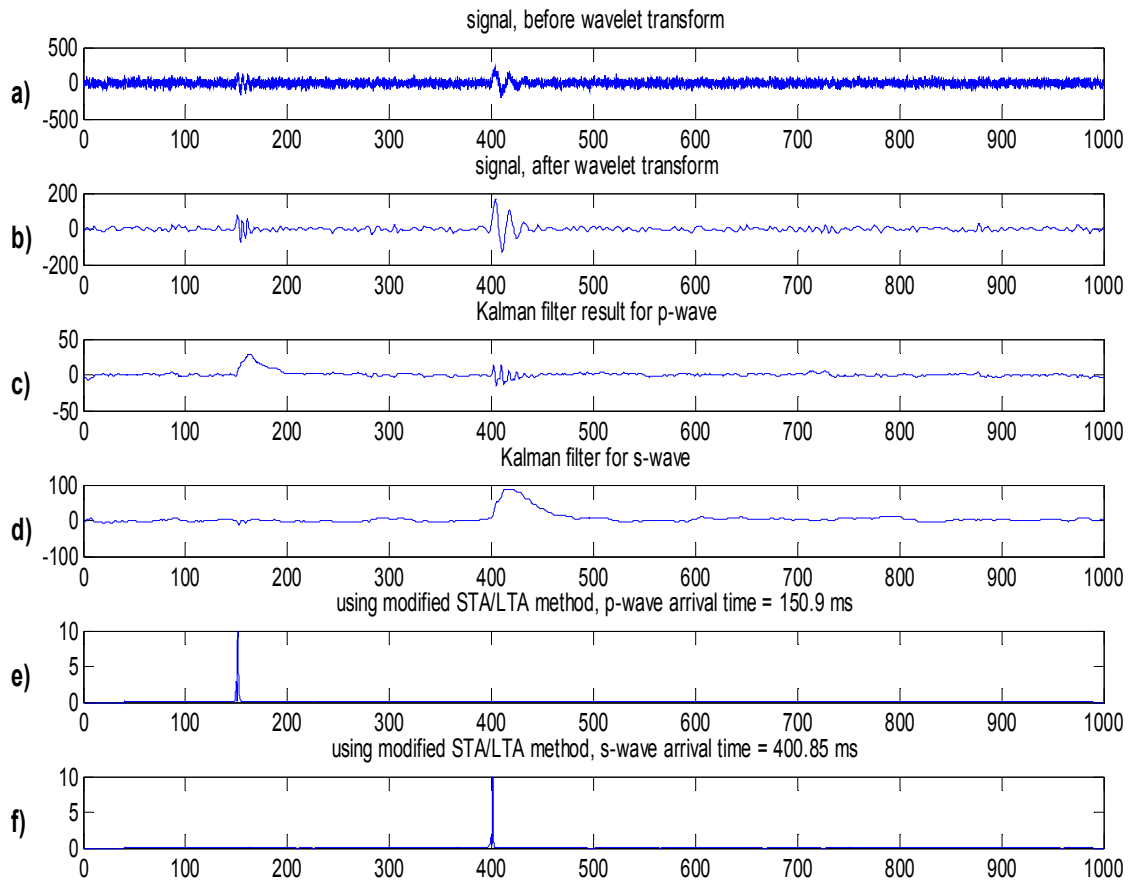


FIG. 1. The results of wavelet transform, Kalman filtering and estimation of the first arrival times using a modified STA/LTA method are shown above. The original signal is denoted by a), after applying wavelet transform b), we can see that the SNR is improved dramatically. The Kalman filtering results (state x_2) for *p*-wave and *s*-wave are shown in c) and d). A modified STA/LTA method which uses the Kalman filtering results is implemented to estimate the first arrival times, the results are shown in e) and f).

Characterization of lava tubes using ground penetrating radar at Craters of the Moon National Monument, USA.

Colin R. Rowell, Adam Pidlisecky, James D. Irving⁴, and Robert J. Ferguson

SUMMARY

Craters of the Moon National Monument is a Pleistocene to Holocene volcanic field in southern Idaho. It consists of numerous lava flows erupted between 15,000 and 2000 years ago. One of the largest lava flows, called the 'Blue Dragon' flow, is approximately 2100 years old and covers an area of 280 km². In many of these larger flows, lava tubes provide an important means of transporting lava underneath the flow over large distances. The goal of this project is to use near-surface geophysical techniques to build images of lava tubes in the sub-surface, and use this information to better understand the mechanisms of lava transport that were active during the eruption.

Ground-penetrating radar (GPR) is a geophysical technique that transmits radio waves into the ground, which are then reflected off of boundaries in the sub-surface. These reflected waves return to the surface to be recorded by the radar device. From these reflections, a 2-dimensional image of the sub-surface can be assembled. This technique was used to image lava tubes at Craters of the Moon National Monument.

GPR data were acquired over known lava tubes in order to assess the usefulness of the method for detecting lava tubes and other lava flow features. A standard GPR processing flow consisting of dewow filter, gain correction, and elevation correction were applied to these data. Additional processing, in the form of phase-shift migration and Gabor deconvolution was also applied to the data set. The migration algorithm corrected for, among other things, the non-vertical incidence of the GPR raypaths at shallow depths, while the deconvolution accounted for the non-stationary nature of GPR signals throughout the time record. These processing steps greatly improved the quality of the GPR images. Lava tubes were successfully imaged to depths of at least 10 meters using elevated antennas, however, voids smaller than about 2 meters were very difficult to distinguish at any depth.

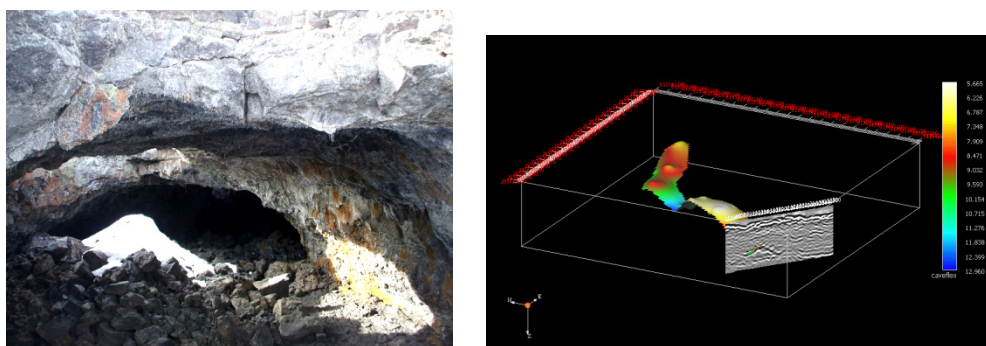


FIG. 1. Left: Interior of Indian Tunnel lava tube. Right: 3D VuPak Image of Beauty Cave.

⁴ School of Engineering, University of Guelph

Iteratively re-weighted least squares inversion for the estimation of density from well logs: part one

A. Nassir Saeed, Laurence R. Lines, and Gary F. Margrave

SUMMARY

A quantitative analysis of density log is established in this study by inverting of density log. The re-weighted inverse algorithm of density log using different constraints in model-structure space have shown stable and fast convergence the final model with few numbers of iterations. The inverted density model has resolved different lithology layers, and successfully delineated gas-bearing sand reservoir of the Blackfoot.

The re-weighted least squares inverse equation of density log is written as

$$(G^T W_d^T R_d W_d G + \lambda W_m^T R_m W_m) m = G^T W_d^T R_d W_d d$$

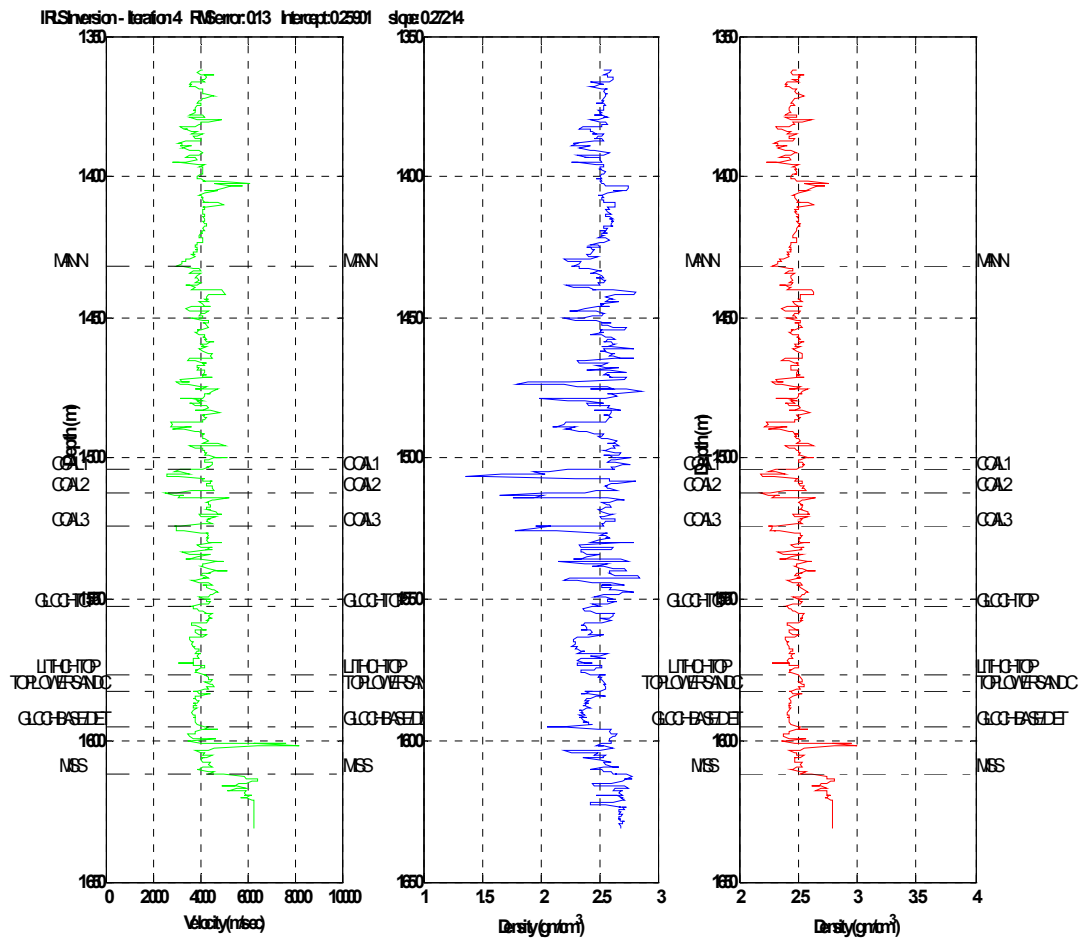


FIG.1. Well 08-08: IRLS inversion of density log using minimum support constraint function.

Iteratively re-weighted least squares inversion for the estimation of density from well logs: part two

A. Nassir Saeed, Laurence R. Lines, and Gary F. Margrave

SUMMARY

Incorporating of constrains in data-misfit domain is tested in this part of study. The inverted density model has resolved different lithology layers, and successfully delineated gas-bearing sand reservoir of the Blackfoot. The additional information incorporated into the weighted matrices used by inverse algorithm has enhanced the interpretation of inverted density log significantly; in particular, the sand base-line as well as separation of sand and carbonate regions. Joint-inversion of Vp- and Vs- logs to predict density log has shown some improvements of final shape of density log.

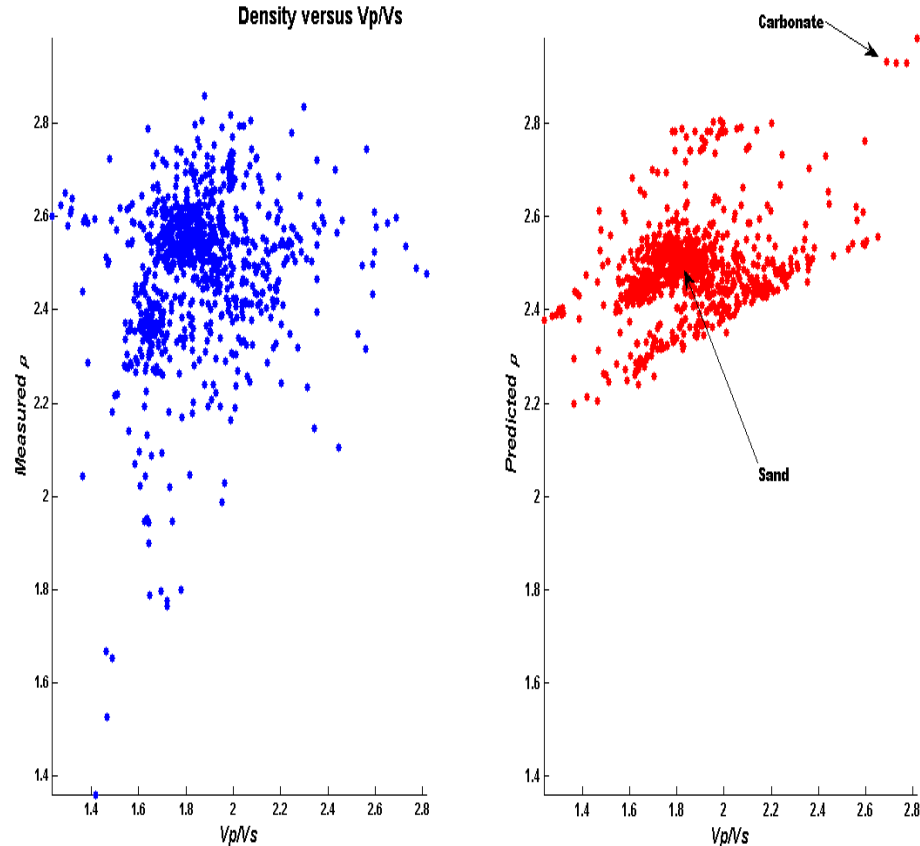


FIG.1. Observed and inverted density versus Vp/Vs ratio.

Mud-rock line estimation via robust locally weighted scattering smoothing method

A. Nassir Saeed, Laurence R. Lines, and Gary F. Margrave

SUMMARY

The robust locally weighted scattering smoothing (LWESS) is another regression method that not only smooths the scatter plot but also guard against outliers that distort the smoothed points. The mud-rock line produced by the robust locally weighted scattering smoothing method, LOWESS, has shown superiority over the Castagna linear regression method in mapping the Glauconitic sand reservoir of Blackfoot area. The produced graph has proven to be a good visualizing tool to discriminate sand and carbonate lines. It also has proven to be an effective DHI tool.

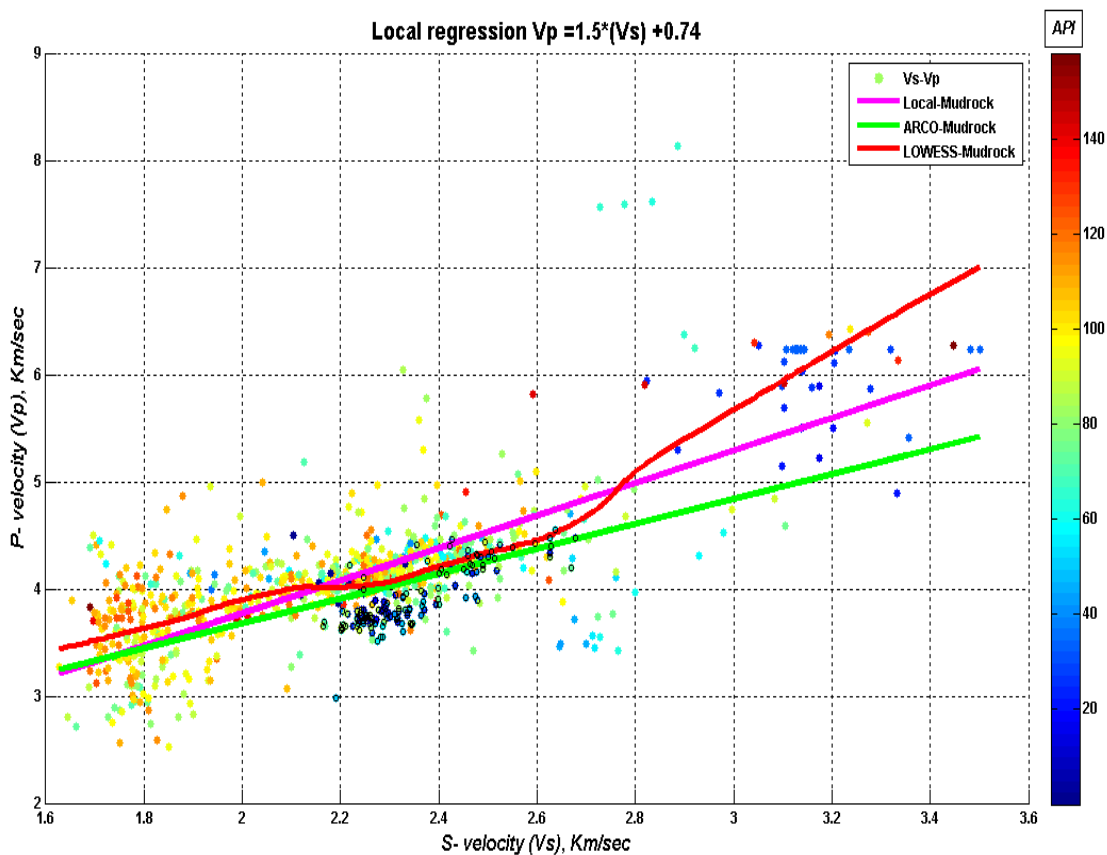


FIG.1. Locally weighted regression method for estimating Mud-rock line. V_s values of productive reservoir sand channel (black dots) are superimposed.

Time-lapse AVO inversion: model building and AVA analysis

A. Nassir Saeed, Laurence R. Lines, and Gary F. Margrave

SUMMARY

Quantitative estimates of the change in reservoir properties can be accomplished by combining rock physics model along with estimated change of P - and S -impedance from time lapse seismic data. The estimated attributes are key steps in discriminating fluid saturation and pressure changes in reservoir.

In this report, we have built a time-lapse model for the Pikes Peak area. The elastic physical parameters are carefully selected based on well logs from the survey area. The synthetic P-P and P-S seismic data generated from the model, using CREWES “SYNGRAM”, are being tested by proposed time-lapse inverse algorithms being developed. The AVA analysis conducted in this study produces information about rock interfaces only, and aids in calibrating physical parameters used in building of the time-lapse model. The rock modulus attributes LambdaRho ($\lambda\rho$) and MuRho ($\mu\rho$) computed from dipole sonic log of the Pikes Peak area help in discriminating lithology, while resistivity and porosity logs give an indication about expected fluid type in the reservoir.

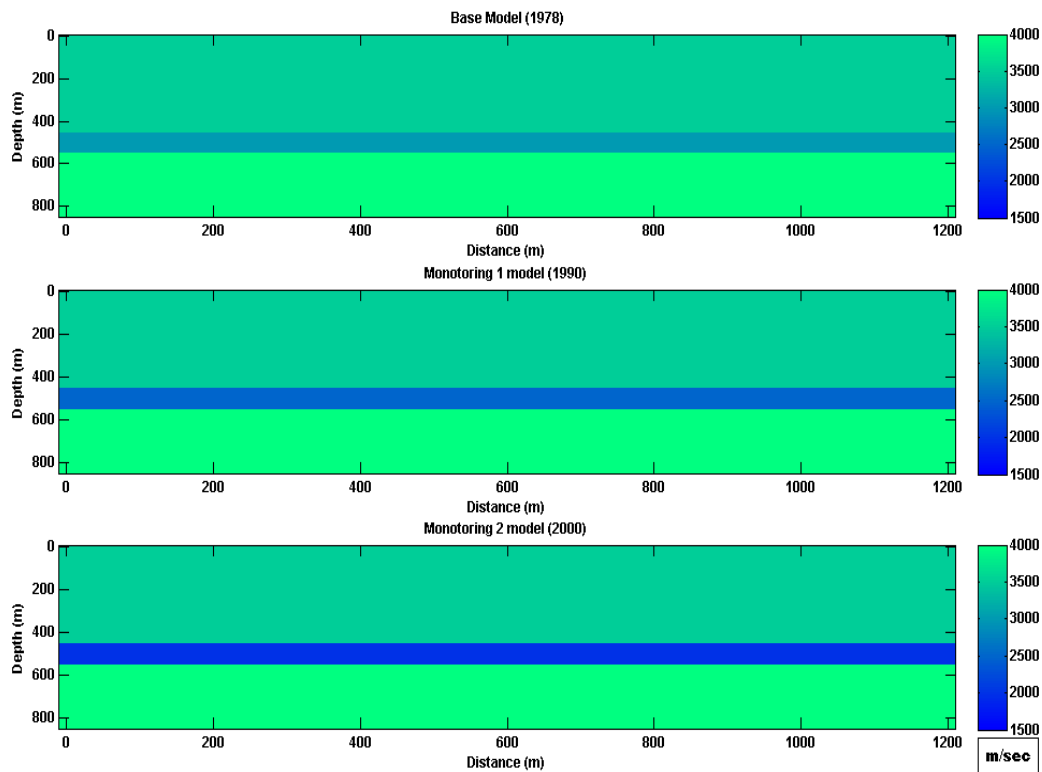


FIG.1. Time-lapse model for the Pikes Peak area.

9C-3D seismic modelling for VTI media

R. K. Sharma and R. J. Ferguson

SUMMARY

For comparison with real seismic data, and with synthetic data derived from fully elastic numerical methods, we present a 9C – 3D numerical modelling approach that is posed in the slowness domain. The slowness domain approach has a number of advantages: 1) multi-pathing with no internal reflection“ simpler event registration”. 2) Parallelizable over temporal frequency. 3) Stable. 4) High frequency. 5) Selectable propagating mode. Following the Fourier decomposition, wavefield extrapolation proceeds as a set of distributed, monochromatic extrapolation steps in depth. 3D phase shift operators in anisotropic media have been used to extrapolate a 3C source wavefield to each grid point. There, source polarization is transformed into the orientation of the multicomponent geophone by applying a rotation matrix on the extrapolated field. The polarization angle (dip) of compression wave computed from the incident angle that is angle between slowness vector and normal to each grid point and the horizontal projection of associated slowness vector at each grid point are the essential parameters of rotation matrix. Traveltimes in anisotropic media are accommodated though plane wave transformation and phase shift, and a propagation angle is produced. For each geophone component, the polarization angle is calculated from the propagation angle. Finally, the desired component for analysis is extracted. Our numerical results demonstrate that all 9 source-receiver combinations are reliably estimate using our procedure.

Figure 1a shows the registered energy versus offset (REVO) of the SV-wave on V component to illustrate that the registered energy decreases with offset. This figure shows the triplication, an interesting property of SV-wave generated by an SV source. Figure 1b illustrate the registered energy versus azimuth (REVA) of SV-wave on the H_2 component.

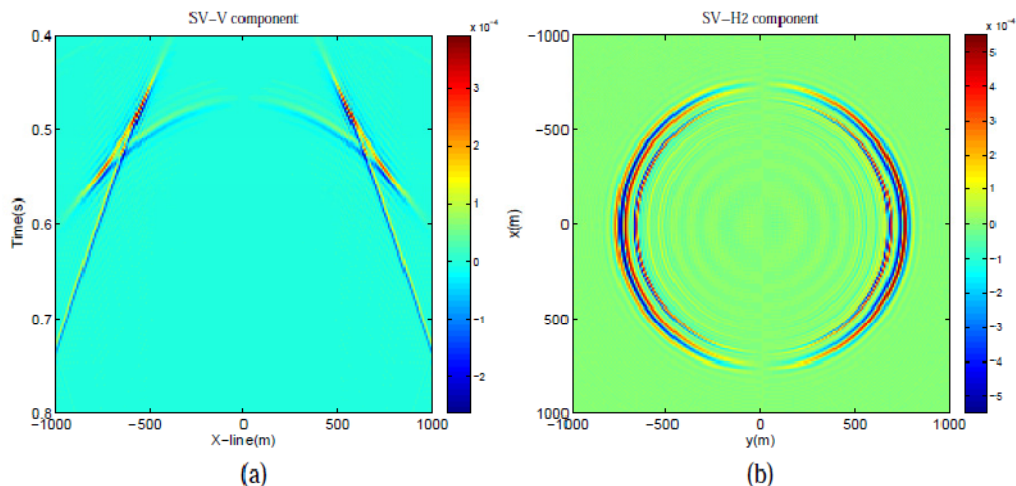


FIG. 1. (a) REVO of SV-wave on V component. The Triplication phenomena occurs in this case. Registered energy decreases with offset. (b) REVA analysis of SV energy on H_2 component demonstrate that H_2 component is more favorable for energy registration in in-line direction and polarity reversal also occur on the either side of the in-line direction.

Phase-shift modelling for HTI media

R. K. Sharma and R. J. Ferguson

SUMMARY

Fractures play an important role in hydrocarbon production as they determine the pathways and volume of crustal fluid movement. We present phase shift modelling for HTI media in the continuation of 9C-3D modelling for VTI media. The only difference from VTI modelling resides on the way of computing polarization angle. Instead of one cross product, the two cross product are taken into account here in order to compute polarization angle. It has been demonstrated that the amplitude and travel time of seismic waves are affected by HTI medium. P- and SH- waves amplitude are highest in the direction of fracture strike while SV-wave amplitude depends on the difference between ϵ and δ . The investigation of the synthetic data for HTI medium in case of SV-wave reveals the triplication behavior of SV-wave in the presence of anisotropy. The location of triplication depends on the absolute value of the difference between ϵ and δ . The presented modelling will be contributive to fracture detection from the surface seismic data since the information about the fracture system can be extracted from the three dimensional behavior of the shear wave splitting. Subsequently, this modelling will be applicable for VSP and micro-seismicity modelling in the presence of anisotropy. Figure 1a shows the time slice of extrapolated SV wavefield. The occurrence of triplication is endorsed by analytic curve. Figure 1b illustrates the time slice of the extrapolated P wavefield. The authentication of the proposed modelling is demonstrated here as analytic curve is analogous to the obtained one.

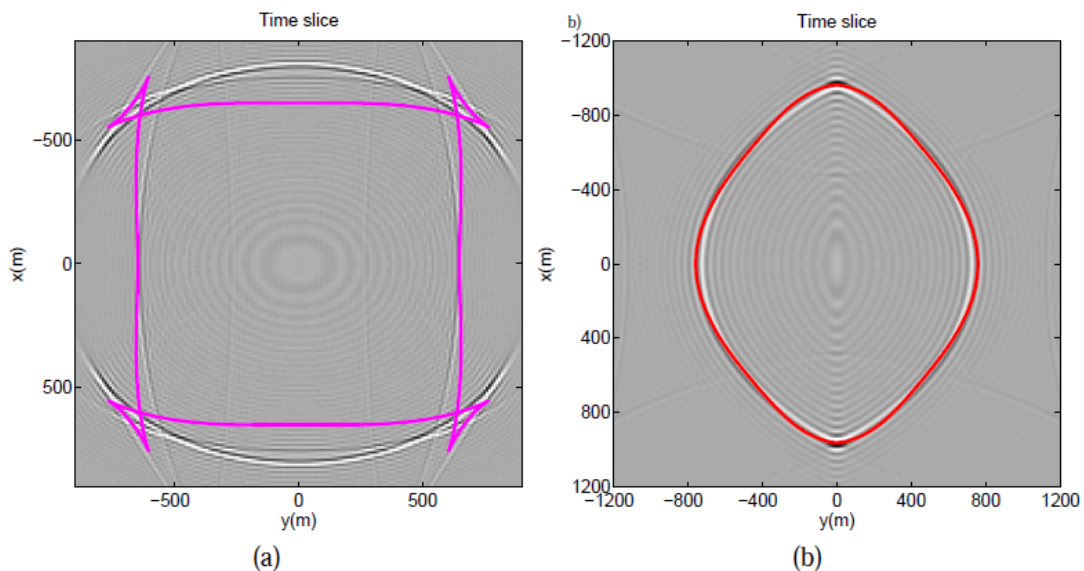


FIG. 1. Time slices (a) and (b) of the extrapolated SV and P wavefield, respectively. The Triplication occurs in SV case. The elliptical time slice of P-wave is overlapping with analytical curve and manifests the azimuthal anisotropy of the medium.

Reflection and Transmission coefficient for VTI media

R. K. Sharma and R. J. Ferguson

SUMMARY

Presently, we obtain the reflection (R) and transmission (T) coefficients in the plane wave domain in behalf of its importance for numerical computations. Classical R and T coefficients has been expressed as a function of the phase angle and can be computed by using the effective ray parameter. To do this, we compute a normal for each individual plane wave based on local velocity that is function of Thomson's parameter of the medium and vector cross-product of this normal with the normal to the reflector yields a ray parameter that is used here to compute the corresponding R and T coefficients for a given plane wave. Now following Graebner's approach, we obtain R and T coefficients in term of Thomson's parameters as these parameters are essential for understanding the seismic waves signatures in the anisotropic media. Another importance of this approach is the automatic adaption of R and T coefficients for HTI media. Further, as the dependency of the reflected waves amplitude on offset has proven to be a valuable exploration tool for direct hydrocarbon detection, we have demonstrated that anisotropy does have considerable influence on the reflection coefficient of seismic waves. Thus, conventional AVO analysis needs to be modified in the presence of the anisotropy on either side of the reflecting boundary. A test of accuracy of Rüger's approximation is also delineated here.

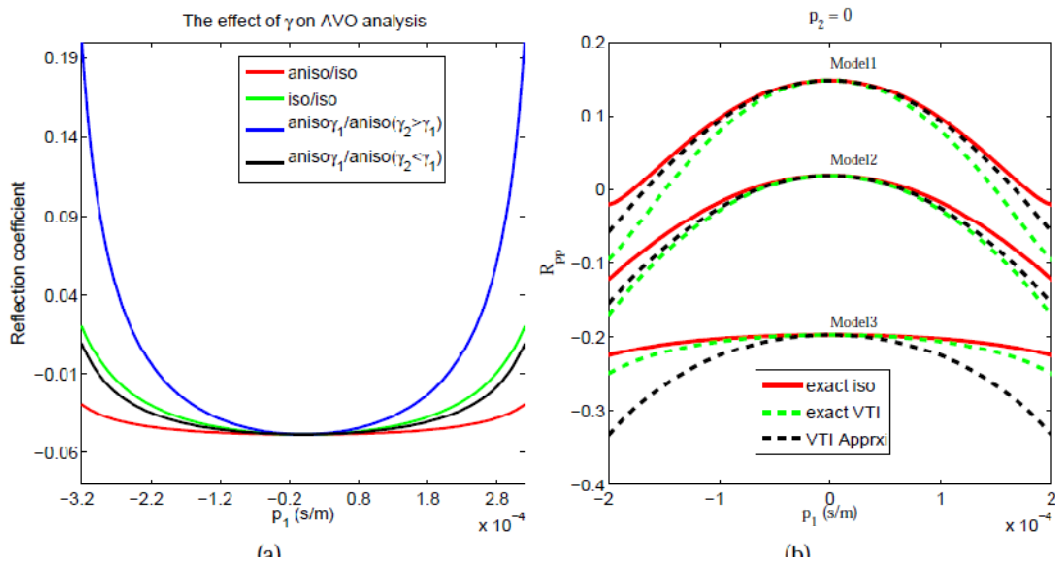


FIG. 1. (a) The influence of Thomson's parameter on the SH wave reflection coefficients curve. (b) R coefficients curves of the P wave for the three VTI ($\delta = 0.12$, $\epsilon = 0.133$) models. The thick red line denotes the exact isotropic reflection coefficient, the dashed green and black lines show the exact and approximated reflection coefficients.

Seismic interpretation of the Redwater Leduc Reef, Alberta

Taher M. Sodagar and Dr. Don C. Lawton

SUMMARY

Approximately 400 line-km of 2D seismic data were reprocessed and interpreted to characterize the Redwater Reef in order to assess its potential for large-scale storage of CO₂. The seismic data, of various vintages, were reprocessed to a common datum in order to provide a uniform character for interpretation of the reef margin and to characterize the internal geometry and facies of the reef.

Interpretation of formation tops in the seismic data was constrained by synthetic seismograms generated from sonic and density logs available from two on-reef and four off-reef wells in the region. The synthetic seismograms tied reasonably well with the surface seismic data for the key formations. Generally, reflections dip gently towards the southwest direction in the 2D seismic datasets and there are no observable faults in the area encompassed by the Redwater Reef.

Devonian age Upper Leduc and Mid-Leduc edges are identified clearly on the 2D seismic lines. Thickening of the reef rim and thinning inside and central of the reef are characteristics of the reef interpreted along individual lines and interpolated through isochron maps. The Cooking Lake and deeper seismic events show time-structure (velocity pull-up) beneath the reef due to higher velocity of the Leduc Formation carbonates compared with the off-reef Ireton shales. A restricted embayment (Duvernay Fm) was mapped from the seismic interpretation into the reef buildup in near the north-west flank and south-west boundaries. Depth-converted seismic event maps compensate for the velocity pull-up beneath the reef except where the shale embayments occurs, since only a single interval velocity for the reef was used in the depth conversion process. Some evidence of dolomitization in the Middle Leduc and Cooking Lake formations was interpreted in seismic lines along western side of the reef. Otherwise, internally to the reef buildup and away from the Duvernay embayments, the seismic character of the Leduc Formation is generally quite featureless.

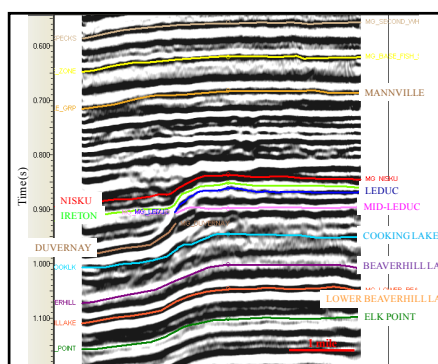


FIG. 1. Interpreted seismic section. North is to the right. This line shows the reef edge clearly and the Duvernay event terminating close to the reef margin.

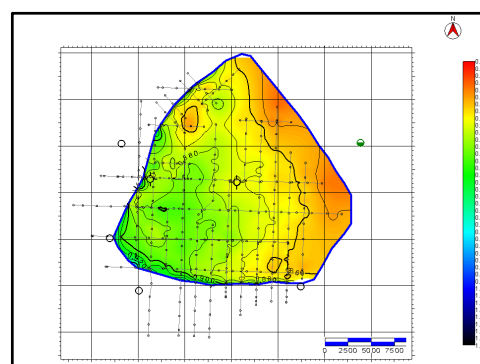


FIG. 2. Time structure map of the Upper Leduc Formation with the Leduc reef edge outlined. The eastern boundary marks the edge of data.

Time-lapse of multi-component seismic modeling of CO₂ fluid replacement in Redwater Leduc Reef, Alberta

Taher M. Sodagar* and Don C. Lawton

SUMMARY

The Devonian Redwater reef, northeast of Edmonton, Alberta, is being evaluated for geological storage of CO₂ for the Heartland Area Redwater CO₂ Storage Project (HARP). It is located close to large sources of CO₂ in the Redwater-Fort Saskatchewan-Edmonton region. The main objective of the study was to build a 2D geological model of the Redwater reef, from the reef center to off-reef, and investigate the seismic response of the reef to CO₂ saturation in the Leduc Formation. Fluid substitution and seismic modeling were undertaken to generate PP and PS synthetic seismic data to study the consequences of CO₂ saturation on the seismic response of the various reef facies and formations below the reef, based on seismic attributes and character.

Common shot ray tracing modeling was undertaken to evaluate variations in the seismic response of the Redwater reef along the 2D line across the margin of the reef for CO₂ saturation in the Upper Leduc interval. The input geological model was based on well data and depth-converted seismic data from the interpretation of legacy 2D seismic lines in the area. Seismic reflections display positive structure below the reef in time sections due to the lateral velocity change from on-reef to off-reef, but are corrected in the depth sections.

Terminations and the lateral position of the Upper Leduc and Middle Leduc events are clear on the pre-stack time-migrated section and a modest improved on the depth-migrated section. Higher amplitudes at the base of Upper-Leduc member are evident near the reef margin due to the higher porosity of the foreslope facies in the reef rim compared to the tidal flat lagoonal facies within the center of the reef. Time-lapse seismic modeling predicts a reasonable amplitude difference for the seismic data before and after CO₂ saturation, particularly for reflections from the Upper Leduc, the top of the reef rim, and the Mid Leduc near the reef edge.

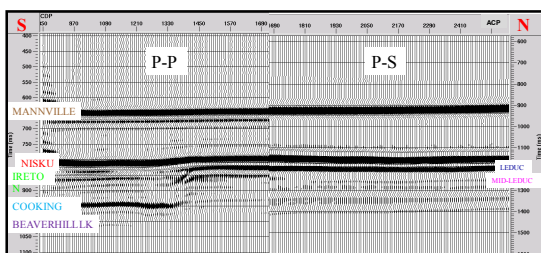


FIG. 1. Comparison and matching the events between PP wave and PS PSTM seismic section from the Redwater Reef model.

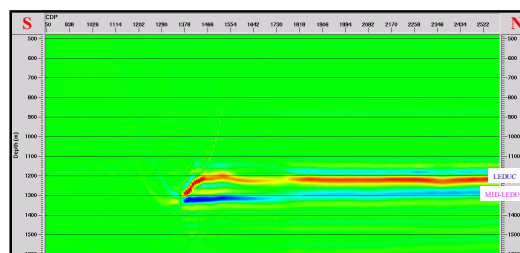


FIG.2. PP difference after PSDM before and after CO₂ replacement.

An assessment of natural and man-made vibrations in Lake Kivu, Rwanda

Robert R. Stewart

SUMMARY

This report overviews the general level of vibrational disturbance to which Lake Kivu, Rwanda has been subjected (e.g., shaking of approximately 10cm/s and 0.1g by recent earthquakes in the magnitude 6 range). These levels are compared to man-made sources, especially those of the exploration seismic community (air guns and sub-bottom sounders). The energy released by marine seismic sources is several orders of magnitude smaller than that of recent Rwandan earthquakes. Interest and concern relates to Lake Kivu because of its vast quantities of dissolved carbon dioxide and methane. Due to its thermohaline structure, the Lake is regarded as stable (although potentially vulnerable to extreme events). The sediments beneath the Lake could be host to hydrocarbons (similar to Lake Albert, Uganda). Thus, there are a number of compelling scientific, hazard reduction, and economic reasons to undertake seismic surveys on the Lake. However, because of the large population around Lake Kivu, potential environmental effects of a seismic survey must be considered. The energy and pressures involved in a seismic survey (using sub-bottom sounders and small airguns) are likely much smaller than those previously experienced in the depths of Lake Kivu. The seismic vibration estimates appear to be safely within Wüest et al.'s (2009) factor of safety and stability criteria.

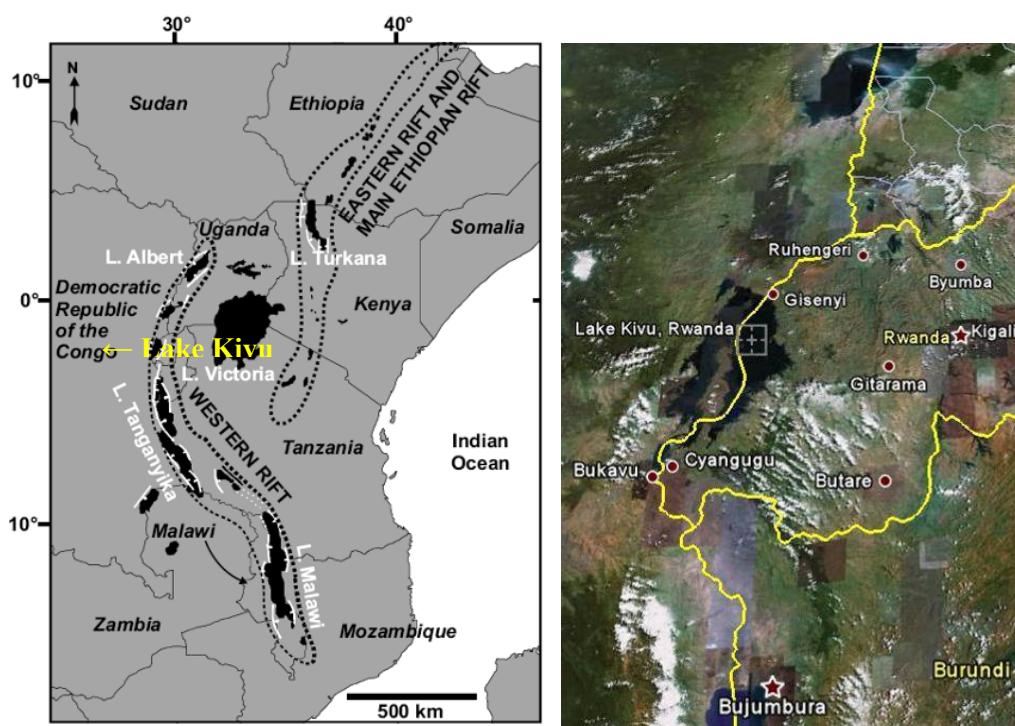


FIG. 1. Map of the East African Rift Zone and Lakes (from Karp et al., 2010) on the left and a satellite image (from Google Earth) on the right.

CDP noise attenuation using local linear models

Todor I. Todorov and Gary F. Margrave

SUMMARY

Seismic noise attenuation plays an important part in a seismic processing flow. Spatial prediction filters, like FX deconvolution, has been successfully applied to seismic volumes. However, since they require uniform spatial sampling, they are not suitable for noise attenuation of CDP gathers. A new method for noise attenuation on CDP gathers, based on local linear models, is developed. The process is applied to synthetic and real data from Alberta oil sands and shows a robust performance while preserving the AVO amplitude variations.

The main steps in the process are:

- frequency slicing by the Borga transform
- predict amplitudes using a local linear fit in offset direction
- compute the absolute error between the predicted and actual amplitudes
- correct the amplitudes with largest absolute error

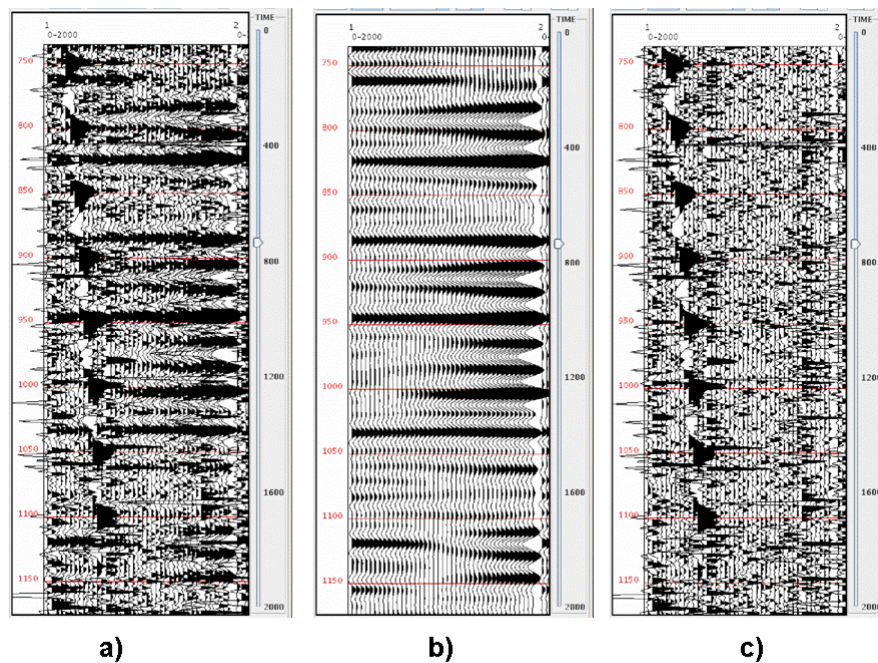


FIG. 1. Noisy gather a), gather after noise attenuation b), and removed noise c).

The seismic quest for estimating heavy oil viscosity

Fereidoon Vasheghani and Laurence R. Lines*

SUMMARY

In heavy oil reservoirs, the enhanced oil recovery (EOR) is largely governed by the mobility of fluids. These EOR methods generally attempt to increase mobility by lowering the fluid viscosity. Hence, it is important to have knowledge of viscosity throughout the reservoir. While viscometers and geochemistry can be used to estimate viscosity from borehole samples, we estimate viscosity between boreholes using cross-borehole seismic combined with rock physics models, since recent research by Vasheghani and Lines (2009) shows the relationship between heavy oil viscosity and seismic Q . Our estimation of viscosity tomograms is achieved by two steps. First, the estimation of Q (inverse attenuation) is achieved using a crossborehole tomography method of Quan and Harris (1997). Then the Biot-squirt rock physics theory (BISQ) is used to convert Q tomograms to estimates of viscosity between boreholes. The details of this research are to be published in the upcoming PhD thesis of Vasheghani (under preparation).

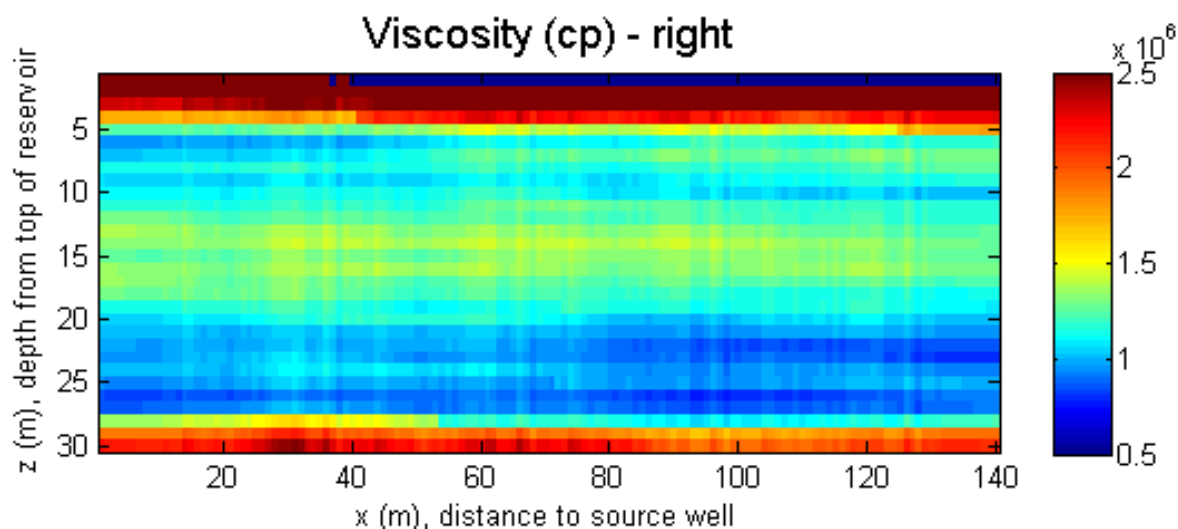


FIG. 1. The viscosity tomogram between wells for a Laricina field in the Wabasca area. The tomogram is obtained by first computing a Q -tomogram and then converting Q -values to viscosity values by using the BISQ rock physics model.

Fluid substitution and seismic modelling in a sandstone aquifer

Virginia C. Vera* and Don C. Lawton

SUMMARY

Fluid substitution and seismic modelling were applied in order to evaluate the Paskapoo Formation as a potential CO₂ geological storage unit. The first stage of this project deals with the application of the Gassmann substitution model using well data and evaluation of property variations due to CO₂ saturation changes. Seismic modelling was undertaken in the area of interest simulating pre, during and post CO₂ injection scenarios. From Gassmann calculations it was found that the P-wave velocity drops between 0 to 20% CO₂ saturation and starts a subtle rise at 30% whereas the S-wave velocity increases directly proportional to CO₂ saturation. The P-wave velocity decreases approximately 7%, the S-wave velocity increases 0.8 %, V_p/V_s decreases an average value of 8% and the basal reflector presents a time delay of 1.6 msec. From seismic modelling it was found that the injection zone can be delineated in the CDP stack section through an amplitude change the top reflector and a time delay for the basal reflector. The reflectivity coefficient was evaluated using the Shuey approximation and qualitative observations of the sections, showing a decrease in the reflectivity with increasing CO₂ saturation, with a major drop in the first 10% and a further amplitude decrease with offset (higher angles). These parameters allow us to estimate the conditions that would help to interpret the real data in further phases of this study.

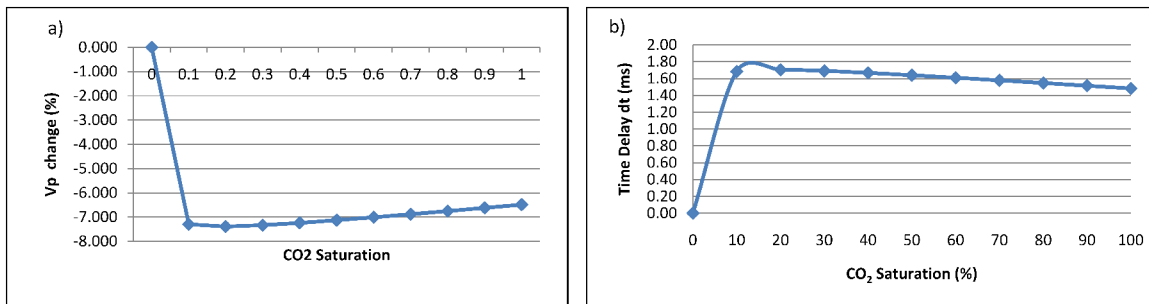


FIG.1. a) P-wave velocity change versus CO₂ saturation. b) Time delay vs. CO₂ saturation.

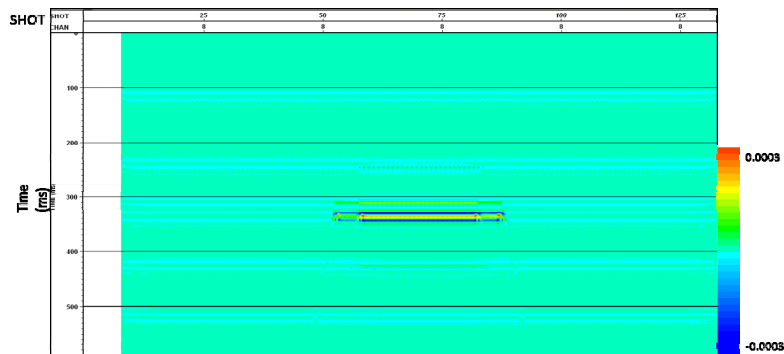


FIG. 2. Difference between 0% CO₂ and 100% CO₂ saturation CDP stack section.

Conventional and non-conventional seismic differencing in time-lapse

Vanja Vracar and Dr. Robert J. Ferguson

SUMMARY

A conventional and non-conventional seismic difference analysis is performed on a 100 % oil saturated reservoir in time-lapse after day 1, 14 and 28. 2D variable velocity plots in time-lapse are passed to a finite-difference algorithm generating zero-offset synthetic seismograms. Synthetics are migrated using Split-step Fourier algorithm and conventionally and non-conventionally differenced. The conventional differencing employs matrix subtraction in MATLAB, a commonly used concept today. Figures a) and b) capture results of conventional differencing after days 1 and 14 and days 1 and 28. Arrow 1 denotes reservoir bottom, whereas, no reservoir top reflection can be identified. Arrows 2 and 3 mark two waterfronts corresponding to differenced models in black. Note a waterfronts to be hard to visualize and the lack of information of remaining reserves. The non-conventional differencing, created employing the inverse data matrix concept, offers improvements. Figures c) and d) capture non-conventional seismic differencing. Note waterfronts and produced reserves volume to be much more obvious to interpret and monitor. Further work triggers a merge of pre-stack migration imaging and inverse data matrix concepts for nonconventional differencing improvements in remaining reserves and adaptation to 3D data sets.

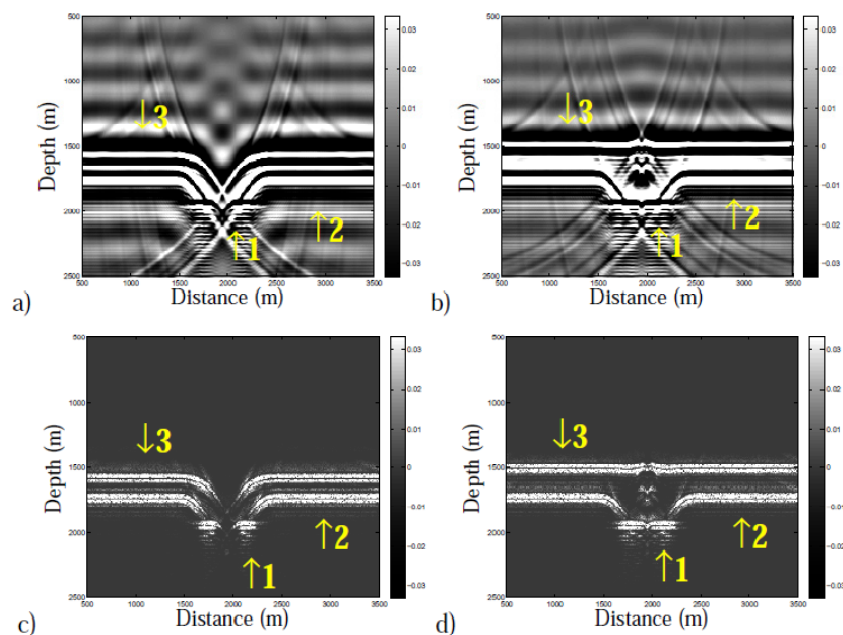


FIG. 1. Models (a) and (b) capture conventional difference of models after days 1 and 14 and days 1 and 28, respectively. Models (c) and (d) capture non-conventional difference of models after days 1 and 14 and days 1 and 28, respectively. Arrow 1, 2 and 3 denote reservoir bottom and two waterfronts, respectively.

Reverse time migration in anisotropic media

Ben D. Wards*, Richard Bale, Gary F. Margrave and Michael P. Lamoureux

SUMMARY

Reverse-time migration (RTM) is a powerful migration method provided that an accurate velocity model can be constructed. Converted wave data, pressure wave energy that has converted into shear wave energy upon reflection, can be used to aid interpretation of pressure wave data. We show how a converted wave RTM can be used to image a simple ramp model, which has a homogenous tilted transverse anisotropic (TTI) overburden. We simplify the propagation of the wavefield necessary for migration by propagating each mode of the elastic wavefield separately by a pseudo-acoustic wave equation. This involves solving the Christoffel equations for the elastic wave equation and creating a pseudo-acoustic wave equation from the derived dispersion relation. Our solutions of the pseudo-acoustics wave equations are based on combining exact dispersion free homogenous solutions.

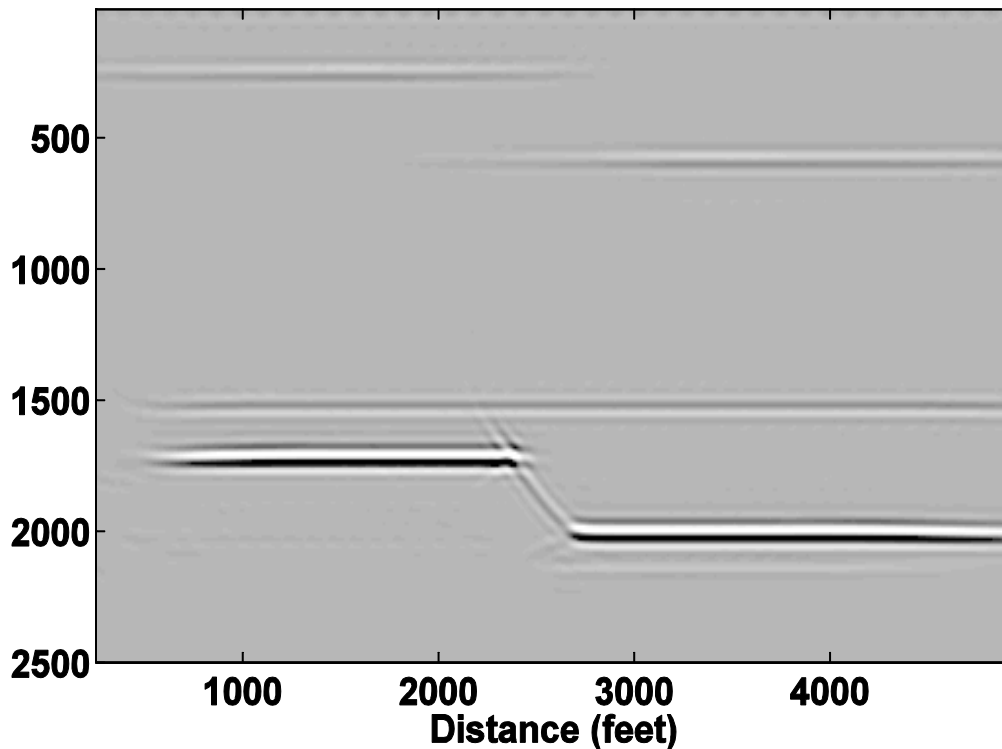


FIG. 1. A PP migrated image of the FRP ramp model which has TTI overburden.

Asymptotic complexity of inverse nonstationary phase shift

Marcus R. Wilson and Robert J. Ferguson

SUMMARY

We perform a speed test on an optimized conjugate-gradient based inversion to correct for surface statics and irregular spatial sampling. An ideally preconditioned scheme is run repeatedly on synthetic trace gathers of random size, up to 2^{15} traces. The runtime and the number of conjugate gradient iterations required for each trial is recorded. Iteratively refined polynomial regression is performed on the resulting data points to estimate the asymptotic complexity of the algorithm, and the number of conjugate gradient iterations is compared with the overall runtime to check for consistency. We find that the ideal preconditioned scheme gives a near optimal runtime of $\mathcal{O}(n^{1.082})$, which indicates that the method could feasibly be preconditioned to run on large data sets.

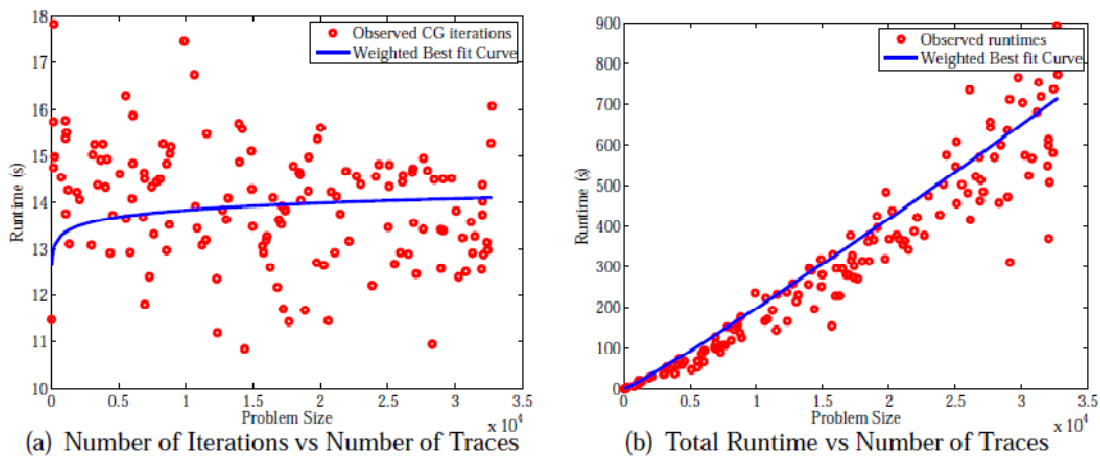


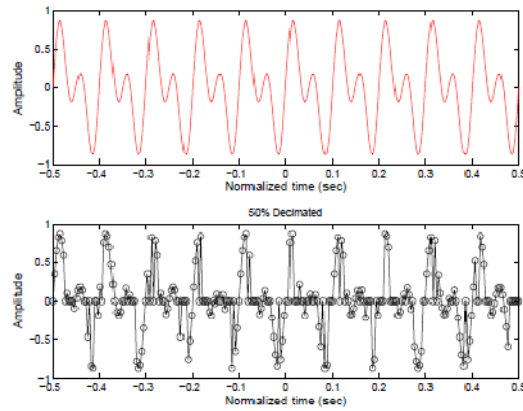
FIG. 1. Number of Iterations and Total Runtimes for $n < 2^{15}$. Regression indicates that the iterations function is given by $C(n) = 11.96n^{0.0158}$, and the runtime function is given by $t(n) = 0.00931n^{1.082}$.

Automatic band limited signal reconstruction

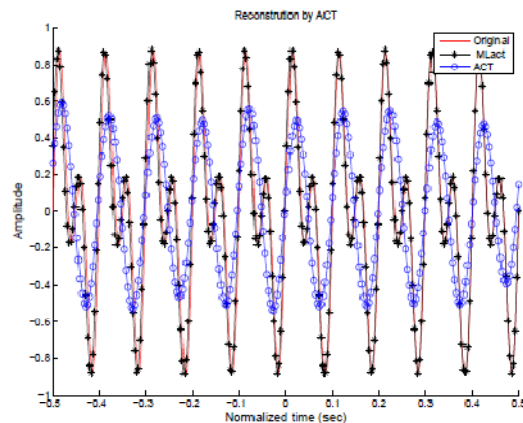
Marcus Wilson, Akshay Gulati and Robert J. Ferguson

SUMMARY

We implement the popular Adaptive weights Conjugate gradient Toeplitz (ACT) algorithm for signal construction. This algorithm is fast and accurate, and we show its effectiveness in several typical trace regularization situations. This algorithm requires an estimate of the bandwidth as input, and overestimating the bandwidth can cause spurious high frequency noise in the reconstruction. As an improvement, we implement a modified version of ACT that is less well known. The Multi-level ACT performs automatic bandwidth detection on its input by performing ACT iteratively to estimate the optimum reconstruction bandwidth. We test this algorithm on a harmonic of unknown bandwidth, and results show that Multi-level ACT is effective when the signal bandwidth can not be accurately estimated. A toolbox has been assembled that can be requested from the authors.



(a) Original harmonic and 50% randomly decimated harmonic



(b) Reconstructed harmonic

FIG. 1. MLACT vs ACT on a 50% randomly decimated harmonic of unknown bandwidth.

Implicit and explicit preconditioning for least-squares nonstationary phase shift

Marcus R. Wilson and Robert J. Ferguson

SUMMARY

An implicit preconditioned conjugate gradient scheme is derived to implement nonstationary phase shift for irregularly sampled seismic data using least squares. This implicit scheme gives fast convergence at all frequencies at the cost of an approximation to the evanescent filter. This results in some error in the phase shifted and regularized data computed. Our implicit scheme suggests an explicit scheme which unfortunately does not perform any better than the standard unconditioned scheme. The fast implicit scheme suggests that an appropriate preconditioner can be found that will reduce the runtime of the algorithm without sacrificing accuracy, and this will result in a robust trace regularization and statics algorithm for use in heterogeneous media.

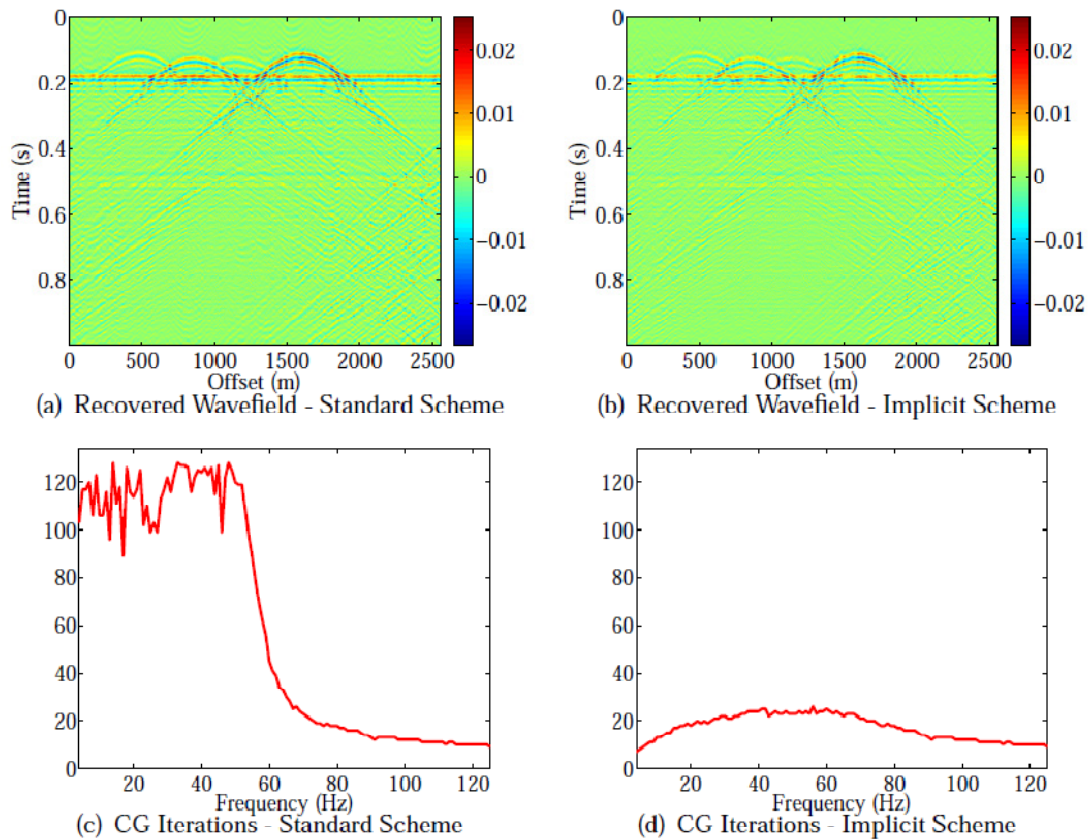


FIG. 1. Recovered wavefields and convergence rates for standard and preconditioned conjugate gradient schemes.

Fermat's principle and ray tracing in anisotropic layered media

Joe Wong

SUMMARY

I consider the path followed by a seismic signal travelling through velocity models consisting of horizontal layers, and describe a ray-bending method based on Fermat's principle, which states that the raypath between the source and receiver must be the one with the least travel time. The intersection points of the least-time raypath with the layer boundaries can be found by a direct-search nonlinear optimization routine. TTI velocity anisotropy can be included in one or more of the layers. An efficient and accurate procedure for producing raypaths and first-arrival times through these layers can be formulated using the Byun/Kumar approximation for TTI group velocities. The method was implemented in MATLAB code, and I present examples of least-time raypaths and travel times for sources and receivers embedded in isotropic and anisotropic layers.

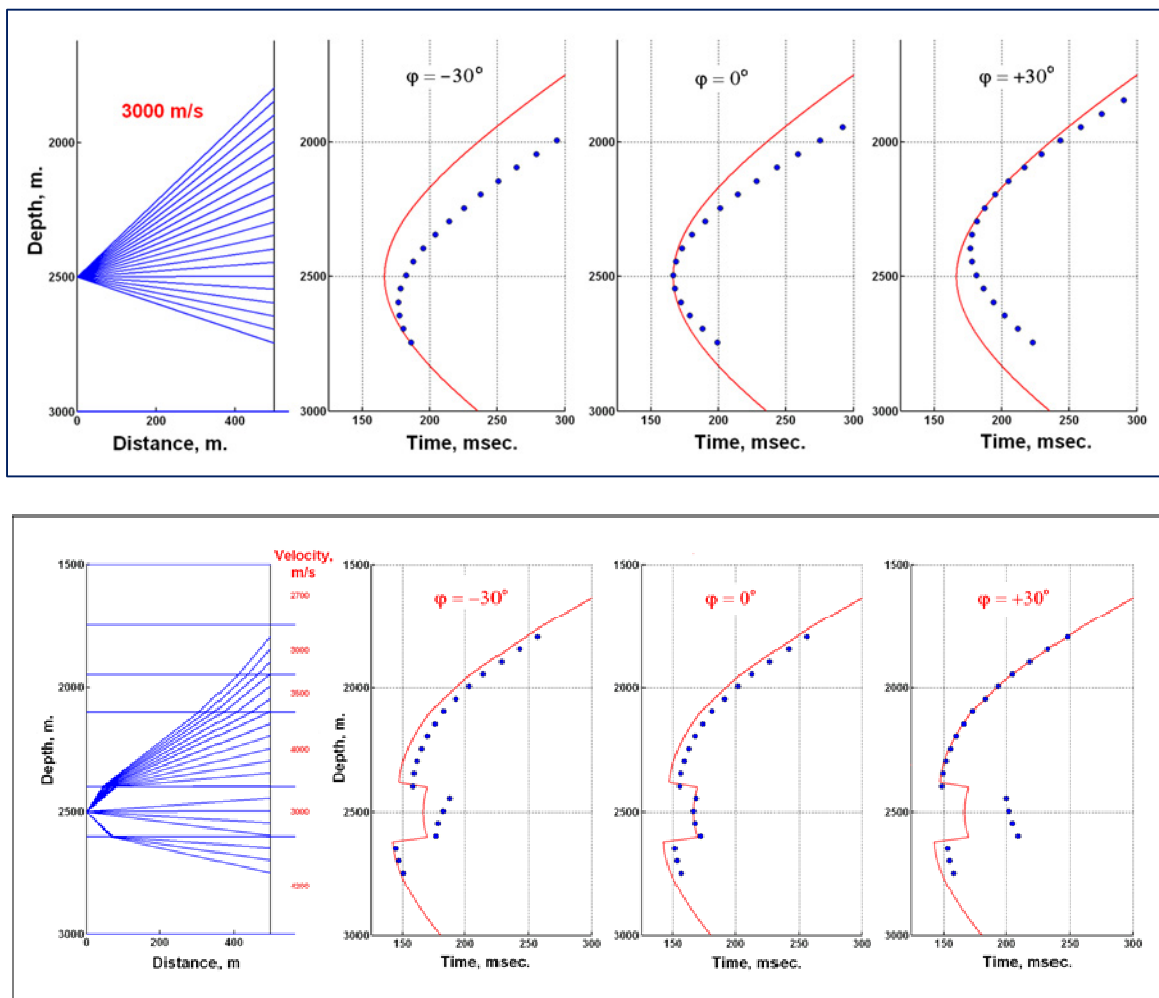


FIG. 1. Raypaths and arrival times for isotropic and TI media. The red curve shows arrival times for the isotropic case. The blue dots are arrival times with tilt angles of -30° , 0° , and $+30^\circ$ for the axis of symmetry of the TI anisotropy. Top: homogeneous model. Bottom: layered model.

Seismic physical modeling measurements on solid surfaces

Joe Wong, Faranak Mahmoudian, Eric Gallant, and Malcolm Bertram

SUMMARY

Using the University of Calgary Seismic Physical Modeling facility, we recorded common source on phenolic and acrylic solid slabs in order to characterize their velocity properties. P and S seismograms were recorded by placing piezoelectric transducers to the solid surfaces using different coupling techniques with various high-viscosity compounds. Analysis of various seismic gathers confirmed that the velocities of the acrylic plastic slab are isotropic. The P- and S-wave velocities of the phenolic slab are clearly orthorhombic. In the presence of significant velocity anisotropy, reflections from flat subsurface boundaries no longer have the normal moveout that follow a hyperbolic trajectory. We observed how velocity anisotropy affected NMO stacking in different azimuthal directions, and determined the form of the non-hyperbolic stacking trajectories that must be applied in order to optimize the stack quality.

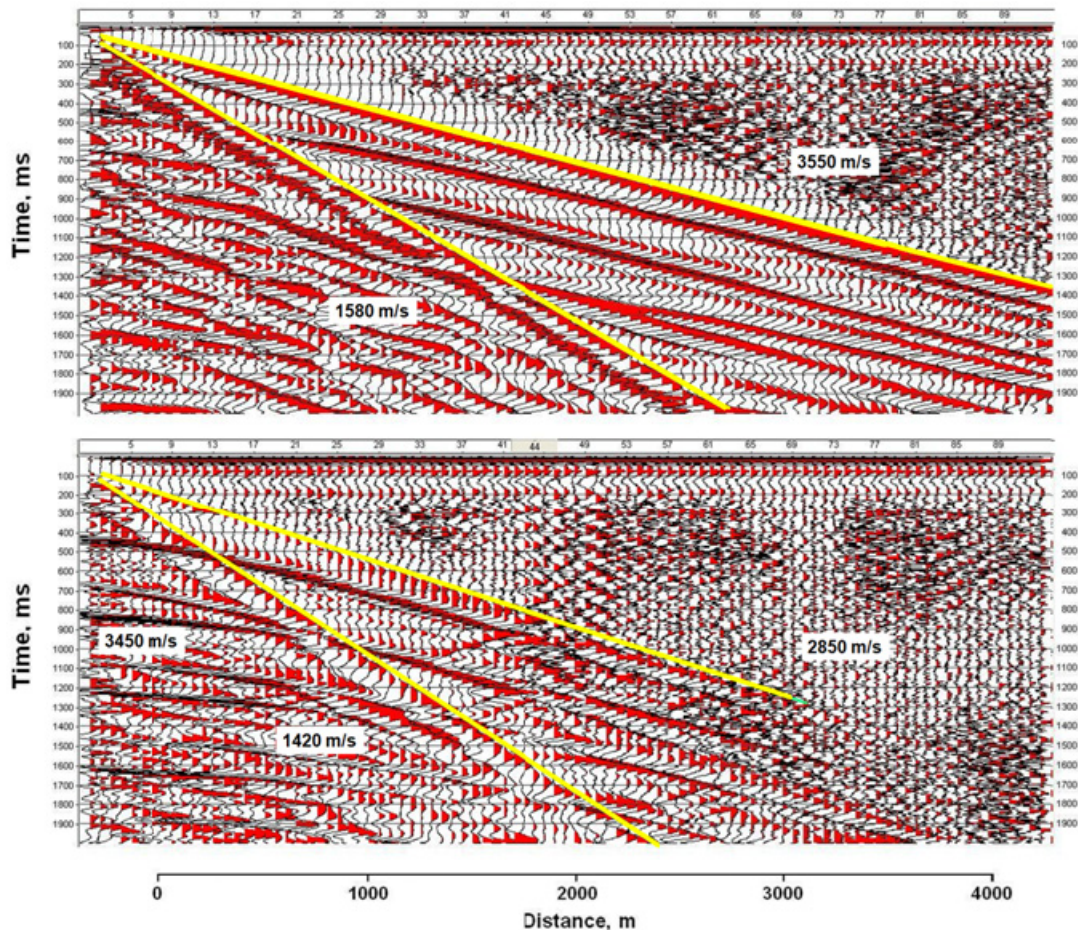


FIG. 1. Two fixed source end-on gathers of seismograms on the anisotropic phenolic slab. Top gather is in the x direction, bottom gather is in the y direction. P-wave velocities are 3550 m/s, 2850 m/s, and 3450 m/s in the x, y, and z directions. Surface wave velocities are 1580 m/s and 1420 m/s in the x and y directions.

Synthetic microseismic datasets

Joe Wong* and Peter M. Manning

SUMMARY

Although passive monitoring of microseismic events induced by hydraulic fracturing has been used for many years, the fundamental problem of locating hypocenters is still plagued by inaccuracies. Different algorithms and processing flows applied to the same dataset often produce radically different estimates of source locations. This is especially true if the acquisition aperture of the recording array is small in angular extent and if the microseismic arrivals are weak compared to the noise.

We have created synthetic microseismic datasets designed to be used with different location algorithms in “blind” tests. Since the hypocenter coordinates for the synthetic data are known, the effectiveness and accuracy of different location methods can be evaluated for various recording geometries and noise levels.

The datasets consist of seismic traces obtained by ray-tracing and finite difference modeling of sources and receiver arrays embedded in horizontally-layered velocity models. Gaussian noise and harmonic noise are added to the synthetic traces to simulate microseismograms different signal-to-noise levels. The modeled data are stored in files with SEG2 format so they conform to field-recorded data files.

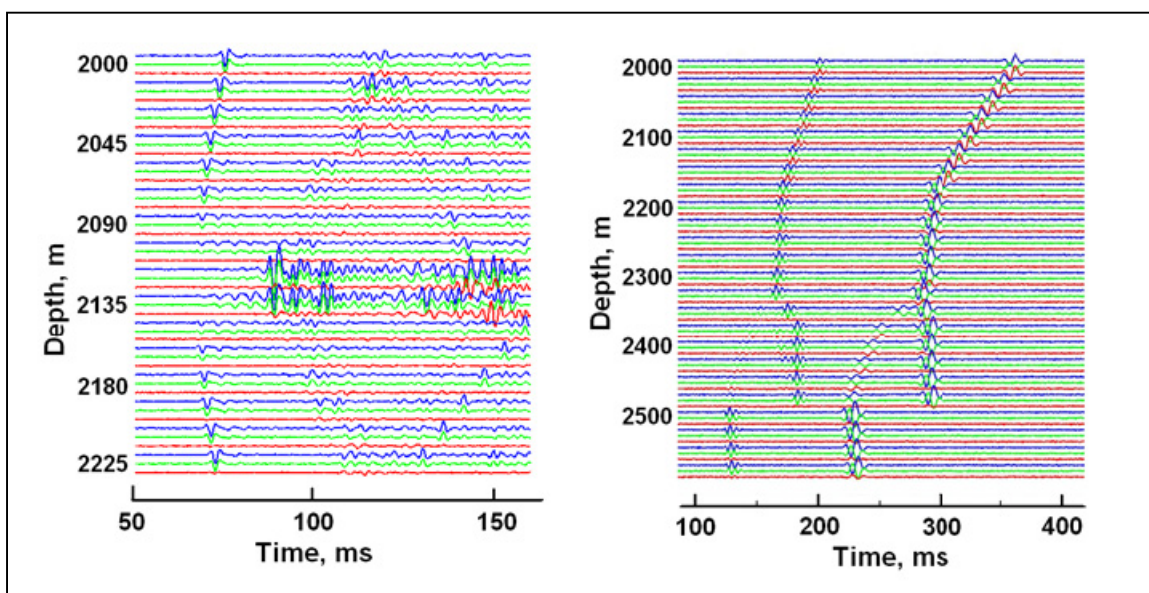


FIG. 1. Synthetic 3C microseismograms through horizontally layered velocity models produced by 2D finite-difference modeling (left), and by ray-tracing (right). The x, y, and z components for individual geophones are plotted as triplets in blue, green, and red. The finite-difference seismograms are rather complex, with mode conversions and grid boundary artifacts clearly visible. The ray-traced seismograms are generated by inserting wavelets at calculated P and S arrival times. They show only the direct arrivals and head waves arrivals, and show true relative amplitudes only for the three components of a single geophone.

Tutorial on the continuous and discrete adjoint state method and basic implementation

Matthew J. Yedlin^{1*}, Daryl G. Van Vorst¹

SUMMARY

This tutorial endeavours to lay out the basic scheme using the adjoint state method for setting up the basic equations for inversion of acoustic, elastic or electromagnetic data. The basic scheme is simple and relies on three basic ingredients consisting of a forward modelling package, the definition of a misfit norm and a gradient descent method. The adjoint state method will be presented in its continuous and discrete forms. The continuous adjoint state method will be developed for the full elastic equations in the time domain, while the discrete adjoint state method will be developed in the frequency domain.

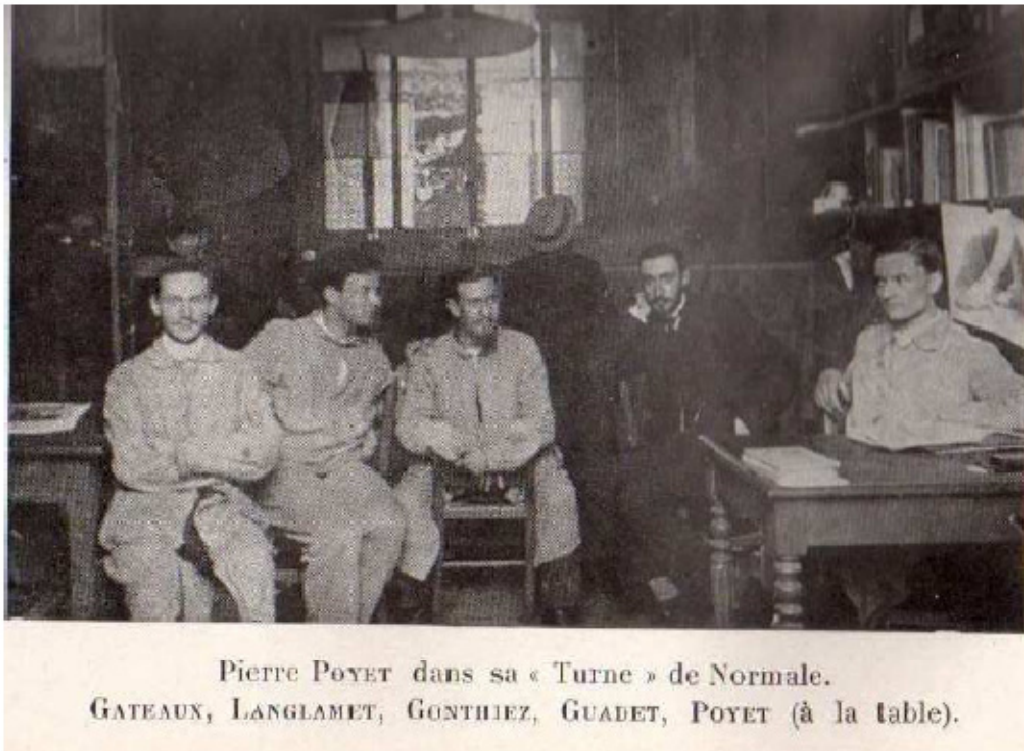


FIG. 1. René Gâteaux (1889-1914), seated at far left in 1908, is the grandfather of the adjoint state method. His work created a formal setting for taking the variation of a functional.

¹ Department of Electrical and Computer Engineering, University of British Columbia

Feasibility of solving least squares Gazdag migration using method of multigrid.

Abdolnaser Yousefzadeh* and John C. Bancroft

SUMMARY

Methods of multigrid have been widely used in solving partial differential equations in physics and mathematics. With the ability of faster recovery of the low frequency components of the solution, they have been used in solving some problems in the exploration geophysics.

Our previous studies showed that the standard method of multigrid is not viable to solve the Kirchhoff least squares prestack migration equation for two reasons. First, the kernel of the main problem is not a diagonally dominant matrix and solvable by the typical multigrid solvers, Jacobi and Gauss Seidel. Second, kernel matrices are extremely large to work with.

This study investigates the feasibility of using multigrid methods in solving a system of Gazdag least squares migration. It is shown by doing least squares migration for each temporal frequency at the time the kernel matrix become smaller, but it is a diagonally non-dominant matrix (Figure 1a). By implementing least squares for each temporal and spatial frequency separately, the kernel matrix remains non-diagonal dominant (Figure 1b). Best scenario is performing least squares migration for each temporal frequency and depth separately at a time. The kernel matrix reduces to a diagonal and easily invertible matrix (Figure 1c).

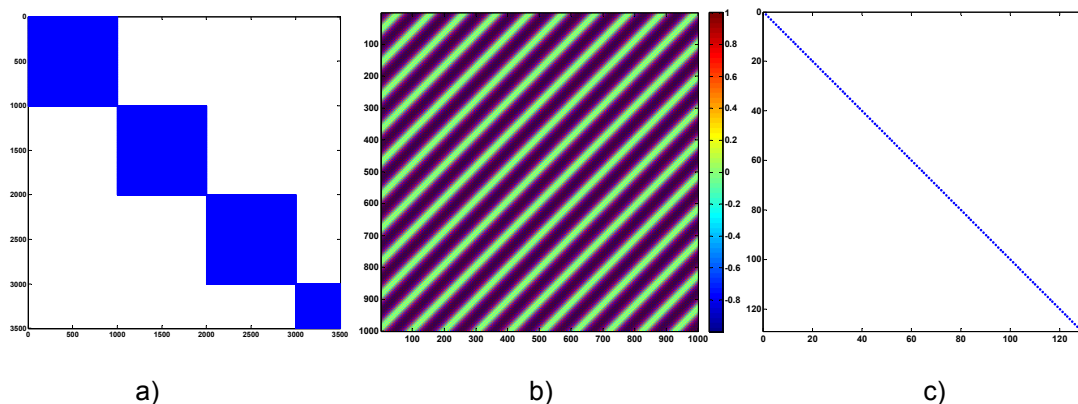


FIG. 1. a) Nonzero elements of the first 3500 rows and columns of matrix Hessian matrix, $\mathbf{G}'\mathbf{G} + \mu^2\mathbf{I}$, for each ω ; b) Real part of the elements in matrix Hessian, when it is constructed for one $\omega = -193.3$, and one k_x ; c) Nonzero elements of the Hessian matrix, when it is constructed for one ω and one depth.

A multiple model and Padé approximation

Dali Zhang, Michael P. Lamoureux, and Gary F. Margrave

SUMMARY

The paper considers rational Padé approximation of the Z -transform function of a time-dependent minimum phase signal. We present a derivation of reflection and transmission coefficients in layered media which are related to infinite impulse response (IIR) filters as a rational function of a special form. We set up the Padé approximation problem using the seismic data directly, with some choice on the rational function form to reduce the dimension of the solution space. The rational $[p, q]$ -Padé approximation of the Z -transform function is formulated as a constrained least squares minimization problem with regularization constraints provided by the minimum phase signal. Results of some numerical experiments in building the Padé approximating filter, and its use as an inverse filter to remove the multiples demonstrate the effectiveness of the presented approach.

RESULTS

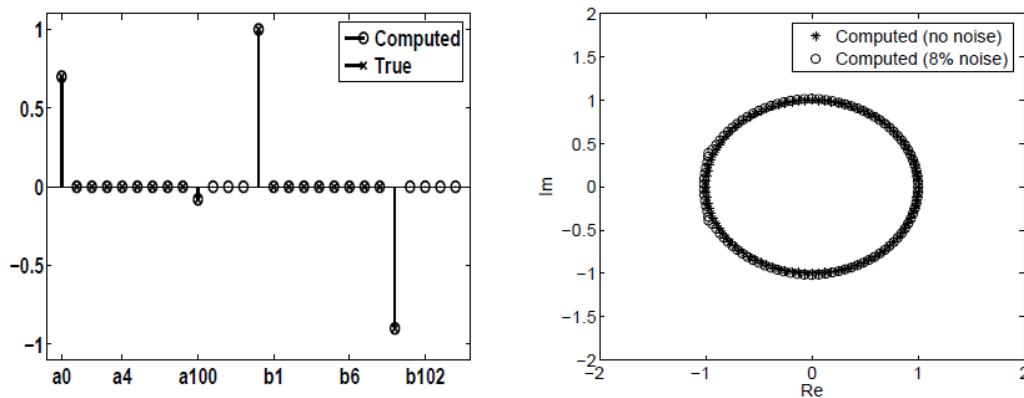


FIG. 1. Reconstruction of Padé coefficients for data with no noise (left). Calculation of poles for the IIR filter function (right).

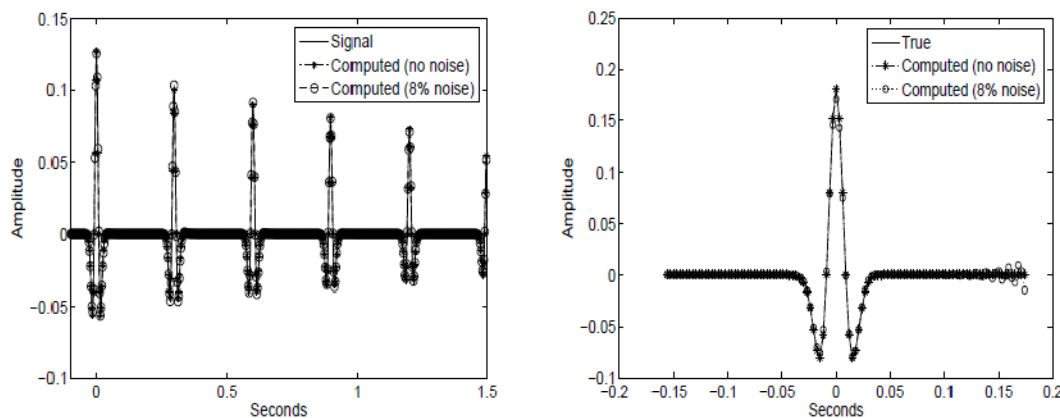


FIG. 2. Left: Reconstruction of the IIR filtered Ricker wavelet (25 Hz dominant frequency). Right: Reconstruction of the Ricker wavelet with a 25 Hz dominant frequency.

AVO processing of walkaway VSP data at the Ross Lake heavy oilfield, Saskatchewan

Zimin Zhang, Robert R. Stewart, and Don C. Lawton

SUMMARY

The AVO processing and analysis of walkaway VSP data was undertaken at the Ross Lake heavy oilfield, Saskatchewan. A walkaway VSP geometry has advantages for AVO analysis over surface seismic data. True amplitude processing is feasible and undesired wave-propagation effects can be minimized. At the top and the base of the target channel sand, the synthetic seismogram and walkaway VSP processing results show a similar amplitude variation with offset for the reflections of both PP and PS data (Figure 1 and Table 1). These results indicate the promise of rock properties inversion using AVO gathers from walkaway VSP.

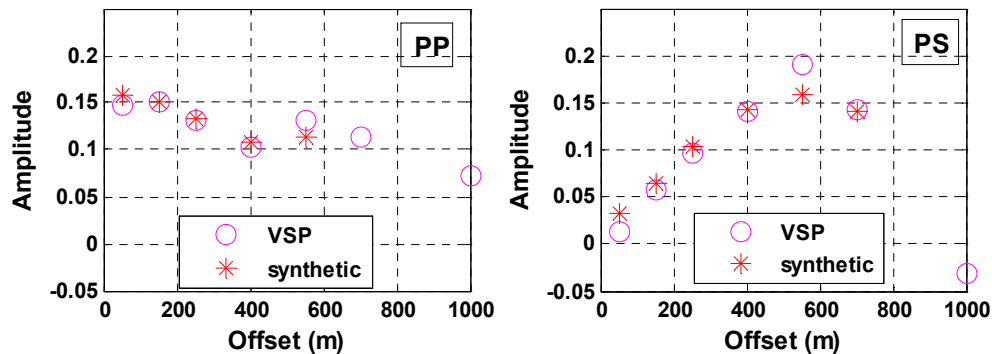


FIG. 1. Comparison between the amplitude at the base of the channel sand from walkaway VSP and synthetic seismograms (generated by Syngram) for PP and PS data. The amplitude of synthetic data were scaled globally to match the amplitude level of VSP data.

Table 1. Amplitude of offset gathers from walkaway VSP data and synthetic seismograms at the base of the channel sand base and their difference.

| Amplitude \ Offset (m) | | 50 | 150 | 250 | 400 | 550 | 700 | 1000 | |
|------------------------|------------------------|---------|---------|---------|---------|---------|---------|---------|--|
| | | | | | | | | | |
| PP | VSP | 0.147 | 0.15137 | 0.13118 | 0.10217 | 0.1313 | 0.11317 | 0.07217 | |
| | synthetic | 0.1577 | 0.1510 | 0.1323 | 0.1082 | 0.1138 | - | - | |
| | mean difference (%) | 0.18 | | | | | - | | |
| | standard deviation (%) | 8.45 | | | | | - | | |
| PS | VSP | 0.01303 | 0.05671 | 0.09677 | 0.14156 | 0.19037 | 0.14256 | -0.0308 | |
| | synthetic | 0.0326 | 0.0640 | 0.01035 | 0.1428 | 0.1578 | 0.1402 | - | |
| | mean difference (%) | - | -0.13 | | | | | - | |
| | standard deviation (%) | - | 11.6 | | | | | - | |

Detecting fractures using time-lapse 3C-3D seismic data

Zimin Zhang, Don C. Lawton and Robert R. Stewart

ABSTRACT

This report presents the interpretation of time-lapse 3C-3D seismic data for fracture detection in a potash mine. Seismic interpretation of the time-lapse 3C-3D surveys saw noticeable amplitude changes and push-down effects at the Dawson Bay Formation and an underlying formation in the 2008 survey compared with the 2004 survey, especially on the converted-wave (P-S) data (Figure 1). V_p/V_s analysis displayed increasing values on the 2008 survey within a particular part of the survey area (Figure 2). Seismic curvature attributes were calculated at the top of the Dawson Bay Formation and the mining level. The curvature maps also suggest that the fractures are well developed in the Dawson Bay Formation.

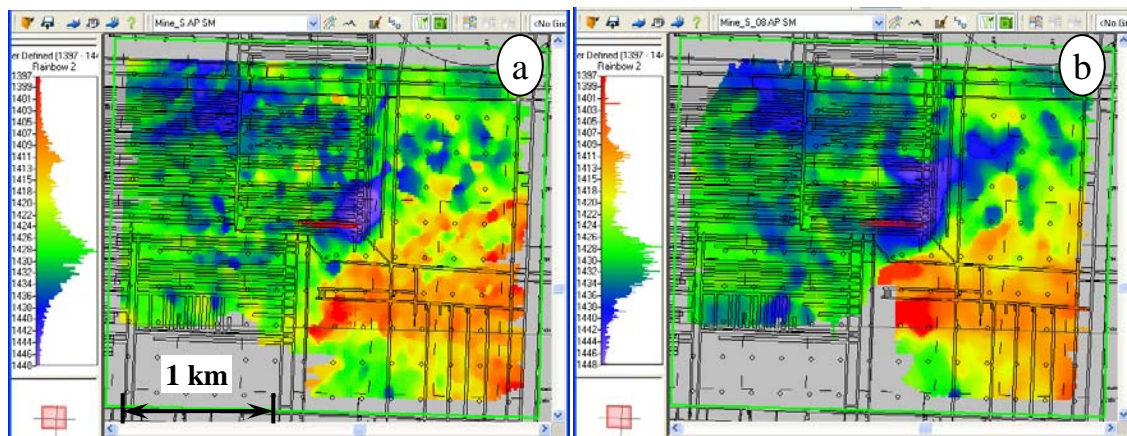


FIG 1. Time structure of the mine level on the PS data, a: 2004 survey; b: 2008 survey; c: PS travel time difference at the mine level between 2008 and 2004 survey.

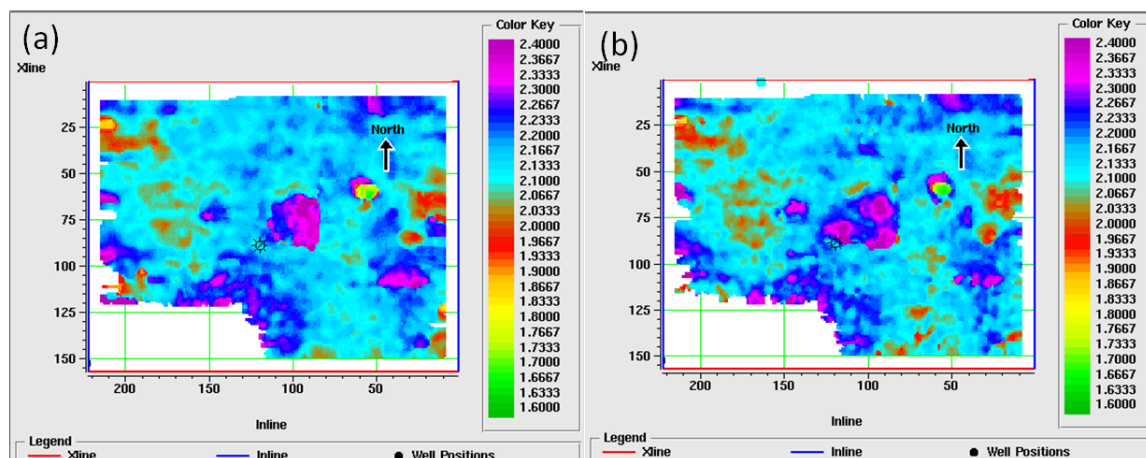


FIG 2. Interval V_p/V_s map from the Birdbear Formation to the Shell Lake anhydrite (including the Dawson Bay Formation). a: 2004 survey; b: 2008 survey.

Estimating seismic attenuation (Qp & Qs) from rock properties

Zimin Zhang, Robert R. Stewart, and Don C. Lawton

SUMMARY

As one of the basic attributes of seismic waves propagating in the earth, attenuation (or Q) has important values in the acquisition, processing, and interpretation of seismic data. The relationship between seismic attenuation and rock properties is investigated in this paper using VSP data and well logs from the Ross Lake heavy oilfield, Saskatchewan. The results reveal that Q values of P- and S-waves correlate to P modulus, V_p/V_s , effective porosity, and shale volume. The equations for Q estimation using these four rock properties were then derived using multiple parameter least-square regression method. The results (Figure 1) show better prediction quality of Q_p ($R^2=0.65$) than Q_s ($R^2=0.48$).

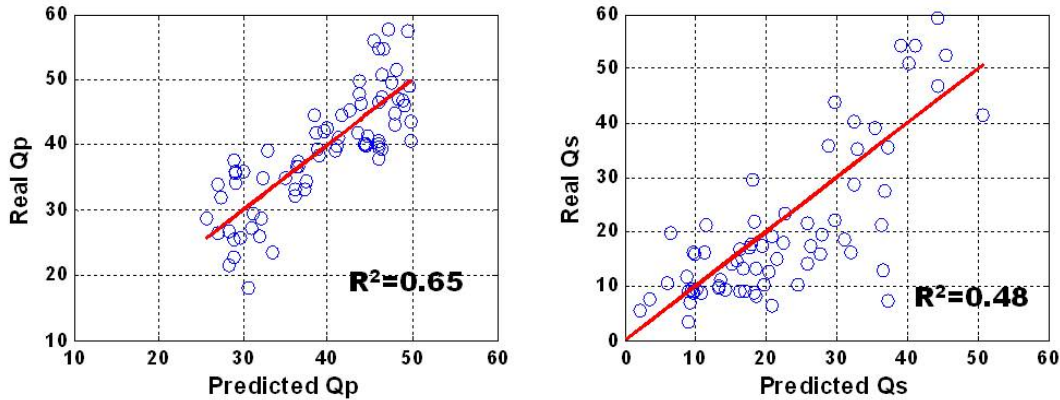


FIG. 1. Comparison between real and predicted Q_p and Q_s values using the following equation:

$$Q_p = 1.95 * M - 13.63 * \frac{V_p}{V_s} + 37 * \phi + 21 * Vsh + 28.6$$

$$Q_s = 66.4 * M - 13.38 * \frac{V_p}{V_s} + 285 * \phi + 101 * Vsh + 210$$

P-S survey design

Liliana M. Zuleta and Don C. Lawton

SUMMARY

Fold, illumination, offset distribution and azimuth distribution were evaluated for PS survey design for two different projects. The first was planned to image an interval of interest from 380 m to 425 m depth, for the Paskapoo Formation, located in the Priddis area. Orthogonal and Slant geometries were tested with different parameters. Good results for the converted wave 3D design were found using a slant geometry design with receiver interval and source interval of 10 m, a receiver line interval of 50 m, a source line interval of 25 m and a maximum offset of 400 m. Fold for the slant geometry design is shown in Figure 1 (left) and it gave better offset and azimuth distribution than the orthogonal geometry design. Illumination was similar in both types of geometries. Optimization of these parameters was reached by changing the receiver and source line intervals to 40 m, balancing quality requirements and cost related to the increase of number of shots when using 25 m as the source line interval. This design was done using CREWES QuadDes software.

A second case study was undertaken where orthogonal and slant designs were also both tested for a project area with a deeper target, of 2160 m, and a shallow horizon of interest at 500 m. Real situations were taken in to consideration such as having to move source lines to pre-existing cut lines and examining the effect of obstructions presented by lakes in the area of the survey. After the analysis, an orthogonal geometry design was chosen with 360 m source line interval, 240 m receiver line interval and 60 m source and receiver station intervals. PS fold for the orthogonal design is shown in Figure 1 (right). The patch selected was 26 lines with 100 receivers per line to have an aspect ratio of about unity for optimum data inversion. This design was undertaken using OMNI software.

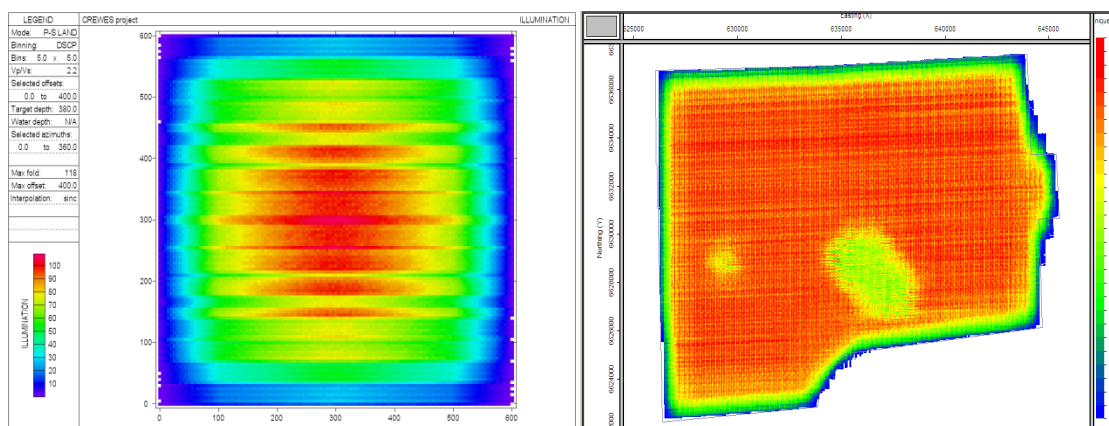


FIG. 1. Left: PS fold for Paskapoo Formation slant design. Right: PS fold for deeper target orthogonal design.